

Rank One Chaos: Theory and Applications

March 30, 2007

QIUDONG WANG*

*Department of Mathematics,
University of Arizona,
Tucson, AZ 85721 USA
dwang@math.arizona.edu*

ALI OKSASOGLU†

*Honeywell Corporation,
11100 N. Oracle Rd.,
Tucson, AZ 85737 USA
ali.oksasoglu@honeywell.com*

Abstract

The main purpose of this tutorial is to introduce to a more application-oriented audience a new chaos theory that is applicable to certain systems of differential equations. This new chaos theory, namely the theory of rank one maps, claims a comprehensive understanding of the complicated geometric and dynamical structures of a specific class of non-uniformly hyperbolic homoclinic tangles. For certain systems of differential equations, the existence of the indicated phenomenon of chaos can be verified through a well-defined computational process. Applications to the well-known Chua's and MLC circuits employing controlled switches are also presented to demonstrate the usefulness of the theory. We try to introduce this new chaos theory by using a balanced combination of examples, numerical simulations and theoretical discussions. We also try to create a standard reference for this theory that will hopefully be accessible to a more application-oriented audience.

*Author for correspondence.

†Also with the Department of Mathematics, University of Arizona, Tucson, AZ 85721 USA.

Contents

1	Introduction	2
2	Periodic Sinks and Observable Chaos	5
2.1	Preliminaries	5
2.2	Numerical simulations	8
2.3	Analytic justifications	12
2.3.1	Newhouse sinks	12
2.3.2	On the existence of tangles with no sinks	15
2.3.3	Observable invariant measures	18
3	A Theory on Rank One Chaos	25
3.1	A brief introduction	25
3.2	Non-uniformly expanding 1D maps	27
3.2.1	Admissible family of non-uniformly expanding 1D maps	27
3.2.2	Dynamical theories on admissible 1D family	29
3.3	A theory of rank one chaos	31
4	A General Framework for Applications	38
4.1	Periodically kicked limit cycles	38
4.2	Hopf bifurcation and rank one chaos	44
5	Application to Circuits and Systems	53
5.1	Rank one chaos in a switch-controlled smooth Chua's circuit	55
5.1.1	Derivation of equations	55
5.1.2	Location of supercritical Hopf bifurcation	57
5.1.3	Normal form and the twist constant	58
5.1.4	The function $\phi(\theta)$ and the existence of rank one chaos	59
5.1.5	Numerical simulations	60
5.2	Multiple switches and asynchronous kicks	63
5.2.1	Derivation of equations	66
5.2.2	Hopf bifurcations and normal form	68
5.2.3	Twist constant and rank one chaos	70
5.2.4	Numerical simulations	71
5.3	Non-Hopf periodic solutions	79
5.3.1	Derivation of equations	84
5.3.2	Numerical simulations	85
6	Concluding Remarks	88
	References	90

1 Introduction

The main purpose of this paper is to introduce to a more application-oriented audience a new chaos theory that is applicable to certain systems of differential equations. This new chaos theory, namely the theory of rank one maps, claims a comprehensive understanding of the complicated geometric and dynamical structures of a specific class of non-uniformly hyperbolic homoclinic tangles. For certain systems of differential equations, the existence of the indicated class of homoclinic tangles is checkable through a well-defined computational process.

Chaos as a dynamical phenomenon can be characterized in descriptive terms by sensitive dependency on initial conditions and unpredictability of evolutions of a generic orbit in the phase space. As was first observed by H. Poincaré [Poincaré, 1890], the occurrences of chaos are closely related to homoclinic tangles created by transversal intersections of the stable and unstable manifolds. Later, the studies of homoclinic tangles led to the discovery of Smale's horseshoe [Smale, 1967], which is a complicated dynamical structure that fulfills the descriptive definition for chaos above and exists in all homoclinic tangles. The conceptual simplicity of the formations of homoclinic tangles and the elegant geometric structure of the horseshoe map have empowered the spreadings of the gospel of modern dynamical systems to other scientific disciplines with a relatively straight forward preaching that

- (i) as a dynamical phenomenon that commonly exists in nonlinear systems, chaos reflects the mathematical actuality of homoclinic tangles;
- (ii) the complicated structure of homoclinic tangles is partly understood through Smale's horseshoes;
- (iii) the existence of the homoclinic tangles and horseshoes can be systematically confirmed through geometric analysis and computations in many systems of applications (see, e.g. [Guckenheimer & Holmes, 1997]).

A comprehensive theory of dynamics has been well-developed for uniformly hyperbolic systems. These are the systems that split the orientations of the phase space *globally* into uniformly expanding and contracting directions. This theory is then extended to the studies of the systems with invariant cones and discontinuities, elucidating important examples such as geodesic flows and billiards (see, e.g., [Anosov, 1967; Bowen, 1975; Sinai, 1970, 1972; Smale, 1967; Wojtkowski, 1983]). An abstract non-uniform hyperbolic theory also emerged in the 1970's and 80's. This theory is applicable to systems in which hyperbolicity is assumed only asymptotically in time and almost everywhere with respect to an invariant measure (see, e.g., [Ledrappier & Young, 1985; Oseledec, 1968; Pesin, 1977; Ruelle, 1976]).

Along the way of these magnificent developments, however, there has remained a gap between the theory and its applications to concrete systems, in particular, between the chaos observed in simulations and its mathematical justifications. The invariant cones property is quite special, and is rarely enjoyed

by systems of real applications. For the new non-uniformly hyperbolic theory to apply to concrete systems, it is necessary to first verify certain *a priori* assumptions such as the positivity of Lyapunov exponents or the existence of SRB measures, but these assumptions are inherently difficult to verify. Consequently, this theory has had trouble in finding its way into the world of concrete applications. With the theory of rank one maps and its applications to concrete systems, we are finally at a point to make the much needed connection.

Non-uniformly hyperbolic tangles are exceedingly complicated structures, and as a participating part, horseshoes are typically *not* observable. To provide valid mathematical justifications for simulation results, one has to look deeper into the tangles to find *observable* dynamical objects. These are, for the systems studied in this paper, *periodic sinks* and *SRB measures*, as we will see momentarily through the various mathematical theories presented in Sec. 2 of this paper. These theories include the theory of Newhouse sinks [Newhouse, 1974; Palis & Takens, 1993], the theories of rank one chaos for maps of various forms and dimensions [Benedicks & Carleson, 1991; Jakobson, 1981; Mora & Viana, 1993; Viana, 1993; Wang & Young, 2001, 2006b] and the theory of SRB measures [Benedicks & Young, 1993; Bowen, 1975; Ruelle, 1976; Sinai, 1972]. In Sec. 3 we present a detailed formulation of the theory of rank one maps following the recent work of Wang & Young [2001, 2006a,b], where the previous theory of Benedicks & Carleson [1985, 1991] on strongly dissipative Hénon maps [Hénon, 1976] is generalized and developed into a form that is potentially applicable to concrete systems.

This tutorial is not only about a mathematical theory, but also about *its applications*. In Sec. 4, we introduce a general setting of periodically kicked systems of ordinary differential equations, to which the theory of rank one chaos is potentially applicable. In particular, we present the studies of Wang & Young [2002a,b] on periodically kicked systems of Hopf bifurcations [Hopf, 1947]. Section 5 is devoted to applications of the theory of Secs. 3 and 4 to certain switch-controlled circuits (or systems). Numerical simulations under the guidance of the analytic computations proposed by the theory of Sec. 4 are presented to demonstrate the usefulness of the theory. The examples used in Sec. 5 are mainly from the work of Wang & Oksasoglu [2005, 2007], Oksasoglu *et al.* [2006] and Oksasoglu & Wang [2006]. The theory of rank one maps has also been applied to other systems of differential equations, see for instances, [Lin, 2006] and [Guckenheimer *et al.*, 2006].

In the writing of the Secs. 2 and 3 of this tutorial, we have placed more emphasis on the explanations of the contents of the theorems we chose to present than on providing proofs, for rigorous proofs are usually way too long to be included. In suitable occasions we would supply sketching outlines and heuristic arguments, through which we hope to at least convey to the reader certain intuitive (but very rough) sense of justifications. More computational details are included in Secs. 4 and 5 with the purpose of providing easy-to-follow steps for the reader in case he/she intends to apply the theory to his/her own problems.

To put what we intend to achieve in perspective, we have, on one hand, rigorous mathematical objects defined to infinitesimal precision. On the other hand, we have simulations carried out on a finite collection of rational numbers within a restricted time frame. What is observed in the latter is at best an imprecise shadow of the former and our task is to match the precise objects through the shadows they cast. Here we are clearly subjected to serious limitations. The dots we connect sometimes are necessarily subjective and judgemental.

The theories and applications we chose to present in this tutorial are only a small sample of what has been achieved in the studies of non-uniformly hyperbolic systems in the last thirty years. Even within such a restricted context, this paper is written as a lecture note of introductory nature, *not* a survey, and the choice of the materials presented is obviously influenced by the research interests of the authors.

2 Periodic Sinks and Observable Chaos

Let S^1 be the unit circle, \mathbb{R} be the real number line and $M = S^1 \times \mathbb{R}$. Let $T_{a,b,L} : M \rightarrow M$ be a three-parameter family of maps defined by

$$(\theta, r) \rightarrow (a + \theta + L \sin 2\pi\theta + r, br + bL \sin 2\pi\theta) \quad (1)$$

where $\theta \in \mathbb{R}/\mathbb{Z}$, $r \in \mathbb{R}$. In this section we use $T_{a,b,L}$ as a motivating example to introduce such objects as *strange attractors*, *Newhouse sinks*, *rank one chaos* and *SRB measures*. Our aim is to provide mathematical justifications for certain numerical observations.

2.1 Preliminaries

Throughout this paper, $|\cdot|$ represents both the absolute value of a real number and the size of a given vector. Let $T : M \rightarrow M$ be a diffeomorphism and DT_z be the Jacobi matrix for T at $z = (\theta, r) \in M$. $z \in M$ is a *periodic point* of period n if $T^n(z) = z$. Let z be a periodic point of period n and λ_1, λ_2 be the two eigenvalues of DT_z^n . z is a *hyperbolic periodic point* if $|\lambda_1| < 1 < |\lambda_2|$, and it is a *periodic sink* if $|\lambda_1|, |\lambda_2| < 1$. For a hyperbolic periodic point $z \in M$ of period n , let

$$\begin{aligned} W^s(z) &= \{z' \in M : \lim_{k \rightarrow +\infty} T^{kn}(z') \rightarrow z\}, \\ W^u(z) &= \{z' \in M : \lim_{k \rightarrow +\infty} T^{-kn}(z') \rightarrow z\}. \end{aligned}$$

$W^s(z)$ is called the *stable manifold* and $W^u(z)$ the *unstable manifold* of z . Both $W^s(z)$ and $W^u(z)$ are 1D curves immersed in M and the eigenvectors of DT_z^n for λ_1 and λ_2 are tangent to $W^s(z)$ and $W^u(z)$, respectively, at z .

We say that $z_0 \in M$ has a *positive Lyapunov exponent* if

$$\limsup_{k \rightarrow \infty} \frac{1}{k} \ln |DT_{z_0}^k u| > 0$$

for some unit vector u in the tangent space of M at z_0 . Positive Lyapunov exponents are a trademark for *local instability* and chaotic dynamics.

A bounded open set $U \subset M$ is a *trapping region* for $T : M \rightarrow M$ if $T(\bar{U}) \subset U$ where \bar{U} is the closure of U . For a given trapping region $U \subset M$, let

$$\Lambda = \cap_{k \geq 0} T^k(\bar{U}).$$

Λ is a compact subset that is *invariant* under T and it is what we will refer to as an *attractor* for T in this paper. We also refer to the set

$$B(\Lambda) := \{z' \in M : \lim_{k \rightarrow \infty} d(T^k(z'), \Lambda) = 0\}$$

as the *basin of attraction* for Λ , where $d(T^k(z'), \Lambda) := \min_{z \in \Lambda} |T^k(z') - z|$. $U \subset B(\Lambda)$ by definition. All these are elementary.

For a given $T : M \rightarrow M$, an attractor for T can be as simple as one point but it can also be a complicated set. Complicated attractors were first encountered with surprises, and were regarded as *strange*. It was soon realized, however, that strange attractors (and *chaos*) are common phenomena in nonlinear systems. They are often associated with

- (a) transversal intersections of stable and unstable manifolds of hyperbolic periodic orbits,
- (b) Smale's horseshoes.

Let us now introduce these two in a little restricted setting of 2D maps from M to M .

Let $z \in M$ be a hyperbolic periodic point for T . We say that $p \in M$ is a point of *transversal intersection* of stable and unstable manifolds of z or, in short, a *homoclinic point* if

- (i) $p \in (W^s(z) \cap W^u(z)) \setminus \{z\}$,
- (ii) p is a non-tangential intersection of $W^s(z)$ and $W^u(z)$, as shown in Fig. 1.

Historically, it was first observed by H. Poincaré that transversal intersections of stable and unstable manifolds give rise to exceedingly complicated dynamical structures, which are since then called *homoclinic tangles*.

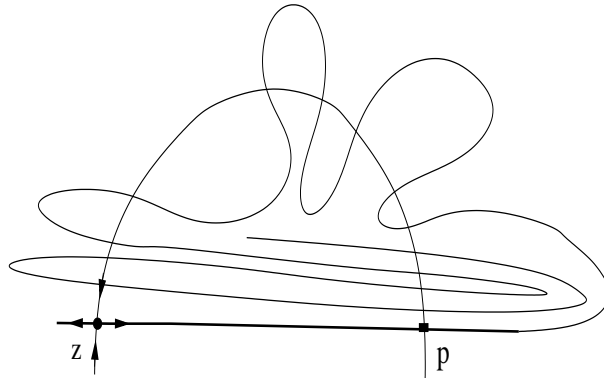


Figure 1: Homoclinic tangles.

A horseshoe is illustrated in Fig. 2, where H_1 and H_2 are the respective images of V_1 and V_2 under a map T . We assume that, in mapping to H_1 and H_2 , V_1 and V_2 are uniformly contracted in the vertical direction and uniformly expanded in the horizontal direction by T . Let

$$D = \bigcap_{k \in \mathbb{Z}} T^k(V_1 \cup V_2).$$

D is an example of what is commonly referred to as Smale's horseshoe.

Horseshoes are best understood through *symbolic dynamics*. Addresses $a(z)$ are first assigned to all $z \in V_1 \cup V_2$ as follows: $a(z) = 1$ if $z \in V_1$ and $a(z) = 2$ if $z \in V_2$. For $z_0 \in D$, let $\{s_k(z_0)\}_{k=-\infty}^{\infty}$ be such that $s_k(z_0) = a(T^k(z_0))$.

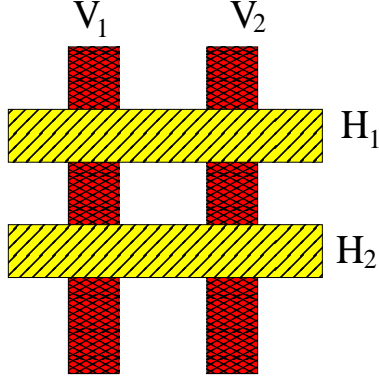


Figure 2: Horseshoe.

$\{s_k(z_0)\}_{k=-\infty}^{\infty}$ is a bi-infinite sequence of 1 and 2's, which we denote as $\mathbf{s}(z_0)$. Observe that $s_k(T(z_0)) = s_{k+1}(z_0)$ for all k . This is to say that $\mathbf{s}(T(z_0))$ is obtained from $\mathbf{s}(z_0)$ by a uniform shift of one position to the left. For the horseshoe in Fig. 2, it is also true that, for any given sequence $\{s_k\}_{k=-\infty}^{\infty}$, $s_k \in \{1, 2\}$, there exists a $z_0 \in D$, so that $a(T^k(z_0)) = s_k$ for all k . In particular, a horseshoe of Fig. 2 contains infinitely many periodic orbits, each corresponding to a cyclic symbolic coding.

Smale observed that horseshoes exist in all homoclinic tangles. Note that a horseshoe of Fig. 2 also implies the existence of homoclinic tangles. To confirm this let us pick two periodic points z_1 and z_2 in D that are arbitrarily close (z_1 and z_2 must exist since we have infinitely many periodic orbits crowded inside of a bounded region in M) and use the fact that, at z_1 and z_2 , the stable and unstable directions are roughly aligned, respectively. We obtain a loop of intersections as shown in Fig. 3(a), from which a homoclinic intersection follows as depicted in Fig. 3(b).

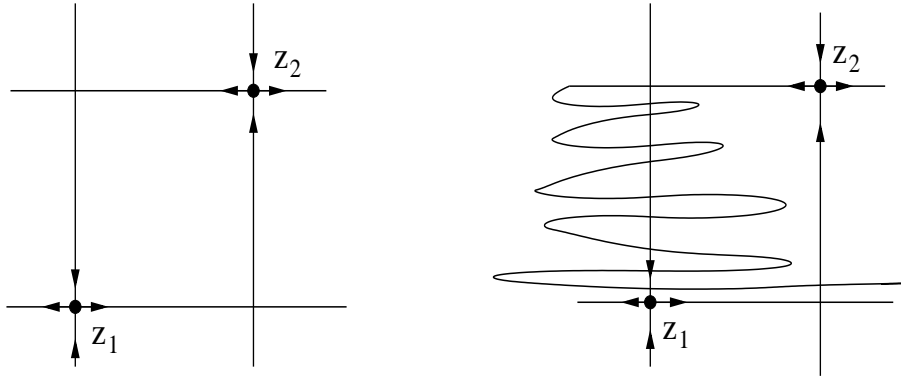


Figure 3: (a) Heteroclinic loop. (b) Homoclinic point.

We now prove the following proposition for $T = T_{a,b,L}$.

Proposition 2.1 *Let $T = T_{a,b,L}$ be as in Eq. (1) and assume that $L \geq 2$, $0 < 2\pi L|b| < 0.1$. Then T has an attractor Λ and inside Λ there exists a horseshoe. It also follows that T admits homoclinic tangles.*

Proof: Let $T = T_{a,b,L}$ and assume that $L \geq 2$ and $0 < 2\pi L|b| < 0.1$. For $z = (\theta, r) \in M$,

$$DT_z = \begin{pmatrix} 1 + 2\pi L \cos 2\pi\theta & 1 \\ 2\pi b L \cos 2\pi\theta & b \end{pmatrix},$$

from which it follows that $\det(DT_z) = b \neq 0$ so T is a diffeomorphism. Let $U = \{(\theta, r) \in M : |r| < 1\}$. $T(\bar{U}) \subset U$ from Eq. (1) so U is a trapping region. Let $\Lambda = \cap_{k \geq 0} T^k(\bar{U})$ be the attractor for T .

Regarding the claim on the existence of a horseshoe in Λ , we first let

$$I_1 = \{\theta : \theta \in [-0.2116, 0.2116]\}, \quad I_2 = \{\theta : \theta \in [0.3151, 0.6849]\}.$$

$V_1, V_2 \subset M$ are such that

$$V_1 = I_1 \times [-1, 1], \quad V_2 = I_2 \times [-1, 1].$$

Let $H_1 = T(V_1)$, $H_2 = T(V_2)$. From Eq. (1) it follows that H_1 crosses both V_1 and V_2 in horizontal direction and so does H_2 , creating a horseshoe as shown in Fig. 2.

For a rigorous proof, we need to further construct *invariant cones* in the tangent space to identify precisely the directions of contraction and expansion for all $z \in V_1 \cup V_2$. We skip this step here. \square

Keeping Proposition 2.1 and its implications for Λ in mind, we now turn to numerical simulations.

2.2 Numerical simulations

In this subsection we present some results from the numerical iterations of $T = T_{a,b,L}$. Numerical experiments are kept direct and simple. Values of parameters (a, b, L) are fixed first, then an initial point $z_0 \in U$ is arbitrarily picked and $z_k = (\theta_k, r_k) := T^k(z_0)$ are numerically computed for $k = 1, 2, \dots$ up to $k = 2^{14}$. (θ, r) are regarded as polar coordinates and their rectangular correspondences (x, y) are obtained through $x = (1 + r) \cos 2\pi\theta$, $y = (1 + r) \sin 2\pi\theta$. To demonstrate the behavior of the map with an initial point randomly picked, the x -coordinate versus time, (k, x_k) , the phase portrait, (x_k, y_k) , and the frequency spectrum of x_k are plotted. Since our goal is to plot Λ through a randomly picked orbit in U , the first 10^3 points of the iteration are dropped. All maps used in this subsection satisfy the assumptions of Proposition 2.1, for which attractors of complicated structures are proved to exist.

Scenario (a) (Periodic sinks) A typical result is shown in Fig. 4. For this plot $L = 2.0$, $b = 0.005$, $a = 0.5$. Initial values are not very relevant, for all our picks produce the same output. For this specific choice of parameters, assumptions

of Proposition 2.1 are obviously satisfied, and thus, it follows that Λ contains homoclinic tangles and horseshoes. They, however, **do not** show up in this simulation.

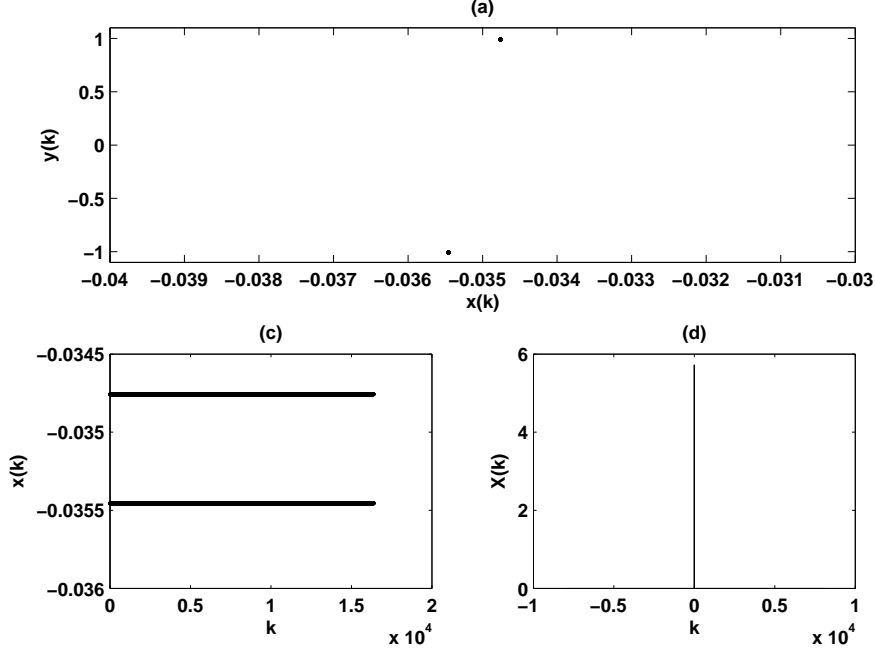


Figure 4: A periodic sink for $L = 2.0$, $b = 0.005$, $a = 0.5$. (a) Phase portrait $x_k - y_k$. (b) Time evolution of x_k . (c) Frequency spectrum of x_k .

Scenario (b) (Chaotic attractors) For a different simulation, we keep $L = 2.0$ and $b = 0.005$ but change a to 0.8. Again, an initial point is randomly picked and, as before, the same type of pictures are plotted in Fig. 5, illustrating a dynamical behavior very different from what appeared in Fig. 4. The phase portrait on the xy -plane is shown in Fig. 5(a). Due to the fact that the attractor is compressed in the r -direction, it is hard to see its structure from the phase portrait of Fig. 5(a). However, the truly complicated structure of the attractor is revealed when a small section of the phase portrait of Fig. 5(a) (indicated with a rectangular area) is magnified as shown in Fig. 5(b). The evolution of the x -coordinate and its frequency spectrum are shown, respectively, in Fig. 5(c) and (d), indicating completely random evolutions in time.

It is also observed that, for different initial conditions, the corresponding plots of Fig. 5(a), (b) and (c) appear identical to the naked eye but the corresponding plots of Fig. 5(d) look completely different. The former hints at the existence of one dominating distribution for almost all orbits in the phase space, and the latter indicates that this distribution manifests itself independently in the phase space by different orbits. These are the critical characteristics of

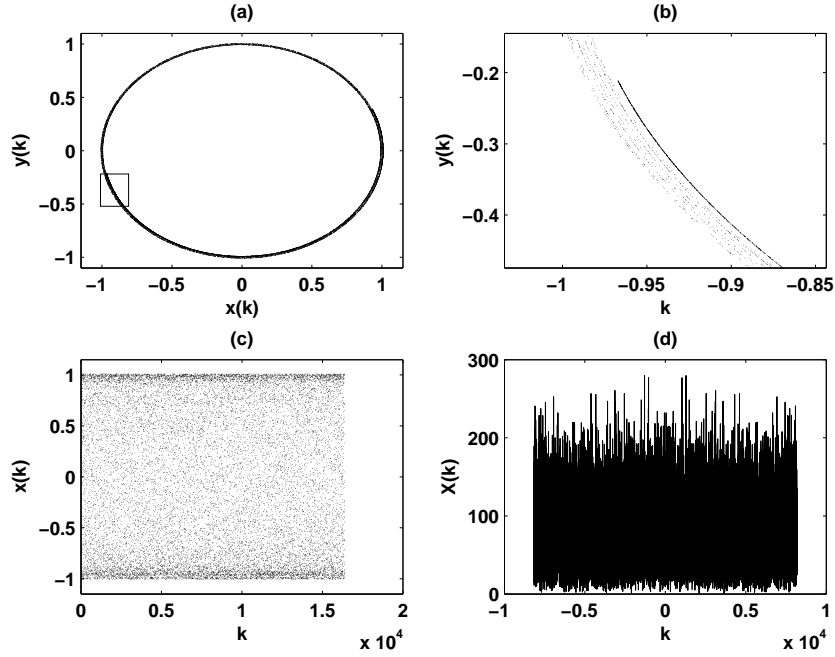


Figure 5: A chaotic attractor for $L = 2.0$, $b = 0.005$, $a = 0.8$. (a) Phase portrait $x_k - y_k$. (b) Magnification of the rectangular area in (a). (c) Time evolution of x_k . (d) Frequency spectrum of x_k .

important consequences for the theory we intend to present in this paper. The issues related to such distributions are further discussed in Sec. 2.3.3.

Over the space of parameters: We continue to fix $L = 2.0$, $b = 0.005$, but now run the parameter a over $[0, 1)$. For each a , we hit one of the two scenarios above. Though the exact locations and periods of the sinks in Scenario (a) and the corresponding plots in Scenario (b) vary as the parameter a varies, the characteristics of all the plots are persistent. In the instances of Scenario (a), periodic sinks, and in the instances of Scenario (b), complicated random structures dominate the scene.

To see the impact of parameter b , we now change b to 0.0001, and keep $L = 2.0$. We again see, for different values of a , one of the two scenarios above. Once again, in the case of Scenario (b), the plots of (x_k, y_k) appear to be a simple closed curve (see, e.g., Fig. 6(a)). Similar to the case of Fig. 5, a simple zoom reveals the complicated structure in the r -direction compressed by strong dissipation. This is shown in Fig. 6(b). Figures 5 and 6 are examples of *rank one chaos*, the mathematical analysis and construction of which are the main theme of this paper.

Let us now vary L . For the rest of the simulations we let $b = 0.005$. We then set $L = 2.0, 2.5, 3.0, 3.5$, respectively, and run a over $[0, 1)$ with an increment of 0.005 totaling 200 simulations for each L . For each combination of

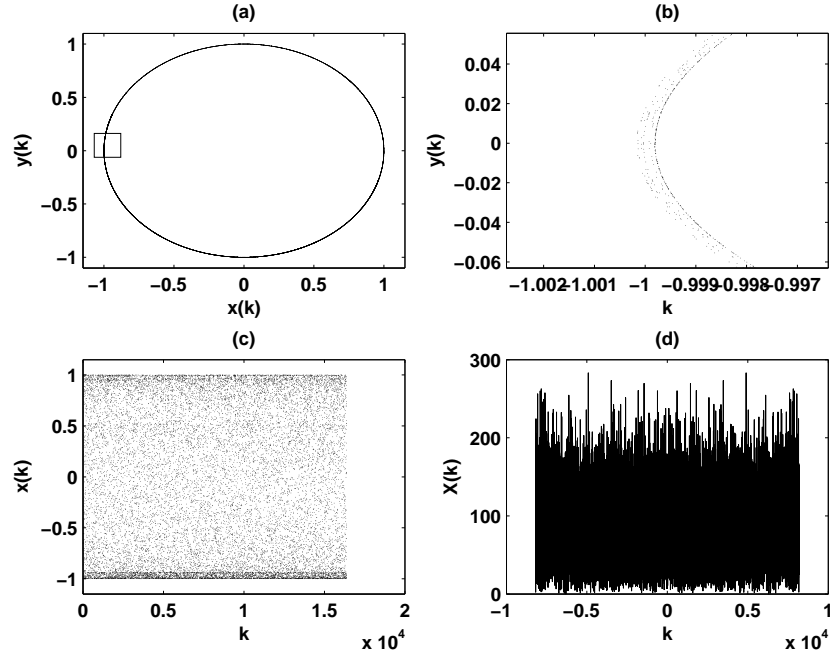


Figure 6: A chaotic attractor for $L = 2.0$, $b = 0.0001$, $a = 0.7$. (a) Phase portrait $x_k - y_k$. (b) Magnification of the rectangular area in (a). (c) Time evolution of x_k . (d) Frequency spectrum of x_k .

(a, b, L) , an orbit randomly picked is plotted. We again end up plotting either a periodic sink (Scenario (a)), or a chaotic attractor (Scenario (b)). Since L determines the strength of expansion of the term $L \sin 2\pi\theta$ in $T_{a,b,L}$, it is intuitively expected that, among the two competing scenarios, smaller L helps Scenario (a), and larger L helps Scenario (b). This is indeed the case. The results of these simulations are given in Table 1. It can be seen from Table 1 that as L increases, Scenario (b) rapidly dominates.

L	Frequency of Scenario (a) (%)	Frequency of Scenario (b) (%)
2.0	14.0	86.0
2.5	11.0	89.0
3.0	5.0	95.0
3.5	2.5	97.5

Table 1: Frequencies of Scenarios (a) and (b) for different choices of L .

We finish this subsection with two remarks:

- (1) The results of the numerical simulations above are typical. They occur frequently in the simulations of systems of various applications. What

we present here is a *prototype* of behavior for systems with non-uniform expansions.

- (2) Proposition 2.1 for $T_{a,b,L}$, though simple and elegant, is far from being sufficient for explaining the numerical plots of this subsection. It appears paradoxical for Scenario (a) since the complicated structures of horseshoes and homoclinic tangles proved to exist by Proposition 2.1 do not show up, i.e., not observed in simulations. For Scenario (b), other than the fact that the plots are complicated, there exists no valid mathematical argument in linking these plots to the objects of Proposition 2.1. As will be seen in Sec. 2.3.3, the plots of Scenario (b) are not those of the horseshoes of Proposition 2.1. They are, in fact, the plots of SRB measures, an *invariant distribution* in the phase space introduced originally by Sinai, Ruelle and Bowen in their study of uniformly hyperbolic systems [Bowen, 1975; Ruelle, 1976; Sinai, 1972].

2.3 Analytic justifications

In this subsection we introduce various mathematical theories developed for the understanding of the numerical observations of the last subsection. These theories, gradually built up by the pure mathematics side of the dynamical systems community since the late 1970's, are fairly sophisticated. All propositions of this subsection are stated for $T_{a,b,L}$ of Eq. (1), a concrete example we use to maintain a sense of unified purpose and direction throughout. These propositions are all backed up by rigorous proofs. We are, however, not interested in presenting the often long and difficult proofs here. The emphasis in our discussions is placed on how to mathematically justify the numerical simulations of Sec. 2.2 based on these propositions.

One major subjective principle we adopt throughout this paper is on the *observability* of an event with regards to numerical simulations of Sec. 2.2. We regard an event in \mathbb{R}^n *observable* only if it happens on a set of positive Lebesgue measure in \mathbb{R}^n . Consequently, events that occur on subsets of Lebesgue measure zero are *not* observable in simulations.

2.3.1 Newhouse sinks

For $T_{a,b,L}$, let us first assume that (a, b, L) satisfies the assumptions of Proposition 2.1. Let $U = \{(\theta, r) : |r| < 1\}$ be the trapping region and $\Lambda = \bigcap_{k>0} T^k(\bar{U})$ be the attractor for T . For a subset $S \subset \Lambda$, let

$$B(S) := \{z \in U : \lim_{k \rightarrow \infty} d(T^k(z), S) = 0\}$$

be the basin of attraction for S . S is observable if $m(B(S)) > 0$ where $m(\cdot)$ stands for the Lebesgue measure, otherwise S is *not* observable as far as the visibility in the numerical experiments of Sec. 2.2 is concerned. For $T_{a,b,L}$, a family of maps of three parameters, there is also an issue of observability in the

parameter space. A dynamical scenario is *observable in the parameter space* only if it holds for a set of parameters of positive Lebesgue measure.

Let us first deal with the seemingly paradoxical situation of Proposition 2.1 and Scenario (a). The horseshoe of Proposition 2.1 and the associated stable manifolds are not observed in the simulations because they form a set of Lebesgue measure zero in M . On the other hand, periodic sinks would have a basin of attraction that is open, therefore, is of positive Lebesgue measure. What appears in the plots of Scenario (a) is hence an indication that, for the map iterated, the attractor Λ contains a periodic sink in addition to the horseshoes of Proposition 2.1, and this sink is the likely destination for a typical orbit starting in $B(\Lambda)$.

For the existence of periodic sinks, here we supply two arguments, one for 1D maps and the other for some 2D maps. First the 1D argument. Let us start with the 1D family $f_{a,L} : S^1 \rightarrow S^1$,

$$f_{a,L}(\theta) = a + \theta + L \sin 2\pi\theta. \quad (2)$$

Let $L > 2$ be fixed, and denote the 1D family $f_{a,L}$ as $f_a : S^1 \rightarrow S^1$. We argue that there is a set for a such that f_a admits periodic sinks. Let $\mathcal{C}(f_a) = \{z \in S^1 : f'_a(z) = 0\}$ be the set of critical points for f_a . For $c_0(a) \in \mathcal{C}(f_a)$ let $c_i(a) = f_a^i(c_0(a))$. For a small interval Δ_0 suitably picked¹ for a , we call $c_i(a) : \Delta_0 \rightarrow S^1$ a critical curve and plot $z = c_i(a)$ on the (z, a) -plane for $i = 0, 1, \dots$. The graph for $z = c_0(a)$ is short and steep, as shown in Fig. 7(a), but in a few iterations as we move forward in time, the critical curve $z = c_i(a)$ will become long, stretching horizontally as shown in Fig. 7(b). Before too long, $z = c_i(a)$ would cross $z = c_0(a)$ (see Fig. 7(c)), generating a parameter \hat{a} such that $c_i(\hat{a})$ comes back to $c_0(\hat{a})$. $c_0(\hat{a})$ is then a super-stable periodic sink. If we keep iterating the parts of $c_i(a)$ that are not yet crossing $c_0(a)$, values of parameters of periodic sinks of higher periods are further generated.

Let us observe that, since sinks persist under small perturbations, a periodic sink for $f_{\hat{a}}$ implies a periodic sink for $T_{a,b,L}$ for all b small and a sufficiently close to \hat{a} . Consequently, (i) periodic sinks are observable in the phase space; and (ii) the maps admitting periodic sinks are observable in the parameter space.

Now a 2D argument. A well-known scenario for periodic sinks on M is as follows. Let $T_\mu : M \rightarrow M$ be a one parameter family of maps. Assume that

(i) (*Dissipative hyperbolic fixed point*) $T = T_0$ has a fixed point p_0 that is hyperbolic ($|\lambda_1| < 1 < |\lambda_2|$ where λ_1, λ_2 are the eigenvalues of DT_{p_0}) and dissipative ($|\lambda_1 \lambda_2| < 1$).

(ii) (*Quadratic tangency*) The stable and unstable manifolds of p_0 have a non-transversal intersection that is non-degenerate, as shown in Fig. 8(a).

¹For the dynamical picture depicted in this paragraph to hold, f_a should satisfy certain technical conditions that are readily verified for $f_{a,L}$ of Eq. (2). These conditions will be introduced later in detail in Sec. 3.2.

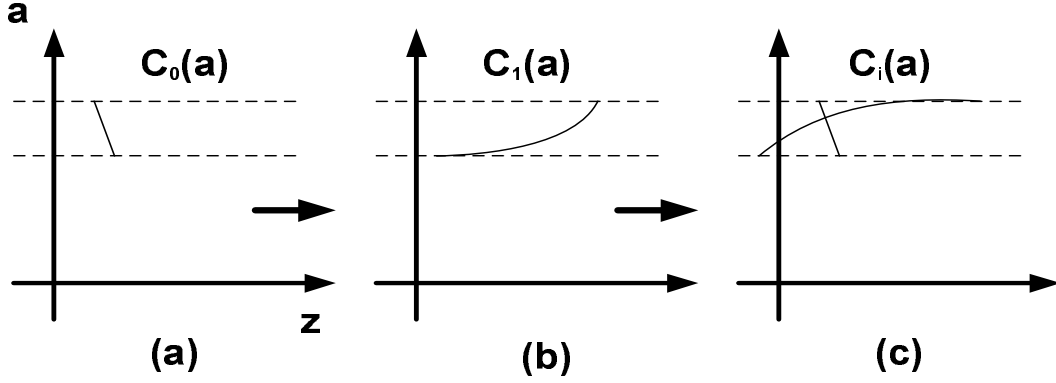


Figure 7: Iterations of critical curves.

(iii) (*Parameter transversality*) Let p_μ be the continuations of p_0 and W_μ^s , W_μ^u be the stable and unstable manifolds of p_μ , respectively. Then, as μ moves through $\mu = 0$, W_μ^u crosses W_μ^s transversally as shown in Fig. 8(b).

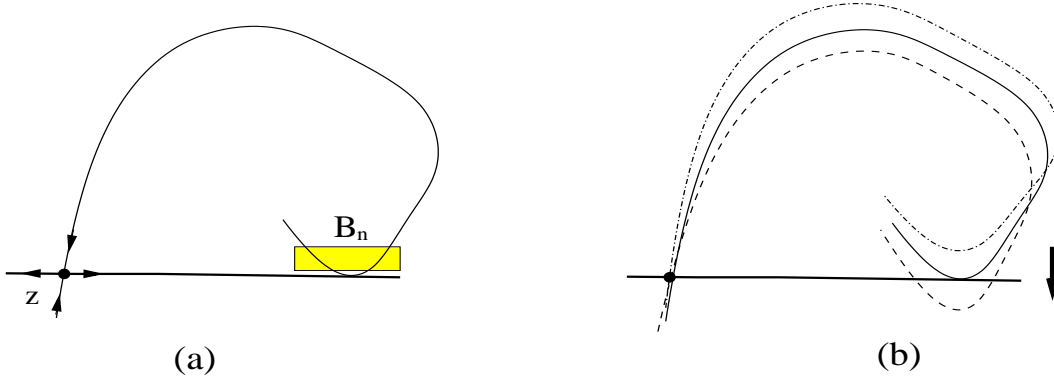


Figure 8: Homoclinic bifurcation.

The following² was observed by Newhouse [Newhouse, 1974; Palis & Takens, 1993].

(1) For every n sufficiently large, there exists an open region B_n (with $\text{diam}(B_n) \rightarrow 0$ as $n \rightarrow \infty$) close to the point of tangency and a range of parameters μ (also depending on n) such that $T_\mu^n(B_n) \subset B_n$ as depicted in Fig. 8(a).

(2) By a proper change of coordinates, $T_\mu^n : B_n \rightarrow B_n$ is transformed to become $\hat{T}_{a,b} : [-2, 2] \times [-2, 2] \rightarrow [-2, 2] \times [-2, 2]$ where $\hat{T}_{a,b}$ is written as

$$(x, y) \rightarrow (1 - ax^2 + y + bu, bv).$$

²These are Newhouse's infinitely many sinks associated with *homoclinic bifurcations*.

Here a, b are constants in μ, λ_i and n , and u, v are functions of (x, y) and μ, λ_i and n , the C^1 -norms of which are bounded from above by constants independent of n .

(3) $b \rightarrow 0$ as $n \rightarrow \infty$, and for every n that is sufficiently large, there exists a range of μ close to $\mu = 0$, such that the corresponding values of a for $\hat{T}_{a,b}$ covers the interval $[1, 2]$.

For any given b that is sufficiently small, it is a triviality to find values of $a \in [1, 2]$ so that $\hat{T}_{a,b}$ has a fixed point that is a sink. It then follows that, for every n that is sufficiently large, there exists μ_n so that $T_{\mu_n}^n$ admits a periodic sink of period n , and hence the existence of infinitely many sinks.

2.3.2 On the existence of tangles with no sinks

The plots of Scenario (b) look very different from those of the periodic sinks of Scenario (a), implicating a form of chaos that is observable. On the other hand, there remains, however unlikely, the possibility that a plot of Scenario (b) is part of a periodic sink of exceedingly long period, reducing the significance of Scenario (b) from an independent dynamical scenario to a particular case of Scenario (a). This possibility, unfortunately, can never be ruled out through numerical computations. It can only be partially ruled out through mathematical analysis. To argue that Scenario (b) is not that of a periodic sink, we would need to prove that the attractor admitting no periodic sinks is *observable* in both the parameter space and the phase space for $T_{a,b,L}$, a rather difficult mathematical task.

Let us start again with 1D maps and with an observation first made by Misiurewicz [1981]. Misiurewicz observed that, in order for a 1D map, such as $f = f_{a,L}$ of Eq. (2), to have no periodic sinks, it suffices that the forward orbits from $\mathcal{C}(f)$ stay a fixed distance away from $\mathcal{C}(f)$. Denoting $\mathcal{C}(f) = \{c^{(1)}, \dots, c^{(q)}\}$, this is to say that we have a $\delta_0 > 0$, so that $d(f^k(c^{(i)}), \mathcal{C}(f)) > \delta_0$ for all $k > 0$ and all $1 \leq i \leq q$. This is the so-called Misiurewicz condition.³

To find maps in a 1D family $\{f_a\}$ satisfying the Misiurewicz condition let us go back to Fig. 7 to study the evolutions of critical curves. For $f_{a,L}$ of Eq. (2), we have

Proposition 2.2 *There exists $L_0 > 2$, such that for all $L > L_0$, there exist values of parameter a such that (i) $f = f_{a,L}$ satisfies the Misiurewicz condition above, and (ii) there exists $\lambda > 0$ such that for almost every $\theta \in S^1$, $\limsup_{k \rightarrow \infty} \frac{1}{k} \ln |(f^k)'(\theta)| > \lambda$.*

Proposition 2.2(ii) rules out the possibility of periodic sinks for f .

Let us be aware that Proposition 2.2 does not mean nearly as much for Scenario (b) as its counterpart in Sec. 2.3.1 meant previously for Scenario (a). Sinks are persistent under small perturbations, and the existence of a periodic sink for one particular map implies the existence of periodic sinks for

³To be completely rigorous, there are other technical conditions imposed. See Sec. 3.2.

an open set of parameter of maps, hence the observability in the parameter space. This is not the case for maps satisfying the Misiurewicz condition. That is, the conclusions of Proposition 2.2 do not necessarily persist under small perturbations because the Misiurewicz condition is not an open condition maintainable in the parameter space. As a matter of fact, for a typical 1D family $\{f_a\}$, the set of parameter values fulfilling the Misiurewicz condition is of Lebesgue measure zero, therefore, it is not observable in the parameter space.

To find more parameters admitting no periodic sinks, it is natural for us to relax the Misiurewicz condition to allow critical orbits approaching $\mathcal{C}(f)$ in controlled manners. This has turned out to be an extremely sophisticated mathematical task over which long theories have been built, first by Jakobson on quadratic maps, then followed by many others [Benedicks & Carleson, 1985; Collet & Eckmann, 1983; Jakobson, 1981; Rychlik, 1988; Thieullen *et al.*, 1994; Wang & Young, 2006a]. In particular, by applying the theory in [Wang & Young, 2006a] to $f_{a,L}$ we obtain

Proposition 2.3 *There exists $L_0 > 2$, such that for all given $L > L_0$, there is a set Δ of positive Lebesgue measure for parameter a , such that for $a \in \Delta$ and $f = f_{a,L}$, there exists $\lambda > 0$ such that for almost every $\theta \in S^1$, $\lim_{k \rightarrow \infty} \frac{1}{k} \ln |(f^k)'(\theta)| > \lambda$.*

The claims of Proposition 2.3 are significantly different from those of Proposition 2.2. By asserting a good parameter set of positive Lebesgue measure, it establishes maps admitting no sinks as a dynamical scenario observable in the parameter space. The likes of Proposition 2.3 are commonly referred to as versions of the Jakobson's theory,⁴ the proofs of which are much harder than that of Proposition 2.2. For proofs of Propositions 2.2 and 2.3, see [Wang & Young, 2002a, 2006a].

To illustrate the differences between the parameter set satisfying Proposition 2.2 and that satisfying Proposition 2.3, let us first recall the construction of the $\frac{1}{3}$ -Cantor set. Starting from the unit interval $[0, 1]$, we first take away the middle third $(\frac{1}{3}, \frac{2}{3})$, then take away the middle third (of size $\frac{1}{9}$ now) again from each of the remaining intervals. We then proceed inductively, taking away the middle third of every interval left over from the previous step along the way. The set that survives all the deletions is the $\frac{1}{3}$ -Cantor set, which we denote as $K_{\frac{1}{3}} \subset [0, 1]$. $K_{\frac{1}{3}}$ is a closed subset of $[0, 1]$ that is nowhere dense (meaning that it contains no intervals), uncountable, and the Lebesgue measure of which is zero. The last clause follows because the sum of the lengths of all intervals we delete along the way totals to one. Note that the number $\frac{1}{3}$ in this construction is not particularly meaningful. Replacing it by any other positive $\varepsilon < 1$ will result in a new Cantor set K_ε and $m(K_\varepsilon) = 0$ for all $\varepsilon > 0$. This is to say that to make ε small would *not* help to increase the measure of K_ε from zero to positive.

⁴Here we are not distinguishing between the uni-modal and the multi-modal cases.

Let us now adopt the following adjustment in the construction of $K_{\frac{1}{3}}$: At step n , instead of deleting the middle $\frac{1}{3}$, we will delete the middle $\frac{1}{3^n}$ of the intervals left over from the earlier steps. Let us denote the set so obtained as $\hat{K}_{\frac{1}{3}}$. $\hat{K}_{\frac{1}{3}}$ remains a closed subset of $[0, 1]$ that is nowhere dense and uncountable. However, it is easy to check that $\hat{K}_{\frac{1}{3}}$ is now a set of positive measure. We call $\hat{K}_{\frac{1}{3}}$ a *fat* Cantor set. Again, in this construction the number $\frac{1}{3}$ is not important. We can use any positive $\varepsilon < 1$ in place of $\frac{1}{3}$ to construct a fat Cantor set \hat{K}_ε of non-zero Lebesgue measure.

With the critical curves evolving in the way as illustrated in Fig. 7, preventing the critical orbits from coming within a fixed distance of $\mathcal{C}(f)$ (the condition for the good parameters of Proposition 2.2) is like constructing a Cantor set K_ε for some ε small in the parameter space. To construct the good parameter set of Proposition 2.3, we allow the critical orbits to come back to $\mathcal{C}(f)$, but neither too close nor too soon. The good parameter set constructed this way is like constructing the fat Cantor set \hat{K}_ε as described in the last paragraph.

We now move to the studies of two dimensional maps. Again, the conclusions of Proposition 2.3 do not persist under small perturbations of a particular 1D map, and the geometric and dynamical structures of attractors of 2D maps $T_{a,b,L}$, $b \neq 0$, are much more complicated than those of the corresponding 1D maps.⁵ Nevertheless, a theory of two-dimensional maps, originally invented for the analysis of strongly dissipative Hénon maps by Benedicks & Carleson [1991], has been developed recently by Wang & Young [2001] into a form that is applicable to a class of maps including $T_{a,b,L}$. In Secs. 3-5 we will discuss the contents of this theory and its applications to certain systems of differential equations. For the moment let us state what we have for $T_{a,b,L}$, $b \neq 0$.

Proposition 2.4 *Let $T_{a,b,L}$ be as in Eq. (1). Then there exists $L_0 > 2$, such that for every $L > L_0$, there exists $b_0 > 0$ sufficiently small so that for all $0 < |b| < b_0$, there exists a set $\Delta_{b,L}$ of positive Lebesgue measure, such that for $a \in \Delta_{b,L}$, $T = T_{a,b,L}$ has a positive Lyapunov exponent for almost all $z \in M$.*

Propositions 2.3 and 2.4 are proved through the theory of rank one maps, which we will discuss in more detail in Sec. 3. For a map of Proposition 2.4, the attractor Λ contains no periodic sinks. Proposition 2.4 claims that attractors of this kind are *observable* in the parameter space.

Based on the conclusions of Proposition 2.4, we will, from this point on, adopt a point of view as follows:

- (1) the plots of Scenarios (a) and (b) are distinct;
- (2) Scenario (a) corresponds to attractors dominated by periodic sinks;
- (3) Scenario (b) corresponds to attractors with no periodic sinks;

⁵See Sec. 3.2 for a detailed description of the geometric and dynamical structures of the critical set for 2D maps.

- (4) a typical orbit of Scenario (b) has a positive Lyapunov exponent.

Remember that positive Lyapunov exponents are trademark for chaos.

We finish this discussion by cautioning that, as analysis requires, the constant b_0 that appears in Proposition 2.4 is exceedingly small. A theory admitting larger b_0 , say to include all $b < 10^{-2}$ would be much more favorable to the position we adopt here. Unfortunately, mathematical analysis has its own limitations and we are not quite there yet.

2.3.3 Observable invariant measures

Next, we try to identify the mathematical objects represented by the chaos structure revealed through the plots of Scenario (b). As we will see momentarily, these are the plots of SRB measures, specific kinds of Borel invariant measures that represent an existing *statistical law* in chaos. Let us start with some elementary measure theory.

A. Borel measures

Let M be a smooth surface compactly embedded in \mathbb{R}^n , m be the Lebesgue measure induced from the surface area. Let \mathcal{B} be the collection of all subsets of M that is m -measurable. \mathcal{B} is the *Borel algebra* for M .

We call a function μ from \mathcal{B} to \mathbb{R}^+ a *Borel measure* if

- (i) $\mu(\emptyset) = 0$, $0 < \mu(M) < \infty$ where \emptyset is the empty set, and
- (ii) for mutually disjoint $A_i \in \mathcal{B}$, $i = 1, \dots$, $\mu(\cup_i A_i) = \sum \mu(A_i)$.

The Lebesgue measure on M is a Borel measure. If the measure of the entire space equals one, then the measure is also called a *probability* measure.

For a given M in \mathbb{R}^n , there are infinitely many ways to define various Borel measures on M . For instances, let $M = [0, 1]$. We first take a finite set of points $P = \{p_1, \dots, p_n\}$ in $[0, 1]$, then define $\mu(A) = \frac{1}{n} \text{card}(A \cap P)$ where $\text{card}(A \cap P)$ is the number of points in $A \cap P$ for $A \in \mathcal{B}$. Measures defined this way are *atomic*, meaning that they are positively defined on isolated points.

We can also define Borel measures of a different kind. First let m be the Lebesgue measure on $[0, 1]$ and $\rho : [0, 1] \rightarrow \mathbb{R}^+$ be a Lebesgue measurable function satisfying $0 < \int_{[0,1]} \rho dm < \infty$, then $\mu : \mathcal{B} \rightarrow \mathbb{R}^+$ defined by

$$\mu(S) = \int_S \rho dm$$

for $S \in \mathcal{B}$ is a Borel measure. Observe that these Borel measures, defined by using density functions ρ , are non-atomic. In fact, for any given $S \in \mathcal{B}$ such that $m(S) = 0$ we have $\mu(S) = 0$.

In general, let μ, ν be two Borel measures defined on the same Borel algebra. We say that μ is *absolutely continuous* with respect to ν if $\nu(A) = 0$ implies $\mu(A) = 0$. For the Borel measures defined on $[0, 1]$ above, the first kind is atomic and the second kind is non-atomic and is absolutely continuous with respect to Lebesgue.

B. Invariant measures and ergodicity

Let T be a smooth mapping from M to M . With regards to T and the various Borel measures on M , there are two conceptually different ways to proceed. The first is to fix a Borel measure μ that is predominately important, such as the Lebesgue measure m induced from a surface area, and study the properties of T with respect to such pre-fixed μ . The second is to find particular Borel measures that are most interesting and suitable for the studies of a given T . Here we emphasize more on the second approach.

A Borel measure μ is an *invariant measure* for T if $\mu(T^{-1}A) = \mu(A)$ for all $A \in \mathcal{B}$. Let μ be an invariant measure for T . μ is an *ergodic* measure for T if all invariant subsets for T are either of full μ -measure or of null μ -measure. Recall that $A \in \mathcal{B}$ is an *invariant subset* for T if $T^{-1}A = A$.

For $S \in \mathcal{B}$ let \mathcal{X}_S be the characteristic function of S defined as follows:

$$\mathcal{X}_S(x) = \begin{cases} 1, & \text{if } x \in S \\ 0, & \text{otherwise} \end{cases}$$

For any given $x \in M$, let

$$I_{S,n}(x) = \frac{1}{n} \sum_{k=0}^{n-1} \mathcal{X}_S(T^k(x)); \quad I_S(x) = \lim_{n \rightarrow \infty} I_{S,n}(x).$$

$I_{S,n}(x)$ is the percentage of the first n points along the orbit starting from x that fall in S and $I_S(x)$ is the limit of this percentage. In general, $I_S(x)$ as a limit does not necessarily exist. It does, however, for μ -almost every $x \in M$ if μ is an ergodic invariant measure for T .

Theorem (Birkhoff's Ergodic Theorem) *Let μ be an ergodic invariant measure for $T : M \rightarrow M$. Then for all $S \in \mathcal{B}$ and for μ -almost every point $x \in M$,*

$$\lim_{n \rightarrow \infty} \frac{1}{n} \sum_{i=0}^{n-1} \mathcal{X}_S(T^i(x)) = \frac{\mu(S)}{\mu(M)}. \quad (3)$$

Birkhoff's Ergodic Theorem [Katok & Hasselblatt, 1995] claims that the space distributions of points of individual trajectories starting from μ -almost every point in M are dictated by μ .

Let us be aware that the amount of information held by an ergodic invariant measure μ about T through Birkhoff's Ergodic Theorem could be minimal. For instance, let $P = \{p_1, \dots, p_n\}$ be a periodic orbit of period n . Then the atomic Borel measure μ supported on P by using $\mu(p_i) = \frac{1}{n}$ is an ergodic invariant measure. With respect to this invariant Borel measure, P is a set of full measure and consequently, Birkhoff's Ergodic Theorem claims that all orbits starting from P are dictated by μ , a completely trivial statement. Invariant measures absolutely continuous with respect to the Lebesgue measure on M are usually much more meaningful. They are supported on m -positive sets, therefore, are at the very least *observable* based on Birkhoff's Ergodic Theorem.

D. Invariant measures and observability

Let us now shift our attention from the support⁶ of μ to its surroundings. Let μ be an invariant measure for T and $x \in M$, not necessarily in the support of μ . We want to figure out an appropriate way to say that the orbit of x is dictated by μ . A naive try would be to copy the conclusions of Birkhoff's Ergodic Theory to say that the orbit of x is dictated by μ if $I_S(x) = \frac{\mu(S)}{\mu(M)}$ for all $S \in \mathcal{B}$. This would be, unfortunately, a bad definition. Let μ be the atomic invariant measure supported on a periodic sink $P = \{p_1, \dots, p_n\}$, and $x \in M$ be sufficiently close to p_1 . The orbit of x is attracted to the periodic orbit of p_1 , and it ought to be obvious that we have every intention to claim that the orbit of x is dictated by μ . The definition proposed above, however, would fail such a claim.

A good definition is as follows: Let $x \in M$ be a starting point, and μ be an invariant measure for T . We say that the space distribution of the points of the orbit starting from x is dictated by μ , or in short, we say that x is *generic* with respect to μ , if for all *continuous* functions $\phi : M \rightarrow \mathbb{R}$,

$$\lim_{n \rightarrow \infty} \frac{1}{n} \sum_{k=0}^{n-1} \phi(T^k(x)) = \frac{1}{\mu(M)} \int_M \phi(x) d\mu. \quad (4)$$

We note that Eq. (3) implies Eq. (4) but the reverse is not true. By replacing the characteristic functions in Eq. (3) with continuous ones, we are now allowed to reach the part of the phase space that is out of the support of μ . This definition will serve us well.

Let m be the Lebesgue measure on M . We say that an ergodic invariant measure μ for $T : M \rightarrow M$ is *observable* if there exists a subset S that is m -positive such that every $x \in S$ is generic with respect to μ . According to Birkhoff's Ergodic Theorem, any ergodic invariant measure μ that is absolutely continuous with respect to m is observable. Any periodic sink would define an observable atomic ergodic invariant measure. On the other hand, atomic measures defined by hyperbolic periodic orbits are in general not observable.

Let us now return to the numerical plots of Sec. 2.2. The plots of Scenario (a) are clearly those of observable atomic ergodic invariant measures representing periodic sinks. The plots of Scenario (b), as we will see momentarily, are the plots of SRB measures, a specific kind of non-atomic invariant measures that dictate the space distributions of points of individual trajectories for at the very least an observable collection of chaotic orbits in M .

E. Absolutely continuous invariant measures for 1D maps

To better understand the plots of Scenario (b), let us take a closer look at the corresponding results of the numerical computations. We start with $f_a = f_{a,L}$. Figure 9(b) is again a case of random evolution of θ_k against time k , and Fig. 9(c) is its frequency spectrum. This is for $L = 2$, $a = 0.6$. The *distribution*

⁶The support $\text{supp}(\mu)$ of a probability measure μ is defined to be the smallest closed set S such that $\mu(S) = 1$.

of the points (histogram) on the orbit is shown in Fig. 9(a) which is obtained as follows: First, we divide $[0, 1]$ for θ into subintervals of $D_j = [\frac{j}{1000}, \frac{j+1}{1000}]$, $0 \leq j \leq 999$. Then we compute the percentages of points of the plotted orbit that fall in each of the subintervals out of the total number of points plotted. The percentage for D_j we denote as μ_j . Let $\rho(\theta) = \sum \mu_j \chi_{D_j}(\theta)$. The graph of $\rho : S^1 \rightarrow [0, 1]$ is then plotted as shown in Fig. 9(a).

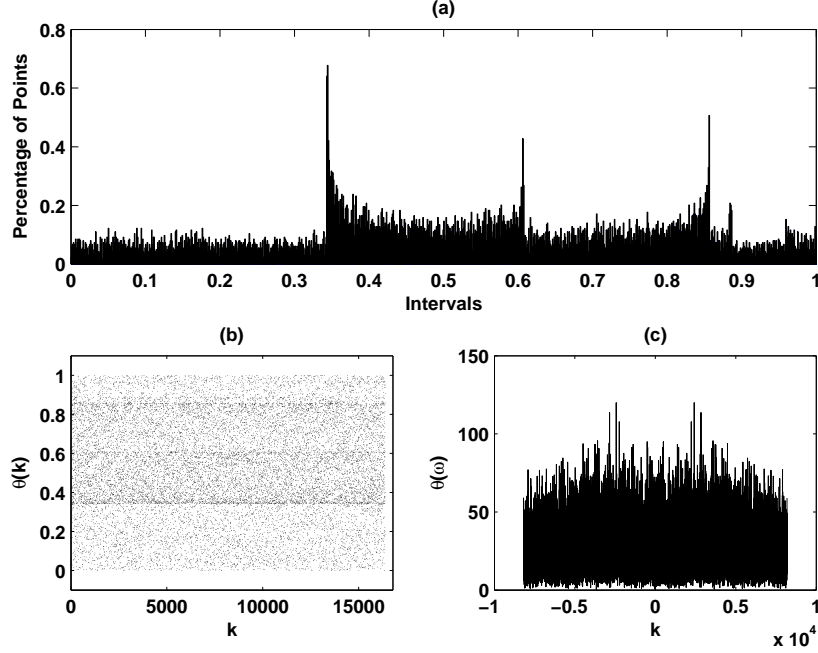


Figure 9: An example of Scenario (b) for 1D maps ($N = 2^{14}$). (a) Histogram for θ_k . (b) Time evolution of θ_k . (c) Frequency spectrum of θ_k .

Next we compute the same histogram using orbits of length up to $k = 2^{15}$ and 2^{16} . These are shown in Figs. 10(a) and 11(a), respectively. The graphs for the distribution are roughly the same. Using different initial values also produce roughly the same plots. These computations hint at the existence of an observable non-atomic ergodic invariant measure for the map plotted. This is indeed proved to be the case, at least for the good maps of Proposition 2.3. We have

Proposition 2.5 *For the good parameters Δ of Proposition 2.3, and for any given $a \in \Delta$, f_a admits an invariant probabilistic measure that is absolutely continuous with respect to Lesbeque.*

For a proof of Proposition 2.5, see [Wang & Young, 2002a].

F. SRB measure for 2D maps

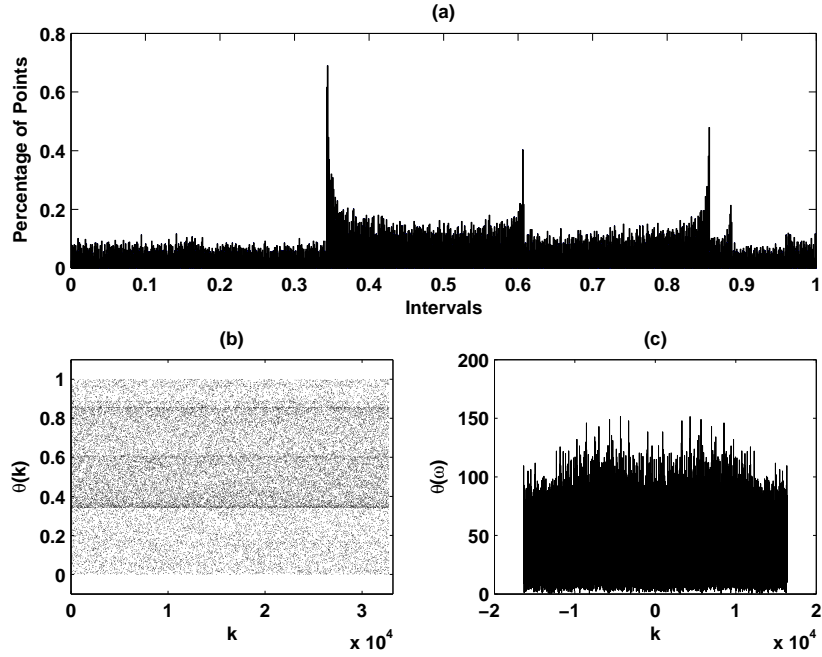


Figure 10: An example of Scenario (b) for 1D maps ($N = 2^{15}$). (a) Histogram for θ_k . (b) Time evolution of θ_k . (c) Frequency spectrum of θ_k .

Let us now consider Scenario (b) for 2D maps $T_{a,b,L} : M \rightarrow M$. The numerical plots again point towards a non-atomic invariant measure μ for T . However, unlike the case of 1D, such invariant measures are *not* absolutely continuous with respect to the Lebesgue measure on M . This is because Λ , the attractor that supports μ , is a set of zero Lebesgue measure in M .

To better comprehend the nature of this new non-atomic invariant measure, let us take a closer look at the plot of Fig. 5(a). It appears that the strongly dissipative nature of T crashes M into Λ along the radial direction, and the absolute continuity of the plotted measure with respect to the Lebesgue measures is preserved only in the angular direction by the expanding nature of $f_{a,L}$ in θ . As a rigorously defined mathematical object, the likes of such invariant measures, crashed in the contractive direction but remaining absolutely continuous with respect to the Lebesgue measures in the directions of expansion, were formally introduced by Sinai, Ruelle and Bowen originally in their studies of axiom A systems [Bowen, 1975; Ruelle, 1976; Sinai, 1972]. These are the so-called *SRB measures*. The development of the theory of SRB measures has had a great impact on the studies of dynamical systems of non-uniform expansions with far reaching consequences. It has provided a critical element for the ergodic theory to become actively involved in the studies of maps such as $T_{a,b,L}$, leading to deeper understandings of the geometric and dynamical properties of certain chaotic attractors.

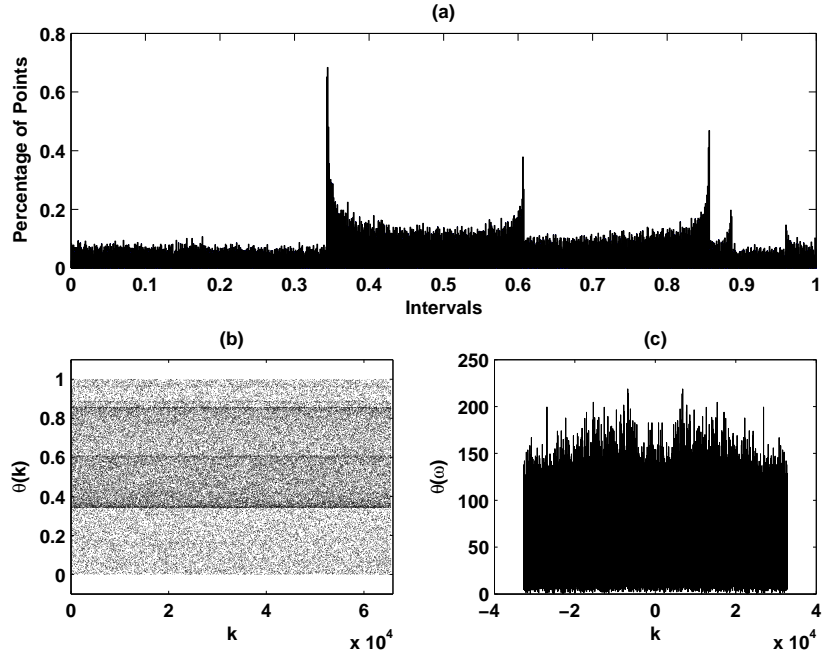


Figure 11: An example of Scenario (b) for 1D maps ($N = 2^{16}$). (a) Histogram for θ_k . (b) Time evolution of θ_k . (c) Frequency spectrum of θ_k .

A formal definition is as follows: A T -invariant Borel measure μ is called an **SRB measure** if

- (i) T has a positive Lyapunov exponent μ -a.e.;
- (ii) the conditional measures of μ on unstable manifolds are absolutely continuous with respect to the Lebesgue measures on these leaves.

Note that (i) requires that μ is supported by a collection of orbits that are chaotic in nature. It is also proved that, in general, the set of points that are generic with respect to an SRB measure is always m -positive, therefore SRB measures are observable.⁷ This last property makes an SRB measure non-ignorable in simulations.

Unfortunately, more sophisticated knowledge from the abstract measure theory and the ergodic theory would be required for further expositions. We refer the more mathematically oriented reader to, for instance, [Young, 1995, 2002], for further reading of the subject. Again, what matters the most for us here about SRB measures is as follows: First, SRB measures are observable objects corresponding to the plots of Scenario (b) in Sec. 2.2 for $T_{a,b,L}$. Second, for a map T admitting chaotic attractors such as those of ours, an SRB measure

⁷This does not follow from Birkhoff's Ergodic Theory because the support of an SRB measure is in general a null m -measure set.

as a dynamical object controls the space distribution of points of individual trajectories from an observable set in the basin of attraction $B(\Lambda)$.

Let us finish this paragraph by a proposition that claims that SRB measures are observable for $T_{a,b,L}$ in both the parameter and the phase spaces. Recall that $U = \{(\theta, r), |r| < 1\}$ is the trapping region.

Proposition 2.6 *For the good parameters of Proposition 2.4, (i) $T = T_{a,b,L}$ admits a unique ergodic SRB measure μ such that $0 < \mu(U) < \infty$; and (ii) Lesbegue almost every point $z \in U$, is generic with respect to μ .*

For a proof of Proposition 2.6, see [Wang & Young, 2001].

Summary: The plots of Sec. 2.2 for both Scenarios (a) and (b) are invariant measures that control the space distribution of individual trajectories for at least an observable set of orbits in the basin of attraction for Λ . For Scenario (a), the invariant measure is atomic, representing a periodic sink. For Scenario (b), it is an SRB measure representing an existing *statistical law* for chaos.

3 A Theory on Rank One Chaos

Various theories of dynamics, including the theories of horseshoes and homoclinic tangles, Newhouse sinks, observable chaos (attractors with no sinks), and SRB measures, are introduced in Sec. 2 to explain the simulation results of Sec. 2.2 for $T_{a,b,L}$. However, propositions for one particular family of maps, such as the ones presented in Sec. 2.3 for $T_{a,b,L}$, are not suitable for applications,⁸ for it is not likely for a real world problem to assume the particular formulas of $T_{a,b,L}$. In this section we introduce a detailed formulation of rank one maps following the work of Wang & Young [2001, 2006a,b], aiming at providing a general framework for applications. A version of Proposition 2.3 for non-uniformly expanding 1D maps is presented in Sec. 3.2 and the work of Wang & Young [2001, 2002b] on rank one chaos is discussed in Sec. 3.3. Note that as specific cases, Propositions 2.3-2.6 are proved through applications of the theorems presented in this section.

3.1 A brief introduction

Let us start with uniformly hyperbolic systems. Assume that M is two-dimensional. Let $T : M \rightarrow M$ be a C^1 diffeomorphism and $\Lambda \subset M$ be T -invariant. We say that Λ is *uniformly hyperbolic* if

- (a) over every point of Λ , there is a well-defined direction in which Λ is *expanding* and there is also another well-defined direction in which Λ is *contracting* under the iterations of T ;
- (b) to make these directions coherent, it is also required that they vary continuously on the entire Λ .

For instance, the horseshoes of Sec. 2.1, including those of Proposition 2.1, are uniformly hyperbolic; the expanding direction for Λ is roughly horizontal and the contracting direction is roughly vertical. This concept can be generalized naturally to the maps of higher dimensions. Chaos associated with uniform hyperbolicity is of relatively simple geometric structure, and the dynamical properties of these systems are well-understood.

A simple and illuminating example of a uniformly hyperbolic attractor is the *axiom A solenoid*. As shown in Fig. 12, let us start with a solenoid S . We perform the following surgery: first, we cut the solenoid open and regard it as a cylinder, then we stretch the cylinder to make it at least twice as long, and compress it to make it very thin. We then put the resulting object back into the original solenoid, wrapping it twice around (again, see Fig. 12). Regarding this surgical process as a mapping T , we obtain a uniformly hyperbolic attractor $\Lambda = \cap_{n \geq 1} T^n(S)$.

⁸This had been in fact a hurdle. For a long time theories were developed exclusively for not exactly $T_{a,b,L}$ in Sec. 2, but the Hénon family and their perturbations [Benedicks & Carleson, 1991; Benedicks & Young, 1993; Mora & Viana, 1993], therefore remained in a form that is much less likely to attract attention from the world of real applications.

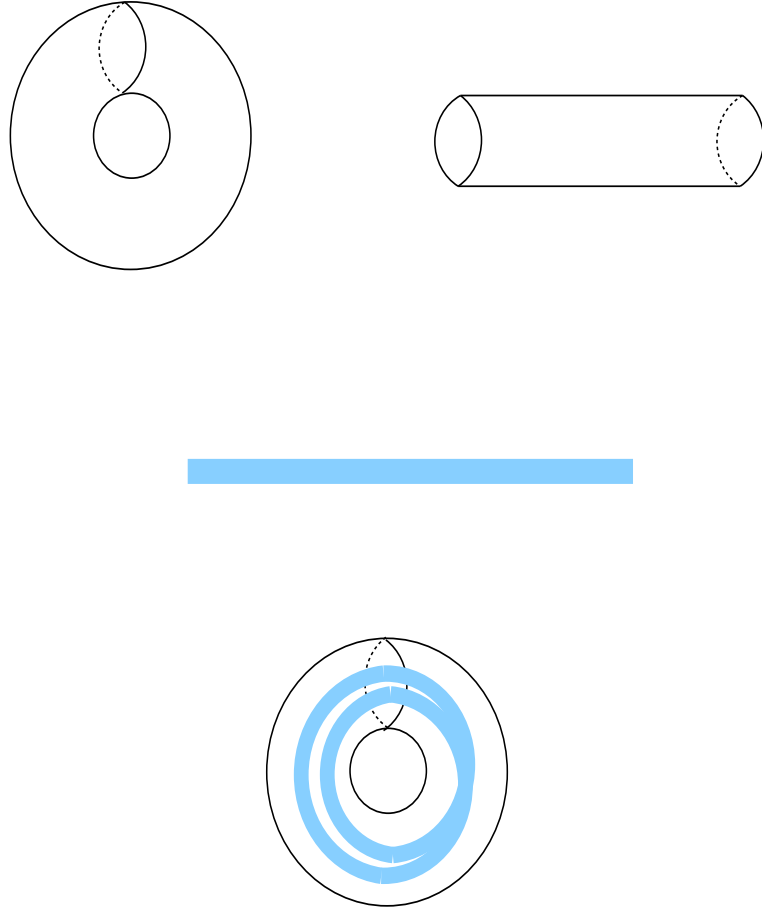


Figure 12: Axiom A Solenoid.

The attractors in real applications, unfortunately, are rarely uniformly hyperbolic. One of the mechanisms for non-hyperbolic behavior, on which we will focus in the rest of this paper, is due to the confusions of the expanding and contracting directions. To provide an example, we modify the construction of the axiom A solenoid by allowing movements in both clockwise and counter-clockwise directions while we wrap the thin tube around. This is depicted in Fig. 13. The changes in the wrapping direction create *turns* at which the expanding and the contracting directions are confused. The maps $T_{a,b,L}$ of Sec. 2 are like the solenoid of Fig. 13, with the critical points of $f_{a,L}$ serving as the “turning points” in wrapping. Rank one maps, which we will soon introduce in Sec. 3.3, model precisely the non-uniformly hyperbolic maps of this kind.

For systems that are uniformly hyperbolic, we have positive Lyapunov exponent everywhere by definition, and the existence of *SRB* measures is proved by Sinai, Ruelle and Bowen [Bowen, 1975; Ruelle, 1976; Sinai, 1972]. For systems that are not uniformly hyperbolic, sinks are allowed to appear, and the existence of positive Lyapunov exponents becomes questionable. Systems such as

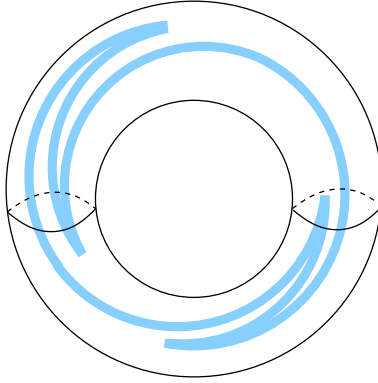


Figure 13: Non-axiom A solenoid.

those depicted in Fig. 13 are exceedingly complicated and notoriously difficult to analyze. Coherent mathematical statements for these systems are subtle, and their proofs are hard to build. The theory we present in this section has come a long way. It originated from Jacobson's theory on quadratic maps [Jakobson, 1981] and the theory of Benedicks and Carleson on strongly dissipative Hénon maps [Benedicks & Carleson, 1991]. Our main objectives here are to properly motivate, and to formally introduce the conclusions of this theory to the reader. Rigorous proofs are out of the scope of this presentation.

3.2 Non-uniformly expanding 1D maps

In this subsection we study the iterations of 1D maps with *critical points*, presenting a theory of non-uniformly expanding 1D maps following primarily Wang & Young [2006a]. Admissible non-uniformly expanding 1D families are introduced in Sec. 3.2.1. This is a setting that takes $f_{a,L}$ in Sec. 2 as a particular case. Propositions parallel to those of Sec. 2 for $f_{a,L}$ are presented in Sec. 3.2.2.

3.2.1 Admissible family of non-uniformly expanding 1D maps

A. Misiurewicz maps. Let I be either an interval or a circle. For $f \in C^2(I, I)$, let $\mathcal{C} = \mathcal{C}(f) = \{x \in I : f'(x) = 0\}$ denote the critical set of f , and let \mathcal{C}_δ denote the δ -neighborhood of \mathcal{C} in I . For $x \in I$, let $d(x, \mathcal{C}) := \min_{\hat{x} \in \mathcal{C}} |x - \hat{x}|$.

Following Wang & Young [2006a], we adopt a definition for Misiurewicz maps that is a little tedious to state but easier to verify in applications. Conceptually they are 1D maps with the following characteristics:

- (a) the critical orbits (orbits of $x \in \mathcal{C}$) stay a fixed distance away from the critical set, and
- (b) the phase space is divided into two regions, \mathcal{C}_{δ_0} (the δ_0 -neighborhood of the critical set \mathcal{C}) and $I \setminus \mathcal{C}_{\delta_0}$; and (i) on $I \setminus \mathcal{C}_{\delta_0}$, f is uniformly expanding;

(ii) for $x \in \mathcal{C}_{\delta_0} \setminus \mathcal{C}$, even though $|f'(x)|$ is small, the orbit of x does not return to \mathcal{C}_{δ_0} again until its derivative has regained a definite amount of exponential growth.

The precise definition is as follows:

Definition 3.1 We say $f \in C^2(I, I)$ is a Misiurewicz map, denoting $f \in \mathcal{M}$, if the following holds for some $\delta_0 > 0$:

- (a) Outside of \mathcal{C}_{δ_0} : there exist $\lambda_0 > 0, M_0 \in \mathbb{Z}^+$ and $0 < c_0 \leq 1$ such that
 - (i) for all $n \geq M_0$, if $x, f(x), \dots, f^{n-1}(x) \notin \mathcal{C}_{\delta_0}$, then $|(f^n)'(x)| \geq e^{\lambda_0 n}$;
 - (ii) if $x, f(x), \dots, f^{n-1}(x) \notin \mathcal{C}_{\delta_0}$ and $f^n(x) \in \mathcal{C}_{\delta_0}$, for any n , then $|(f^n)'(x)| \geq c_0 e^{\lambda_0 n}$.
- (b) Inside \mathcal{C}_{δ_0} : (i) $f''(x) \neq 0$ for all $x \in \mathcal{C}_{\delta_0}$;
- (ii) for all $\hat{x} \in \mathcal{C}$ and $n > 0$, $d(f^n(\hat{x}), \mathcal{C}) \geq \delta_0$;
- (iii) for all $x \in \mathcal{C}_{\delta_0} \setminus \mathcal{C}$, there exists $p_0(x) > 0$ such that $f^j(x) \notin \mathcal{C}_{\delta_0}$ for all $j < p_0(x)$ and $|(f^{p_0(x)})'(x)| \geq c_0^{-1} e^{\frac{1}{3}\lambda_0 p_0(x)}$.

Condition (a) in Definition 3.1 says that on $I \setminus \mathcal{C}_{\delta_0}$, f is essentially uniformly expanding. (b)(ii) says that for $x \in \mathcal{C}_{\delta_0} \setminus \mathcal{C}$, if n is the first return time of $x \in \mathcal{C}_{\delta_0}$ to \mathcal{C}_{δ_0} , then $|(f^n)'(x)| \geq e^{\frac{1}{3}\lambda_0 n}$. (To see this, use (b)(ii) followed by (a)(ii)).

Claim 2.1 Let $f \in C^3(I, I)$ be such that

- (i) $S_f(x) < 0$ where $S_f(x)$ denotes the Schwarzian derivative of f ,⁹
- (ii) $f''(\hat{x}) \neq 0$ for all $\hat{x} \in \mathcal{C}$,
- (iii) if $f^n(x) = x$, then $|(f^n)'(x)| > 1$, and
- (iv) for all $\hat{x} \in \mathcal{C}$, $\inf_{n>0} d(f^n(\hat{x}), \mathcal{C}) > 0$.

Then $f \in \mathcal{M}$.¹⁰

Claim 2.2 Let $f_{a,L} : S^1 \rightarrow S^1$ be given by

$$f_{a,L}(\theta) = \theta + a + L\Phi(\theta)$$

where $a, L \in \mathbb{R}$ and $\Phi : S^1 \rightarrow S^1$ is a Morse function¹¹ (the right side is mod 1). Then there exists $L_0 > 0$ such that for all $L \geq L_0$, there exists an $\mathcal{O}(\frac{1}{L})$ -dense set of a for which $f_{a,L} \in \mathcal{M}$.

Claim 2.2 is an important technical proposition for us in applying the theory of rank one maps in Sec. 3.3 to the family $T_{a,b,L}$ of Sec. 2 and the other systems of applications in Secs. 4 and 5. We refer the more technically oriented reader to [Wang & Young, 2002a, Lemma 5.3] for a proof. $f_{a,L}$ in Sec. 2 is a special case of Claim 2.2 for which $\Phi(\theta) = \sin 2\pi\theta$.

B. Admissible family of 1D maps. We continue to introduce admissible families following [Wang & Young, 2006a]. Assume that $F(x, a) : I \times (a_1, a_2) \mapsto I$ is

⁹Recall that $S_f(x) = \frac{f'''(x)f'(x) - \frac{3}{2}f''(x)^2}{f'(x)^2}$.

¹⁰(i)-(iv) are the properties used traditionally in defining Misiurewicz maps, among which (iii) is not directly checkable and (i) is often not fulfilled in applications.

¹¹ $\Phi(\theta)$ is a Morse function if it is C^2 and all its critical points are non-degenerate.

C^2 and let $\{f_a \in C^2(I, I) : a \in (a_1, a_2)\}$ be the one-parameter family of one-dimensional maps defined through $f_a(x) := F(x, a)$. We say that f_a is an admissible family if it satisfies two conditions. The first is that it contains a Misiurewicz map f_{a^*} . The second compares the movement of critical points and critical orbits of f_a with respect to parameter a at a^* . This one is a little long to state.

To be more precise, first we assume that there exists $a^* \in (a_1, a_2)$ such that f_{a^*} is a Misiurewicz map satisfying Definition 3.1. We define the continuations of critical points as follows: For every $c \in \mathcal{C}(f_{a^*})$, continuations $c(a) \in \mathcal{C}(f_a)$ satisfying $c(a^*) = c$ is well-defined around a^* following Definition 3.1(1)(a). Let $\mathcal{C}(f_{a^*}) = \{c^{(1)}(a^*) < \dots < c^{(q)}(a^*)\}$ be the critical set for f_{a^*} . Continuation of $c^{(i)}(a^*)$ is denoted as $c^{(i)}(a)$.

Next we define the continuations of critical orbits. For $c^{(i)}(a^*) \in \mathcal{C}(f_{a^*})$, denote $\xi(a^*) = f_{a^*}^{(i)}(c^{(i)}(a^*))$. Then for all a that is sufficiently close to a^* , there exists $\xi(a)$, a unique continuation of $\xi(a^*)$, such that the orbits $\{f_{a^*}^n(\xi(a^*))\}_{n \geq 0}$ and $\{f_a^n(\xi(a))\}_{n \geq 0}$ have the *same itineraries*, by which we mean that, for any given $n \geq 0$, if $f_{a^*}^n(\xi(a^*)) \in (c^{(j)}(a^*), c^{(j+1)}(a^*))$ then $f_a^n(\xi(a)) \in (c^{(j)}(a), c^{(j+1)}(a))$.¹² Furthermore, $a \mapsto \xi(a)$ is differentiable (this is proved in Sec. 4.2 of [Wang & Young, 2006a]). Note that $\xi(a)$ is not to be confused with $f_a(c^{(i)}(a))$.

Definition 3.2 *Let $F(x, a) : I \times (a_1, a_2) \mapsto I$ be C^2 , and $\{f_a\}$ be such that $f_a(x) := F(x, a)$. We say that $\{f_a\}$ is an admissible family if the following holds:*

- (a) *There exists $a^* \in (a_1, a_2)$ such that $f_{a^*} \in \mathcal{M}$ is a Misiurewicz map.*
- (b) *Let $c(a)$ and $\xi(a)$ be continuations of $c(a^*) \in \mathcal{C}(f_{a^*})$ and $\xi(a^*) = f_{a^*}(c(a^*))$;*

$$\frac{d}{da} f_a(c(a)) \neq \frac{d}{da} \xi(a) \quad \text{at } a = a^*.$$

It is also proved in [Wang & Young, 2002a] that Definition 3.2(b) holds for $f_{a,L}$ in Claim 2.2. So under the assumption that $L > L_0$ is sufficiently large, $f_{a,L}$ of Claim 2.2 is an admissible family. In particular, this applies to $f_{a,L}$ in Sec. 2.

Admissible families are defined by abstract conditions that are in principle checkable. Through these definitions we hope to build a dynamical theory that is flexible enough to be applied to certain systems of ordinary differential equations.

3.2.2 Dynamical theories on admissible 1D family

Let $f_a, a \in (a_1, a_2)$ be an admissible 1D family, and $f_{a^*} \in \mathcal{M}$ for some $a^* \in (a_1, a_2)$. First we claim that there are many parameters of periodic sinks around

¹²The end of I in the interval case is denoted as $c^{(0)}$ and $c^{(q+1)}$. If I is a circle, then we use the cyclic convention $c^{(1)}(a) < \dots < c^{(q)}(a) < c^{(q+1)}(a) := c^{(1)}(a)$.

a^* . To prove this claim we argue along the lines of the first part of Sec. 2.3.1, iterating critical curves as shown in Fig. 7. Using the notations of Sec. 2.3.1, the critical curves $c_n(a)$, defined inductively by $c_n(a) = f_a(c_{n-1}(a))$, satisfying

$$\begin{aligned} \frac{d}{da}c_n(a) &= \frac{\partial F(c_{n-1}(a), a)}{\partial c_{n-1}(a)} \frac{d}{da}c_{n-1}(a) + \frac{\partial F(c_{n-1}(a), a)}{\partial a} \\ &= f'_a(c_{n-1}(a)) \frac{d}{da}c_{n-1}(a) + \partial_a f_a(c_{n-1}(a)). \end{aligned} \quad (5)$$

Observe that $|\partial_a f_a|$ is uniformly bounded, therefore negligible provided that $|\frac{d}{da}c_n(a)|$ is sufficiently large, a condition guaranteed to hold for some large n through Definition 3.2(b).¹³ It then follows that, under the assumption that the critical curves stay out of \mathcal{C}_{δ_0} ,

$$\frac{d}{da}c_n \sim (f_a^n)'(c_1(a))$$

grows exponentially in magnitude according to the assumptions of Definition 3.1(a). Consequently, with $c_n(a^*)$ staying out of \mathcal{C}_{δ_0} , the critical curve would cross \mathcal{C}_{δ_0} repeatedly, creating parameters which admit periodic sinks. Since periodic sinks persist under small perturbations, they are observable in both the parameter and the phase spaces.

Along the same lines of thinking, next we construct the set of parameter $a \in (a_1, a_2)$ for which f_a satisfies Definition 3.1(b)(ii), a necessary condition for f_a to be a Misiuriewicz map. To simplify the situation let us for the moment deal only with maps of one critical point (the uni-modal case). We iterate the critical curves forward in time, deleting the part that is over \mathcal{C}_{δ_0} along the way. The deletions would chop the critical curves into small pieces, each of which we iterate forward. Clearly, parameters surviving all deletions are those satisfying Definition 3.1(b)(ii) in (a_1, a_2) . Excluding the deleted pieces on (a_1, a_2) along the way, we would construct in (a_1, a_2) a parameter set that appears very similar to a Cantor set with, say, a fixed proportion of deletions.

To obtain a correspondence of Proposition 2.3, that is, to construct a parameter set of *positive* Lebesgue measure admitting no periodic sinks, we again follow the same lines of thinking, iterating critical curves forward in time. We, however, relax the rule of deletion as follows: Instead of deleting the critical curves over \mathcal{C}_{δ_0} , we delete those over \mathcal{C}_{δ_n} where $\delta_n = \min\{\delta_0, e^{-\alpha n}\}$ for some $\alpha > 0$. By exponentially shrinking the proportions of deletion, we end up constructing a fat Cantor set of positive measure. These parameters are the ones admitting no periodic sinks.

Let us caution that, in reality, the construction of the indicated fat Cantor set of parameters is not as easy as it sounds in this brief outline. By allowing critical orbits to come back close to the critical set, we risk the much needed expansions of critical curves, and the potential losses of derivatives at close returns to $\mathcal{C}(f)$ need to be controlled with caution (the issue of derivative

¹³This is the purpose of this rather technical assumption.

recovery). The mappings from $c_n(a)$ to $c_{n+1}(a)$ are obviously not linear so the proportion of deletions on (a_1, a_2) is not exactly the same as the proportion of deletions on $c_{n+1}(a)$. This nonlinearity also needs to be carefully maintained along the way of iterations (distortion estimates). These issues are carefully settled for maps of one critical point primarily through the work of Jakobson [1981] and Benedicks & Carleson [1985]. Allowing more than one critical point would introduce additional complexities in the construction of good parameters. For a complete treatment of this issue, see [Wang & Young, 2006a].

Let us end this discussion by stating in precise terms the primary results of [Wang & Young, 2006a] for a given admissible family of 1D maps.

Proposition 3.1 *Let $f_a, a \in (a_1, a_2)$ be an admissible family of 1D maps satisfying Definition 3.2. Then there is a positive measure set $\Delta \subset (a_1, a_2)$, such that for all $a \in \Delta$, $f = f_a$ satisfies the following: Let $\mathcal{C}(f) = \{x : f'(x) = 0\}$ be the critical set, then for all $\hat{x} \in \mathcal{C}(f)$,*

- (a) $d(f^n(\hat{x}), \mathcal{C}(f)) > \min\{\delta_0, e^{-\alpha n}\}$ for all $n \geq 1$; and
- (b) $(f^n)'(f(\hat{x})) > ce^{\lambda n}$ for some $c, \lambda > 0$ for all $n \geq 1$.

We also have

Proposition 3.2 *Let $\{f_a\}$ and Δ be the same as in Proposition 3.1. Then, for $f = f_a, a \in \Delta$,*

- (a) *there exists $\lambda > 0$ such that for almost all $x \in I$, $\limsup_{n \rightarrow \infty} \frac{1}{n} \ln |(f^n)'(x)| > \lambda$;*
- (b) *f admits an invariant measure that is absolutely continuous with respect to Lebesgue.*

Propositions 3.1 and 3.2 together are sufficient to make maps without periodic sinks an observable dynamical scenario in both the parameter and the phase spaces. By the fact that $f_{a,L}$ of Claim 2.2 is admissible, which is proved in [Wang & Young, 2002a], Propositions 2.2, 2.3 and 2.5 follow from Propositions 3.1 and 3.2.

3.3 A theory of rank one chaos

Let $M = I \times [-1, 1]$ where I is either an interval or a circle, $\Delta_0 = (a_1, a_2) \times (0, b_1)$ and let $T_{a,b} : M \rightarrow M, (a, b) \in \Delta_0$ be a two-parameter family of 2D maps. Let us assume that $T_{a,b}$ assumes the general form

$$T_{a,b} : \begin{pmatrix} x \\ y \end{pmatrix} \mapsto \begin{pmatrix} F(x, y, a) + b u(x, y, a, b) \\ b v(x, y, a, b) \end{pmatrix}. \quad (6)$$

We also assume that

- (C1) For any given $(a, b) \in \Delta_0$, $T_{a,b}$ is a diffeomorphism from M to its image; and as functions in (x, y, a) , the C^3 -norms of $F(x, y, a)$, $u(x, y, a, b)$ and $v(x, y, a, b)$ are uniformly bounded.

- (C2) Let $f_a := F(x, 0, a)$. $\{f_a\}, a \in (a_1, a_2)$ is an admissible family of 1D maps satisfying Definition 3.2.
- (C3) Let $f_{a^*}, a^* \in (a_1, a_2)$ be a Misiurewicz map of Definition 3.2(a) and $\mathcal{C}(f_{a^*})$ be the critical set of f_{a^*} . Then for $\hat{x} \in \mathcal{C}(f_{a^*})$,

$$\left. \frac{\partial}{\partial y} F(x, y, a) \right|_{(\hat{x}, 0, a^*)} \neq 0.$$

Definition 3.3 Let $T_{a,b} : M \rightarrow M$ be as in Eq. (6). $T_{a,b}$ is an admissible family of rank one maps if it satisfies (C1)-(C3).

In one sentence, $T_{a,b}$ is an admissible family of rank one maps if it is a non-degenerate 2D unfolding of an admissible 1D family. (C1) imposes the usual 2D regularity and (C3) requires in particular that the unfolding is not singular in the direction of y . $T_{a,b,L}$ in Sec. 2 is an example of an admissible family of rank one maps if L is sufficiently large. Another example is the Hénon family $(x, y) \rightarrow (1 - ax^2 + y, bx)$ around $a^* = 2$.

We now consider the correspondences of Scenarios (a) and (b) of Sec. 2 for a given admissible family of rank one maps. That periodic sinks are observable in both the parameter and the phase spaces follows again from the fact that the periodic sinks of 1D maps are persistent under small perturbations. It is an easy exercise to prove that, if a particular $f_{\hat{a}}$ has a periodic sink, then so does all $T_{a,b}$ for a sufficiently close to \hat{a} and $|b|$ sufficiently small. This way the issue of observability for Scenario (a) is quickly disposed of.

The hard part is to justify the observability of Scenario (b) in the parameter space, that is, to prove the existence of a parameter set Δ of positive measure, for which the attractor of $T_{a,b}, (a, b) \in \Delta$ admits no periodic sinks. From this point on, this scenario will be referred to as *rank one chaos*. To prove the observability of rank one chaos in the parameter space for an admissible family, we imitate the 1D theory of Sec. 3.2, and as a starting point we try to draw a corresponding version of Proposition 3.1 for $T_{a,b}$. An immediate hurdle for us in repeating the claims of Proposition 3.1 is how to identify the set of critical points for a 2D map $T_{a,b}$, over which we wish to impose a rule of the likes of Proposition 3.1(a). As it turns out, to this question there is no straight and easy answer as in the case of 1D maps. To find an answer we need to take a closer look at how $T_{a,b}$ acts on M .

For $T = T_{a,b}$ let $R_0 := I \times [-Kb, Kb]$ where $K > 0$ be such that $T(R_0) \subset R_0$. Define $R_n = T^n(R_0)$. $\{R_n\}$ is a decreasing sequence of neighborhoods of the attractor $\Lambda := \bigcap_{n=0}^{\infty} R_n$. Let δ be a small positive number such that $d(f^n(\hat{x}), \mathcal{C}) \gg \delta$ for all $\hat{x} \in \mathcal{C}$ and $n > 0$, where $f = f_{a^*}$ and \mathcal{C} is the set of critical points for f . Define

$$\mathcal{C}^{(0)} = \{(x, y) \in R_0 : |x - \hat{x}| < \delta \text{ for some } \hat{x} \in \mathcal{C}\}.$$

$\mathcal{C}^{(0)}$ is a collection of vertical strips of width 2δ .

The picture of $R_1 = T(R_0)$ is rather simple. T maps the connected components of $R_0 \setminus \mathcal{C}^{(0)}$ to vertically compressed and horizontally stretched horizontal strips, and the components of $\mathcal{C}^{(0)}$ become small quadratic turns connecting these strips. Under one more iteration of T , new turns are created from the intersections of R_1 and $\mathcal{C}^{(0)}$, and the images of the old turns are kept away from $\mathcal{C}^{(0)}$. Let us keep iterating forward in time. As far as the images of all the quadratic turns are prevented from coming back to $\mathcal{C}^{(0)}$, we can maintain a relatively simple and clean picture of sharp turns connected by horizontal strips for R_n . This is depicted in Fig. 14. Since T is obtained by perturbing a Misiurewicz map, this simple picture of R_n would last at least up to $n = N_0 = \mathcal{O}(\log \delta)$.

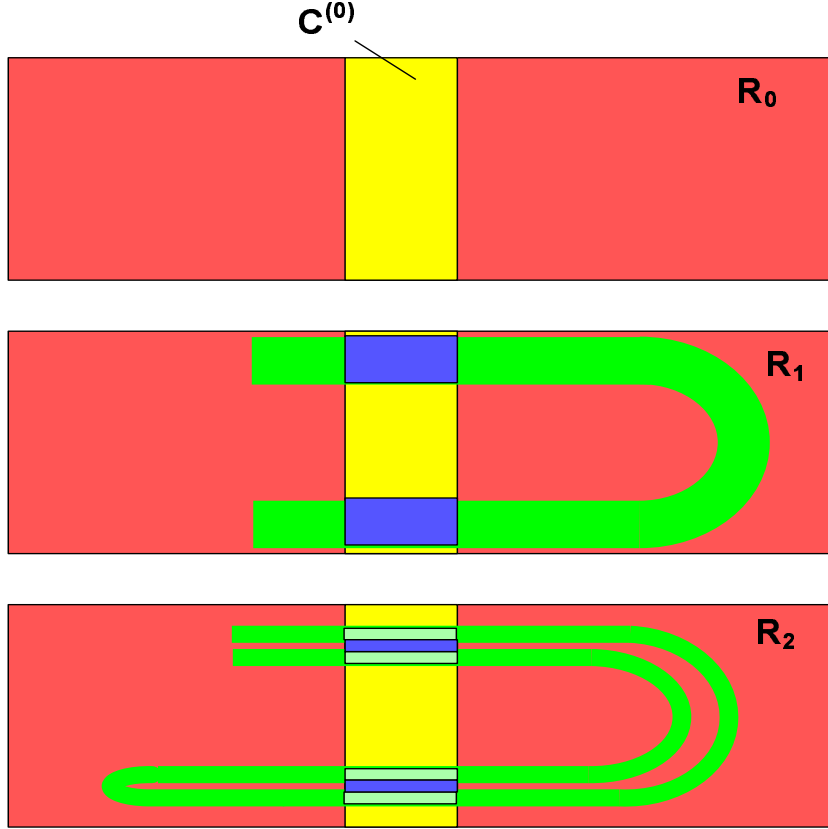


Figure 14: R_0 , $\mathcal{C}^{(0)}$ and their images.

We now study the structure of $\mathcal{C}^{(0)} \cap R_n$. As long as the images of the turns are kept away from coming back to $\mathcal{C}^{(0)}$, $R_n \cap \mathcal{C}^{(0)}$ is a collection of thin, horizontal strips crossing $\mathcal{C}^{(0)}$, and the intersection of R_{n+1} with each of the strips of $R_n \cap \mathcal{C}^{(0)}$ is again a collection of thinner strips. Again, see Fig. 14.

However, the horizontal size of the images of the turns does grow and will eventually intersect $\mathcal{C}^{(0)}$. So the best we could hope for in terms of getting a nested structure of horizontal strips of Fig. 14 for $R_n \cap \mathcal{C}^{(0)}$ is to make the tips

of the turns on the boundary of R_n stay out of $\mathcal{C}^{(0)}$. This is depicted in Fig. 15. Such geometric pictures kept forever would give the correspondences of the 1D Misiurewicz maps in 2D.

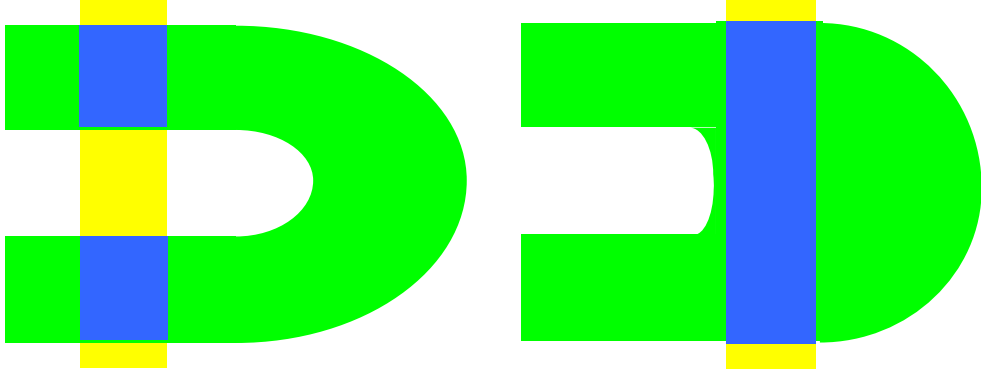


Figure 15: Two ways to maintain the nested structure of $R_n \cap \mathcal{C}^{(0)}$.

To obtain the correspondences of the good maps of Proposition 3.1, we have to allow the tips of the turns to come back to $\mathcal{C}^{(0)}$. Consequently the nested structure of horizontal strips of Fig. 14 could not last forever. We will, however, impose a rule of slow return similar to Proposition 3.1(a), and shrink the length of the horizontal strips of Fig. 14 gradually to maintain a nested structure with dwindling horizontal scale.

The theorem below is a formulation of a correspondence of Proposition 3.1 for $T_{a,b}$ based on these ideas. For $z_0 \in R_0$, let $z_i = T^i(z_0)$. If w_0 is a tangent vector at z_0 , let $w_i = DT^i(z_0)w_0$. A curve in R_0 is called a $C^2(b)$ -**curve** if the slopes of its tangent vectors are $\mathcal{O}(b)$ and its curvature is everywhere $\mathcal{O}(b)$.¹⁴

Theorem 1 *Let $T_{a,b}, (a,b) \in (a_1, a_2) \times (0, b_1)$ be an admissible family of rank one maps. Then for every $b > 0$ sufficiently small, there is a positive measure set $\Delta_b \subset (a_1, a_2)$ such that the following holds for $T_{a,b}, a \in \Delta_b$. In what follows, $\alpha, \delta, c > 0$ and $0 < \rho < 1$ are positive constants, and $b \ll \alpha, \delta, \rho, e^{-c}$.*

- (1) **Critical regions and critical set.** *There is a Cantor set $\mathcal{C} \subset \Lambda$ called the critical set given by $\mathcal{C} = \bigcap_{k=0}^{\infty} \mathcal{C}^{(k)}$ where the $\mathcal{C}^{(k)}$ is a decreasing sequence of neighborhoods of \mathcal{C} called critical regions.*

Geometrically:

(i) $\mathcal{C}^{(0)} = \{(x, y) \in R_0 : d(x, \mathcal{C}) < \delta\}$ where \mathcal{C} is the set of critical points of $f_{a^*} \in \mathcal{M}$.

(ii) $\mathcal{C}^{(k)}$ has a finite number of components called $Q^{(k)}$ each one of which is diffeomorphic to a rectangle. The boundary of $Q^{(k)}$ is made up of two $C^2(b)$ segments of ∂R_k ($R_k = T^k(R_0)$) connected by two vertical lines:

¹⁴The requirement on the curvature is a requirement on second derivative, which we must impose for this theorem to hold.

the horizontal boundaries are $\approx \min(2\delta, \rho^k)$ in length, and the Hausdorff distance between them is $\mathcal{O}(b^{\frac{k}{2}})$.

(iii) $\mathcal{C}^{(k)}$ is related to $\mathcal{C}^{(k-1)}$ as follows: $Q^{(k-1)} \cap R_k$ has at most finitely many components, each of which lies between two $C^2(b)$ subsegments of ∂R_k that stretch across $Q^{(k-1)}$ as shown in Fig. 16. Each component of $Q^{(k-1)} \cap R_k$ contains exactly one component of $\mathcal{C}^{(k)}$.

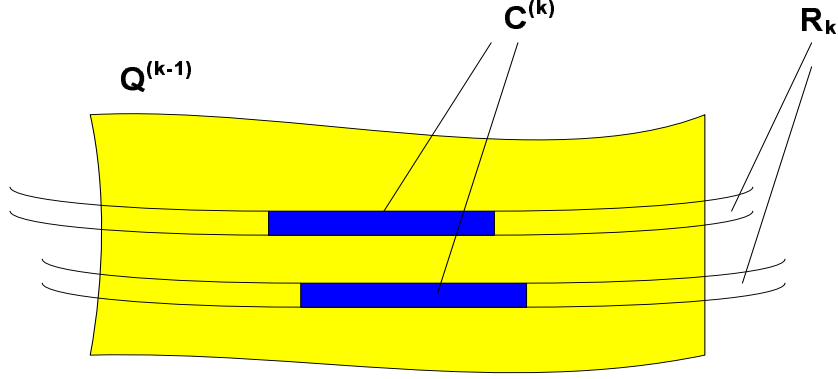


Figure 16: Critical regions.

Dynamically: On each horizontal boundary γ of $Q^{(k)}$ there is a unique point z located within $\mathcal{O}(b^{\frac{k}{4}})$ of the midpoint of γ with the property that if τ is the unit tangent vector to γ at z , then $DT^n(z)\tau$ decreases in length exponentially as n tends to ∞ .

(2) **Properties of critical orbits.** For $z \in R_0$, let $d_{\mathcal{C}}(z)$ denote the following notion of “distance to the critical set”: If $z \notin \mathcal{C}^{(0)}$, let $d_{\mathcal{C}}(z) = \delta$; if $z \in \mathcal{C}^{(0)} \setminus \mathcal{C}$, let k be the largest number with $z \in \mathcal{C}^{(k)}$, and define $d_{\mathcal{C}}(z)$ to be the horizontal distance between z and the midpoint of the component of $\mathcal{C}^{(k)}$ containing z . Then for all $z_0 \in \mathcal{C}$:

- (i) $d_{\mathcal{C}}(z_j) \geq \min\{\delta, e^{-\alpha j}\}$ for all $j > 0$;
- (ii) $\|DT^j(z_0)\binom{0}{1}\| \geq K^{-1}e^{cj}$ for all $j > 0$.

This theorem, though very long to lay out, is a direct parallel of Proposition 3.1. Theorem 1(2)(i) corresponds to Proposition 3.1(a) and Theorem 1(2)(ii) to Proposition 3.1(b). Theorem 1(1) is a detailed identification of the set of critical points, which is now an infinite set. This theorem ([Wang & Young, 2001]), together with a generalization to higher dimensions ([Wang & Young, 2006b]), forms the core of what we will refer to as the theory of rank one chaos. Proof of Theorem 1 is based on an analytic machinery originally invented by Benedicks & Carleson [1991] in their studies of strongly dissipative Hénon maps. It involves complicated analytical schemes, the details of which are unfortunately not suitable for us to pursue further in this paper.

Let us finish by presenting a parallel of Proposition 3.2, which, when combined with Theorem 1, confirms that

- (1) attractors without periodic sinks are observable in both the parameter and the phase spaces, and
- (2) these attractors do admit SRB measures dominating the statistical behavior of almost all orbits in R_0 .

First let us further assume that, for $T_{a,b}$,

- (C4) there exists $K > 1$ such that for arbitrary $(x_1, y_1), (x_2, y_2) \in R_0$,

$$K^{-1} < \frac{|\det DT_{a,b}(x_1, y_1)|}{|\det DT_{a,b}(x_2, y_2)|} < K.$$

Theorem 2 *Let $T_{a,b}, (a, b) \in (a_1, a_2) \times (0, b_0)$ be an admissible family of rank one maps satisfying also (C4), and let Δ be the good parameter set of Theorem 1. Then,*

- (1) $T = T_{a,b}$ has a positive Lyapunov exponent for Lebesgue-almost every $z_0 \in R_0$.
- (2) T admits finitely many ergodic SRB measures, which we denote as $\mu_1, \mu_2, \dots, \mu_r$;
- (3) Lebesgue almost all points $z_0 \in R_0$ are generic with respect to one of the SRB measures in (2).

Both Theorems 1 and 2 are proved in [Wang & Young, 2001]. Let us note that Theorem 2(1) implies that T admits no periodic sinks, and Theorem 2(2) confirms the observability of SRB measures in the phase space. Since $T_{a,b,L}$ in Sec. 2 is an admissible family of rank one maps for L large, and $\det(DT_{a,b,L}(z)) = b$ for all $z \in M$, Propositions 2.4 and 2.6 follow from Theorems 1 and 2.

Rank one chaos for maps of dimension > 2 . A similar theory for rank one maps of higher dimensions is further developed in [Wang & Young, 2006b]. We now proceed to define the dynamical systems under consideration. Let $M = I \times D_{m-1}$ where I is either an interval or a circle and D_{m-1} is an $(m-1)$ -dimensional disk, $m \geq 2$. Points in M are denoted by (x, \mathbf{y}) where $x \in I$ and $\mathbf{y} = (y^1, \dots, y^{m-1}) \in D_{m-1}$. We consider a 2-parameter family of maps $T_{a,b} : M \rightarrow M$, $a \in (a_1, a_2)$, $b \in (0, b_1)$ in the form of

$$T_{a,b} : \begin{pmatrix} x \\ y^1 \\ \vdots \\ y^{m-1} \end{pmatrix} \mapsto \begin{pmatrix} F(x, y^1, \dots, y^{m-1}; a) + bu(x, y^1, \dots, y^{m-1}; a, b) \\ bv^1(x, y^1, \dots, y^{m-1}; a, b) \\ \vdots \\ bv^{m-1}(x, y^1, \dots, y^{m-1}; a, b) \end{pmatrix} \quad (7)$$

where

- (C1) $(x, \mathbf{y}, a) \mapsto F(x, \mathbf{y}; a)$, $u(x, \mathbf{y}; a, b)$ and $v^i(x, \mathbf{y}; a, b)$, $i \leq m-1$, are C^3 and their C^3 -norms are bounded above by a constant independent of b ;
- (C2) $f_a := F(x, \mathbf{0}; a)$ is an admissible family of 1D maps;

(C3) let $a^* \in (a_1, a_2)$ be such that $f_{a^*} \in \mathcal{M}$; then for every $x_0 \in \mathcal{C}(f_{a^*})$, there exists $j \leq m - 1$ such that

$$\left. \frac{\partial F(x, \mathbf{y}; a)}{\partial y^j} \right|_{(x_0, \mathbf{0}, a^*)} \neq 0;$$

(C4) let us further assume that there exists $K > 1$ such that for arbitrary $(x_1, \mathbf{y}_1), (x_2, \mathbf{y}_2) \in M$,

$$K^{-1} < \frac{|\det DT_{a,b}(x_1, \mathbf{y}_1)|}{|\det DT_{a,b}(x_2, \mathbf{y}_2)|} < K.$$

We call $T_{a,b}$ in Eq. (7) satisfying (C1)-(C4) above an *admissible family of rank one maps of dimension m* . In short, $T_{a,b}$ is a non-degenerate unfolding of an admissible 1D family into a phase space of m dimensions. Let $R_0 = \{(x, \mathbf{y}) \in M : |\mathbf{y}| < Kb\}$ be such that $T_{a,b}(R_0) \subset R_0$.

A main difference between the two dimensional theory and the theory of higher dimensions is as follows: In two dimensions, the geometric structure of Theorem 1(1) is maintained by inductively using $R_{k+1} = T^{k+1}(R_0)$ intersecting $\mathcal{C}^{(k)}$, which we can control by imposing Theorem 1(2)(i) on the tips of the turns on the boundaries of R_{k+1} . In dimensions > 2 , the boundaries of R_k are no longer curves; they are surfaces of dimension $m - 1$, the geometry of which is impossible to control. Consequently, the nested structure of Theorem 1(1) for $\mathcal{C}^{(k)} \cap R_{k+1}$ cannot be maintained for all $k > 0$ and we are in need of major modifications in formulating a generalized version of Theorem 1(1) to maps of higher dimensions [Wang & Young, 2006b].

Let us finish this section by stating one more theorem that is parallel to Theorem 2 in 2D for maps of higher dimensions.

Theorem 3 *Let $T_{a,b}, (a, b) \in (a_1, a_2) \times (0, b_1)$ be an admissible family of rank one maps of dimensions $m > 2$. Then there exists $b_0 > 0$ such that for all $b < b_0$, there exists a set Δ_b of positive Lebesgue measure, such that for $T = T_{a,b}, a \in \Delta_b$,*

- (1) $T = T_{a,b}$ has a positive Lyapunov exponent for Lebesgue-almost every $z_0 \in R_0$.
- (2) T admits finitely many ergodic SRB measures, which we denote as $\mu_1, \mu_2, \dots, \mu_r$;
- (3) Lebesgue almost all points $z_0 \in M$ are generic with respect to one of the SRB measures in (2).

4 A General Framework for Applications

In this section we present a specific way of applying the theory of rank one chaos to certain systems of ordinary differential equations. We prove that, by periodically kicking a periodic solution that is asymptotically stable, we induce a time- T map that assumes the form of Eq. (7). As a particular case, the time- T maps of periodically kicked Hopf limit cycles are subsequently studied. Most of the ideas and the results presented in this section originate from [Wang & Young, 2002a,b].

4.1 Periodically kicked limit cycles

Let $\mathbf{x} \in \mathbb{R}^m$ be the phase variable and t be the time. We start with an autonomous ordinary differential equation

$$\frac{d\mathbf{x}}{dt} = \mathbf{f}(\mathbf{x}) \quad (8)$$

and assume that Eq. (8) has an asymptotically stable periodic solution which we write in parametrized form as $\mathbf{x} = \mathbf{p}(s)$ where $s \in \mathbb{R}$ is the curve length from $\mathbf{p}(s)$ to $\mathbf{p}(0)$. $\mathbf{p}(s) = \mathbf{p}(s + L_0)$ is a vector-valued periodic function of period L_0 where L_0 is the total length. We assume that $\mathbf{f}(\mathbf{x})$ is C^4 in a small neighborhood of this periodic solution. To Eq. (8), we add a time-periodic forcing term $\varepsilon P_{T,p}(t)\Phi(\mathbf{x})$ to obtain a new nonautonomous system

$$\frac{d\mathbf{x}}{dt} = \mathbf{f}(\mathbf{x}) + \varepsilon P_{T,p}(t)\Phi(\mathbf{x}) \quad (9)$$

where $P_{T,p}(t) = \sum_{n=-\infty}^{\infty} P_p(t - nT)$ is a periodic pulsetrain of period T , $P_p(t) = \frac{1}{p}$ for $0 < t \leq p$ and $P_p(t) = 0$ otherwise, $\Phi(\mathbf{x})$ is C^4 representing the shape of the forcing and ε its magnitude. In what follows we assume

$$p \ll \varepsilon \ll 1 \ll T \quad (10)$$

and we show that, in the vicinity of the periodic solution $\mathbf{x} = \mathbf{p}(s)$, the time- T map of Eq. (9), which we denote as F_T , is a map of the form of Eq. (7) with the corresponding u and v^i uniformly bounded from above in magnitude, indicating that Eq. (9) represents a natural setting to which the theory of Sec. 3 potentially applies.

(A) A preliminary change of coordinates. First we introduce a change of variables. The old phase variables are $\mathbf{x} = (x_1, \dots, x_m)$ and the new phase variables are $\mathbf{u} = (s, \mathbf{y})$ where $s \in S^1 := [0, L_0)$, $\mathbf{y} = (y_1, \dots, y_{m-1})$. s and y_1, \dots, y_{m-1} are defined as follows. First, s is the parameter in $\mathbf{p}(s)$, representing the curve length. To define $\mathbf{y} = (y_1, \dots, y_{m-1})$, we denote $\mathbf{e}_m(s) = \frac{d}{ds}\mathbf{p}(s)$. Since s is the curve length, $|\mathbf{e}_m(s)| = 1$. Let $(\mathbf{e}_1(s), \mathbf{e}_2(s), \dots, \mathbf{e}_{m-1}(s))$ be a set of unit vectors such that $\mathbf{e}_1(s), \dots, \mathbf{e}_{m-1}(s)$ and $\mathbf{e}_m(s)$ form an orthonormal basis of \mathbb{R}^m for all $s \in [0, L_0)$. For $\mathbf{x} \in \mathbb{R}^m$ that is sufficiently close to the

periodic solution $\mathbf{x} = \mathbf{p}(s)$, there is a unique $s \in [0, L_0)$ and $(m-1)$ -vector $\mathbf{y} = (y_1, \dots, y_{m-1})$ such that

$$\mathbf{x} = y_1 \mathbf{e}_1(s) + \dots + y_{m-1} \mathbf{e}_{m-1}(s) + \mathbf{p}(s). \quad (11)$$

Denote $\mathbf{e}(s) = (\mathbf{e}_1(s), \dots, \mathbf{e}_m(s))^T$ and let

$$\mathbf{e}'(s) = \mathbf{k}(s)\mathbf{e}(s)$$

where $\mathbf{k}(s) = (k_{i,j}(s))$ is the m by m skew symmetric matrix of curvatures. We further write

$$\mathbf{k}_i(s) = (k_{1,i}(s), \dots, k_{m-1,i}(s))$$

for $i \leq m$. \mathbf{k}_i is the i -th row of the matrix $\mathbf{k}(s)$. Differentiating with respect to t on both sides of Eq. (11) we have

$$\begin{aligned} \frac{d\mathbf{x}}{dt} &= \sum_{i=1}^{m-1} \left(\mathbf{e}_i(s) \frac{dy_i}{dt} + y_i \mathbf{e}'_i(s) \frac{ds}{dt} \right) + \mathbf{p}'(s) \frac{ds}{dt} \\ &:= \mathbf{f}(\mathbf{x}) + \varepsilon P_{T,p}(t) \Phi(\mathbf{x}), \end{aligned} \quad (12)$$

from which it follows that

$$\begin{aligned} \frac{ds}{dt} &= \frac{1}{1 + \mathbf{k}_m(s)\mathbf{y}} [\mathbf{f}(s, \mathbf{y})\mathbf{e}_m(s) + \varepsilon P_{T,p}(t) \Phi(s, \mathbf{y})\mathbf{e}_m(s)] \\ \frac{dy_i}{dt} &= \mathbf{f}(s, \mathbf{y})\mathbf{e}_i(s) + \varepsilon P_{T,p}(t) \Phi(s, \mathbf{y})\mathbf{e}_i(s) - \mathbf{k}_i(s)\mathbf{y} \frac{ds}{dt} \end{aligned} \quad (13)$$

where $i = 1, \dots, m-1$, and $\mathbf{f}(s, \mathbf{y})$ and $\Phi(s, \mathbf{y})$ are the expressions of $\mathbf{f}(\mathbf{x})$ and $\Phi(\mathbf{x})$ in new variables (s, \mathbf{y}) , respectively. Observe that in the new phase variable $\mathbf{u} = (s, \mathbf{y})$, $\mathbf{y} = \mathbf{0}$ represents the periodic solution $\mathbf{x} = \mathbf{p}(s)$. The vector field of Eq. (13) is well-defined for all \mathbf{y} that is sufficiently close to $\mathbf{y} = \mathbf{0}$.

Periodic forcing in Eq. (13) is turned on at $t = kT$ then turned off at $t = kT + p$. We call $[kT, kT + p)$ a *forcing period* and $[kT + p, (k+1)T)$ a *relaxation period*. With the forcing in action for $t \in [kT, kT + p)$, Eq. (13) becomes

$$\begin{aligned} \frac{ds}{dt} &= \frac{1}{1 + \mathbf{k}_m(s)\mathbf{y}} [\mathbf{f}(s, \mathbf{y})\mathbf{e}_m(s) + \varepsilon \frac{1}{p} \Phi(s, \mathbf{y})\mathbf{e}_m(s)] \\ \frac{dy_i}{dt} &= \mathbf{f}(s, \mathbf{y})\mathbf{e}_i(s) + \varepsilon \frac{1}{p} \Phi(s, \mathbf{y})\mathbf{e}_i(s) - \mathbf{k}_i(s)\mathbf{y} \frac{ds}{dt} \end{aligned} \quad (14)$$

and with the forcing de-activated for $t \in [kT + p, (k+1)T)$, Eq. (13) becomes

$$\begin{aligned} \frac{ds}{dt} &= \frac{1}{1 + \mathbf{k}_m(s)\mathbf{y}} \mathbf{f}(s, \mathbf{y})\mathbf{e}_m(s) \\ \frac{dy_i}{dt} &= \mathbf{f}(s, \mathbf{y})\mathbf{e}_i(s) - \frac{\mathbf{f}(s, \mathbf{y})\mathbf{e}_m(s)}{1 + \mathbf{k}_m(s)\mathbf{y}} \mathbf{k}_i(s)\mathbf{y}. \end{aligned} \quad (15)$$

We denote $\mathbf{u}_0 = (s_0, \mathbf{y}_0)$, $\mathbf{u}_p = (s_p, \mathbf{y}_p)$ and let $\hat{\mathbf{u}}(\mathbf{u}_0, t)$ be the solution of Eq. (14) satisfying $\hat{\mathbf{u}}(\mathbf{u}_0, 0) = \mathbf{u}_0$, and $\mathbf{u}(\mathbf{u}_p, t)$ be the solution of Eq. (15) satisfying $\mathbf{u}(\mathbf{u}_p, 0) = \mathbf{u}_p$. Then the time- T map is given by $F_T = G \circ \kappa$ where

$$\mathbf{u}_p := \kappa(\mathbf{u}_0) = \hat{\mathbf{u}}(\mathbf{u}_0, p), \quad G := G_{T-p}(\mathbf{u}_p) = u(\mathbf{u}_p, T - p). \quad (16)$$

(B) Map κ at the end of a forcing period. We introduce a new time $\hat{t} = \frac{1}{p}t$. For $t \in [0, p)$, $\hat{t} \in [0, 1)$. We re-write Eq. (14) as

$$\begin{aligned} \frac{ds}{d\hat{t}} &= \mathcal{O}(p) + \frac{\varepsilon \Phi(s, \mathbf{y}) \mathbf{e}_m(s)}{1 + \mathbf{k}_m(s) \mathbf{y}} \\ \frac{dy_i}{d\hat{t}} &= \mathcal{O}(p) + \varepsilon \Phi(s, \mathbf{y}) \mathbf{e}_i(s) - \mathbf{k}_i(s) \mathbf{y} \frac{\varepsilon \Phi(s, \mathbf{y}) \mathbf{e}_m(s)}{1 + \mathbf{k}_m(s) \mathbf{y}}. \end{aligned} \quad (17)$$

where $\mathcal{O}(p)$ represents terms with a factor of p in front. In a similar way, the rest of the terms on the right side of Eq. (17) can be written as terms of $\mathcal{O}(\varepsilon)$, and we have from Eq. (17) that for $\hat{t} \leq 1$,

$$s(\hat{t}) = s_0 + \mathcal{O}(\varepsilon) + \mathcal{O}(p), \quad \mathbf{y}(\hat{t}) = \mathbf{y}_0 + \mathcal{O}(\varepsilon) + \mathcal{O}(p). \quad (18)$$

With the assumption $p \ll \varepsilon$, we can ignore the $\mathcal{O}(p)$ terms. Let

$$U_\varepsilon = \{(s, \mathbf{y}) : |\mathbf{y}| < \varepsilon\}.$$

For $\mathbf{u}_0 = (s_0, \mathbf{y}_0) \in U_\varepsilon$, we have from Eq. (18)

$$s(\hat{t}) = s_0 + \mathcal{O}(\varepsilon), \quad \mathbf{y}(\hat{t}) = \mathcal{O}(\varepsilon). \quad (19)$$

With Eq. (19) at hand, we now write the second equation of Eq. (17) as

$$\frac{dy_i}{d\hat{t}} = \mathcal{O}(p) + \varepsilon (\Phi(s_0, 0) \mathbf{e}_i(s_0) + \mathcal{O}(\varepsilon)), \quad (20)$$

from which we obtain that at $\hat{t} = 1$,

$$\mathbf{y}(1) = \mathbf{y}_0 + \varepsilon(\phi(s_0) + \mathcal{O}(\varepsilon))$$

where

$$\phi(s_0) = (\Phi(s_0, \mathbf{0}) \mathbf{e}_1(s_0), \dots, \Phi(s_0, \mathbf{0}) \mathbf{e}_{m-1}(s_0)).$$

In summary, for $\mathbf{u}_0 \in U_\varepsilon$, $\mathbf{u}_p = (s_p, \mathbf{y}_p) := \kappa(\mathbf{u}_0)$ is such that

$$s_p = s_0 + \mathcal{O}(\varepsilon), \quad \mathbf{y}_p = \mathbf{y}_0 + \varepsilon(\phi(s_0) + \mathcal{O}(\varepsilon)). \quad (21)$$

(C) Map G at the end of a relaxation period. We now study the solutions of Eq. (15). For $i = 1, \dots, m$, let

$$\psi_i(s, \mathbf{y}) := \mathbf{f}(s, \mathbf{y}) \mathbf{e}_i(s).$$

$\psi_i(s, \mathbf{y})\mathbf{e}_i$ is the projection of $\mathbf{f}(s, \mathbf{y})$ onto \mathbf{e}_i . We have for $\mathbf{y} = \mathbf{0}$,

$$\psi_1(s, \mathbf{0}) = \psi_2(s, \mathbf{0}) = \cdots = \psi_{m-1}(s, \mathbf{0}) = 0, \quad \psi_m(s, \mathbf{0}) = |\mathbf{f}(s, \mathbf{0})|$$

because $\mathbf{f}(s, \mathbf{0})$ and $\mathbf{e}_m(s)$ are in the same direction on $\mathbf{y} = \mathbf{0}$. Expanding $\psi(s, \mathbf{y})$ in terms of \mathbf{y} we have, for $i \leq m-1$,

$$\psi_i(s, \mathbf{y}) = \psi_i^{(1)}(s)\mathbf{y} + \mathcal{O}(\mathbf{y}^2)$$

where

$$\psi_i^{(1)}(s) = \left. \frac{\partial}{\partial \mathbf{y}} (\mathbf{f}(s, \mathbf{y})\mathbf{e}_i(s)) \right|_{\mathbf{y}=\mathbf{0}}.$$

Note that $\psi_i^{(1)}$ are $(m-1)$ -vectors for $i \leq m-1$. We also have for $\psi_m(s, \mathbf{y})$

$$\psi_m(s, \mathbf{y}) = \psi_m^{(0)}(s) + \psi_m^{(1)}(s)\mathbf{y} + \mathcal{O}(\mathbf{y}^2)$$

where

$$\psi_m^{(0)}(s) = |\mathbf{f}(s, \mathbf{0})|, \quad \psi_m^{(1)}(s) = \left. \frac{\partial}{\partial \mathbf{y}} (\mathbf{f}(s, \mathbf{y})\mathbf{e}_m(s)) \right|_{\mathbf{y}=\mathbf{0}}.$$

From Eq. (15) we obtain

$$\begin{aligned} \frac{dt}{ds} &= b_0(s) + (\mathbf{b}_1(s) + \mathcal{O}(\mathbf{y}))\mathbf{y} \\ \frac{d\mathbf{y}}{ds} &= (\mathbf{a}(s) + \mathcal{O}(\mathbf{y}))\mathbf{y} \end{aligned} \tag{22}$$

where $\mathbf{a}(s)$ is an $(m-1)$ by $(m-1)$ matrix, and the i -th row of $\mathbf{a}(s)$ is

$$\mathbf{a}_i(s) = \frac{\psi_i^{(1)}(s)}{\psi_m^{(0)}(s)} - \mathbf{k}_i(s).$$

We also have

$$b_0(s) = \frac{1}{\psi_m^{(0)}(s)} > 0,$$

and

$$\mathbf{b}_1(s) = \frac{1}{\psi_m^{(0)}(s)} \left(\mathbf{k}_m - \frac{\psi_m^{(1)}(s)}{\psi_m^{(0)}(s)} \right).$$

Note that by writing the equations in the form of Eq. (22), we are switching the roles of t and s , regarding t as one of the phase variables and s as the time variable. Observe that all the functions on the right side of Eq. (22) are periodic with period L_0 in s .

We now apply Floquet's theory to the second item of Eq. (22). Let $\mathbf{P}(s)$ be the matrix of fundamental solutions of the equation

$$\frac{d}{ds}\mathbf{y} = \mathbf{a}(s)\mathbf{y},$$

By introducing new coordinates $\mathbf{z} := \mathbf{Q}^{-1}(s)\mathbf{y}$, where $\mathbf{P}(s) = \mathbf{Q}(s)e^{\mathbf{A}s}$, Eq. (22) is transformed into

$$\begin{aligned}\frac{dt}{ds} &= b_0(s) + (\mathbf{b}_1(s)\mathbf{Q}(s) + \mathcal{O}(\mathbf{z}))\mathbf{z} \\ \frac{d\mathbf{z}}{ds} &= (\mathbf{A} + \mathcal{O}(\mathbf{z}))\mathbf{z}\end{aligned}\tag{23}$$

where $\mathbf{Q}(s)$ is periodic matrix and \mathbf{A} is a constant matrix that is negative-definite. Let $\{\lambda_i\}$ be the eigenvalues of \mathbf{A} and $\lambda > 0$ be such that $\lambda_i < -\lambda$ for all i . Note that by definition $b_0(s) > 0$ for all s . In using Eq. (23), we regard (t, \mathbf{z}) as phase variables and s as time. Let $(t(s), \mathbf{z}(s))$ be the solution of Eq. (23) satisfying $t(s_p) = 0, \mathbf{z}(s_p) = \mathbf{z}_p$. We have from Eq. (23),

$$\begin{aligned}t(s) &= \int_{s_p}^s b_0(\tau)d\tau + \int_{s_p}^s \mathcal{K}(\tau)d\tau. \\ |\mathbf{z}(s)| &< Ce^{-\frac{\lambda}{2}(s-s_p)}|\mathbf{z}_p|\end{aligned}\tag{24}$$

where

$$\mathcal{K}(\tau) = (\mathbf{b}_1(\tau)\mathbf{Q}(\tau) + \mathcal{O}(\mathbf{z}(\tau)))\mathbf{z}(\tau).\tag{25}$$

Equation (24) is what we use for the solutions in the relaxation period.

(D) *The time-T map $F_T = G \circ \kappa$. Let $M := \{(s, \mathbf{z}) : |\mathbf{z}| < \tilde{K}^{-1}\varepsilon\}$ where $\tilde{K} = \max_{s \in [0, L_0]} \|\mathbf{Q}(s)\|$, and $F_T : (s_0, \mathbf{z}_0) \rightarrow (s_T, \mathbf{z}_T)$ be the time-T map for $(s_0, \mathbf{z}_0) \in M$. For $\kappa : (s_0, \mathbf{z}_0) \rightarrow (s_p, \mathbf{z}_p)$ we have from Eq. (21)*

$$s_p = s_0 + \mathcal{O}(\varepsilon), \quad \mathbf{z}_p = \mathbf{z}_0 + \varepsilon(\mathbf{Q}^{-1}(s_0)\phi(s_0) + \mathcal{O}(\varepsilon));\tag{26}$$

and for G we have

$$\begin{aligned}T - p &= \int_{s_p}^{s_T} b_0(\tau)d\tau + \int_{s_p}^{s_T} \mathcal{K}(\tau)d\tau. \\ |\mathbf{z}_T| &< Ce^{-\frac{\lambda}{2}(s_T-s_p)}|\mathbf{z}_p|\end{aligned}\tag{27}$$

where $\mathcal{K}(\tau)$ is as in Eq. (25). To obtain F_T we combine Eqs. (26) and (27). Note that $G : (s_p, \mathbf{z}_p) \rightarrow (s_T, \mathbf{z}_T)$ is implicitly defined through Eq. (27).

To fit $F_T : M \rightarrow M$ into the form of Eq. (7), we need to first introduce parameters a and b . Denote

$$T_0 = \int_0^{L_0} b_0(s)ds$$

and let $n \geq 0$ be the largest integer such that

$$T - p - nT_0 > 0.$$

(i) We define

$$a = T - p - nT_0, \quad b = e^{-\frac{\lambda}{10}nL_0}.\tag{28}$$

Observe that, as $T \rightarrow \infty$, $b \rightarrow 0$ and $a \in [0, T_0)$.

(ii) We also define a function $g_a(s_0, \mathbf{z}_0)$ implicitly by letting

$$a + nT_0 = \int_{s_p}^{g_a(s_0, \mathbf{z}_0)} b_0(s) ds + \int_{s_p}^{\infty} \mathcal{K}(s) ds. \quad (29)$$

(iii) We write $F_T : (s_0, \mathbf{z}_0) \rightarrow (s_T, \mathbf{z}_T)$ as

$$s_T = g_a(s_0, \mathbf{z}_0) + bu; \quad \mathbf{z}_T = b\mathbf{v}. \quad (30)$$

To show that F_T is in the form of Eq. (7), we now prove $|u|, |\mathbf{v}| < 1$ for T sufficiently large. First, for \mathbf{v} , we have $\mathbf{v} = b^{-1}\mathbf{z}_T$, and from Eq. (24) it follows that

$$|\mathbf{v}| < e^{\frac{1}{10}\lambda nL_0} e^{-\frac{1}{2}\lambda(s_T - s_p)} < 1.$$

For the last inequality, let us note that $s_T \approx nL_0$.

Estimation for u is as follows. By definition $u = b^{-1}(s_T - g_a(s_0, \mathbf{z}_0))$. We have

$$|s_T - g_a(s_0, \mathbf{z})| \leq K \left| \int_{s_T}^{g_a(s_0, \mathbf{z}_0)} b_0(s) ds \right| = K \left| \int_{s_T}^{\infty} \mathcal{K}(s) ds \right| < K\lambda^{-1} e^{-\frac{1}{2}\lambda s_T}.$$

To obtain the first inequality we use $b_0(s) > 0$ for all s and let $K^{-1} = \min_{s \in [0, L_0]} b_0(s)$. For the last inequality we use Eq. (24) for $\mathbf{z}(s)$, and for the middle equality we compare the first items of Eqs. (27) and (29).

(E) 1D limit $g_a(s, 0)$ and the existence of rank one chaos. To apply the theory of Sec. 3 we need to further verify conditions (C1)-(C4) for F_T in Eq. (30). We caution that in principle there is no reason *a priori* for (C1)-(C4) to hold for F_T . In fact, the general setting of infrequent kicks (T large) of small magnitude (ε small) to a stable periodic solution does not favor chaos. To get the kind of expansions assumed in (C2), we need additional assumptions on ε , $\Phi(\mathbf{x})$ and the properties of Eq. (8) around $\mathbf{p}(s)$.

Let us be more concrete by presenting a specific example, through which we hope to provide to the reader some conceptual understanding of the various factors that determine the properties of the 1D limit $g_a(s, 0)$ and the existence of rank one chaos. For this example let us assume $m = 2$. We drop all $\mathcal{O}(\mathbf{y})$ terms in Eq. (22), and assume that

$$\mathbf{Q}(s) = Id, \quad \mathbf{a}(s) = -\lambda, \quad b_0(s) = 1, \quad \mathbf{b}_1(s) = B$$

where λ and B are constants. Note that λ here represents the attractive strength of the periodic solution $\mathbf{y} = \mathbf{0}$, and B represents the strength of *shearing*, that is, the change of the angular velocity for the solutions of the unforced equation with respect to their distances from the periodic solution $\mathbf{y} = \mathbf{0}$. It then follows from Eq. (29) that

$$g_a(s_0, \mathbf{0}) = a + s_0 + \mathcal{O}(\varepsilon) + \frac{\varepsilon B}{\lambda}(\phi(s_0) + \mathcal{O}(\varepsilon)).$$

This function is almost in the form of $f_{a,L}$ of Claim 2.2 with

$$L = \frac{\varepsilon B}{\lambda}$$

where ε represents the magnitude of the forcing. ε, λ and B are three independent parameters. For the theory of Sec. 3 to apply we need L large. This could be achieved with either a sufficiently small λ (weak stability) and/or a sufficiently large B .

In conclusion, periodically kicking a weakly stable periodic solution with strong shearing is more likely to create rank one chaos.

4.2 Hopf bifurcation and rank one chaos

In this subsection we discuss a particular setting of Eq. (9) for the applications of the theory of rank one maps. The stable limit cycles freshly coming out of a generic supercritical Hopf bifurcation [Hopf, 1947; Marsden & McCracken, 1976] are periodically kicked to produce rank one chaos. This is a particular case where the time- T maps F_T can be semi-explicitly computed to the extend that conditions of (C1)-(C4) are readily checked. Observe that the attractive strength of Hopf limit cycles can be made as weak as desired. The strength of shearing in this case is determined by the third order term of the normal forms for the Hopf bifurcation.

(I) Statement of Results. Let $\mathbf{x} \in \mathbb{R}^m$ ($m \geq 2$) be the phase variable and $t \in \mathbb{R}$ be the time. Consider the following μ -dependent system of differential equations

$$\frac{d\mathbf{x}}{dt} = A_\mu \mathbf{x} + \mathbf{f}_\mu(\mathbf{x}) \quad (31)$$

where A_μ is a real m by m matrix and $\mathbf{f}_\mu(\mathbf{x})$ is a vector-valued real analytic function in \mathbf{x} defined on a given neighborhood of $\mathbf{x} = \mathbf{0}$ such that $\mathbf{f}_\mu(\mathbf{0}) = \mathbf{0}$, $D_{\mathbf{x}}\mathbf{f}_\mu(\mathbf{0}) = \mathbf{0}$. Both A_μ and $\mathbf{f}_\mu(\mathbf{x})$ are smooth dependents of μ at and around $\mu = 0$. Let $\{\lambda_i\}_{i=1}^m$ be the eigenvalues of A_μ . We assume that

(A1) *There is a conjugated pair $\lambda_{1,2} = a(\mu) \pm \omega(\mu)\sqrt{-1}$ such that $a(0) = 0, \omega(0) \neq 0$, and $\frac{d}{d\mu}a(0) > 0$. In addition, there exists $c > 0$ such that $Re(\lambda_i) < -c, i \geq 3$.*

Corresponding to $\lambda_{1,2}$, Eq. (31) has a 2-dimensional local center manifold W^c at $\mathbf{x} = \mathbf{0}$, and the equations for the solutions on W^c can be written in a complex variable z in the normal form as

$$\dot{z} = (a(\mu) + i\omega(\mu))z + k_1(\mu)z^2\bar{z} + k_2(\mu)z^3\bar{z}^2 + \dots \quad (32)$$

where $k_1(\mu), k_2(\mu), \dots$ are complex numbers. Note that by transforming z to cz , k_1 is changed to $|c|^2 k_1$. This is, however, the only ambiguity for k_1 . In particular, the sign of $Re(k_1(0))$ and $\arg(k_1(0))$ are uniquely determined.

The ratio of the real and the imaginary parts of the coefficient k_1 above is particularly important for us. Let us denote from this point on that

$$k_1(\mu) = -E(\mu) + \sqrt{-1}F(\mu).$$

Our next assumption is that

(A2) $E(0) > 0$.

We say that Eq. (31) has a generic supercritical Hopf bifurcation at $\mathbf{x} = 0$ for $\mu = 0$ if (A1) and (A2) hold for Eq. (31). It is well-known that, under the assumptions (A1) and (A2), an asymptotically stable periodic solution of size $\mathcal{O}(\mu^{\frac{1}{2}})$ bifurcates out of $\mathbf{x} = 0$ on the center manifold for $\mu > 0$. This periodic solution will be referred to as the *Hopf limit cycle*. See the depiction in Fig. 17.

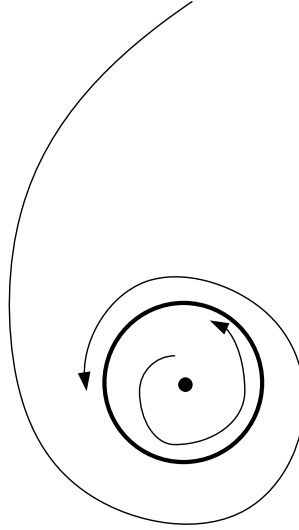


Figure 17: A supercritical Hopf bifurcation.

We now add a time-dependent forcing term to Eq. (31) to form a new equation

$$\frac{d\mathbf{x}}{dt} = A_\mu \mathbf{x} + \mathbf{f}_\mu(\mathbf{x}) + \varepsilon \Phi(\mathbf{x}) P_{T,p}(t) \quad (33)$$

where $\Phi(\mathbf{x})$, $P_{T,p}(t)$ are the same as in Sec. 4.1. Let (r, \mathbf{s}) be the polar coordinates for $\mathbf{x} \in \mathbb{R}^m$. This is to say that $r = |\mathbf{x}|$, $\mathbf{s} = \frac{1}{|\mathbf{x}|} \mathbf{x}$. We have $\mathbf{x} = r\mathbf{s}$ where $r \in \mathbb{R}^+$ and $\mathbf{s} \in S^{m-1}$ is such that $|\mathbf{s}| = 1$.

Let us assume that for $\Phi(\mathbf{x})$

(A3) $\Psi(r, \mathbf{s}) := \frac{1}{r} \Phi(r\mathbf{s})$ as a function of r and \mathbf{s} is C^4 on $[0, \hat{\varepsilon}) \times S^{m-1}$ for some $\hat{\varepsilon} > 0$.

Let $\mathbf{x} \rightarrow L_\mu \mathbf{x} := (x, y, \mathbf{w})^T$ be a linear coordinate change that transforms Eq. (33) into

$$\begin{aligned}\dot{x} &= ax - \omega y + f_x + \varepsilon \Phi_x P_{T,p}(t) \\ \dot{y} &= \omega y + ay + f_y + \varepsilon \Phi_y P_{T,p}(t) \\ \dot{\mathbf{w}} &= A^{(s)} \mathbf{w} + f_{\mathbf{w}} + \varepsilon \Phi_{\mathbf{w}} P_{T,p}(t)\end{aligned}\tag{34}$$

so that $A^{(s)}$ is an $(m-2)$ by $(m-2)$ matrix of eigenvalues of negative real part, and

$$(f_x, f_y, f_{\mathbf{w}})^T = L_\mu \mathbf{f}_\mu(L_\mu^{-1}(x, y, \mathbf{w})^T), \quad (\Phi_x, \Phi_y, \Phi_{\mathbf{w}})^T = L_\mu \Phi(L_\mu^{-1}(x, y, \mathbf{w})^T).$$

Denote the polar coordinates for (x, y, \mathbf{w}) as $(\hat{r}, \hat{\mathbf{s}})$. This is to say that $\hat{r} = \sqrt{x^2 + y^2 + |\mathbf{w}|^2}$, $\hat{\mathbf{s}} = \frac{1}{\hat{r}}(x, y, \mathbf{w})$. Let

$$\Psi_x(\hat{r}, \hat{\mathbf{s}}) := \frac{1}{\hat{r}} \Phi_x(\hat{r} \hat{\mathbf{s}}); \quad \Psi_y(\hat{r}, \hat{\mathbf{s}}) := \frac{1}{\hat{r}} \Phi_y(\hat{r} \hat{\mathbf{s}}); \quad \Psi_{\mathbf{w}}(\hat{r}, \hat{\mathbf{s}}) := \frac{1}{\hat{r}} \Phi_{\mathbf{w}}(\hat{r} \hat{\mathbf{s}}).$$

$\Psi_x(\hat{r}, \hat{\mathbf{s}}), \Psi_y(\hat{r}, \hat{\mathbf{s}}), \Psi_{\mathbf{w}}(\hat{r}, \hat{\mathbf{s}})$ are C^4 in $(\hat{r}, \hat{\mathbf{s}})$ according to (A3). Finally we let

$$\phi(\theta) = \cos \theta \Psi_x(0, \hat{\mathbf{s}}_0) + \sin \theta \Psi_y(0, \hat{\mathbf{s}}_0)\tag{35}$$

where $\hat{\mathbf{s}}_0 = (\cos \theta, \sin \theta, \mathbf{0})$, $\theta \in [0, 2\pi]$.

The time- T map of Eq. (33) is denoted as $F_{\mu, \varepsilon, T, p}$ where μ is the bifurcation parameter of the unperturbed Eq. (31) and ε, T, p are the parameters of forcing. Also recall that $k_1(\mu) = -E(\mu) + iF(\mu)$ where k_1 is as in Eq. (32). Let us assume that

- (a) (A1)-(A3) hold for Eq. (33);
- (b) $\phi(\theta)$ in Eq. (35) is a Morse function; and
- (c) μ, ε, p are such that $0 < \mu < 1$, $0 < p \ll \varepsilon \ll 1$.

Then, we have

Theorem 4 *Let the values of μ, p and ε be fixed and assume that (a)-(c) above hold. We regard the period T of the forcing as a parameter and denote $F_T = F_{\mu, \varepsilon, T, p}$. Then there exists a constant K_1 , determined exclusively by $\phi(\theta)$, such that if*

$$\left| \varepsilon \frac{F(0)}{E(0)} \right| > K_1,$$

then there exists a positive measure set $\Delta \subset (\mu^{-1}, \infty)$ for T , so that for $T \in \Delta$, F_T has a strange attractor Λ admitting no periodic sinks. This is to say that there exists an open neighborhood U of Λ in \mathbb{R}^m such that F_T has a positive Lyapunov exponent for Lebesgue almost every point in U . Furthermore, F_T admits an ergodic SRB measure, with respect to which almost every point of U is generic.

In Sec. 5 we will present various examples of applications of Theorem 4 to switch-controlled circuits and systems.

A slightly different version of Theorem 4 is proved in [Wang & Young, 2002b]. To prove Theorem 4, we need to first compute the time-T map using the normal forms in the vicinity of a Hopf limit cycle. Then we need to further verify (C1)-(C4) for the time-T map computed. Since in this case our computations are focused on a small neighborhood of the center of a Hopf bifurcation, the resulting formula for the time-T map is more explicit than the formula derived for a periodically kicked arbitrary limit cycle in Sec. 4.1. As a matter of fact, the time-T map we obtain at the end is an unfolding of a 1D family in the form of $f_{a,L}$ of Claim 2.2 in Sec. 3.1, with a and b correspondingly extracted from $T - p$ through Eq. (28) in Sec. 4.1 and $L \approx \varepsilon \left| \frac{F(0)}{E(0)} \right|$. The actual process of computing F_T and checking (C1)-(C4) for Eq. (33) are long, and we refer the reader to [Lu *et al.*, 2007; Wang & Young, 2002a,b] (in particular to [Lu *et al.*, 2007]), for detailed derivations, which we have no choice but skip here. We, however, would compute the time-T map and identify the 1D limit for a simplified case, through which we hope to illustrate the main ideas involved.

(II) A simplified system. To simplify the issue we first assume $m = 2$ so the strongly stable directions represented by \mathbf{w} in Eq. (34) are completely dropped. Second we assume that Eq. (34), now with only two equations of (x, y) , is in the normal form. For notational simplicity, let us also assume $a(\mu) = \mu$. Consequently, we are going to compute the time-T map of the following system of equations

$$\begin{aligned}\dot{x} &= \mu x - \omega y - E(x^2 + y^2)x - F(x^2 + y^2)y + \mathcal{O}((x^2 + y^2)^{\frac{5}{2}}) + \varepsilon \Phi_x P_{T,p}(t) \\ \dot{y} &= \omega x + \mu y + F(x^2 + y^2)x - E(x^2 + y^2)y + \mathcal{O}((x^2 + y^2)^{\frac{5}{2}}) + \varepsilon \Phi_y P_{T,p}(t).\end{aligned}\tag{36}$$

First we need to introduce a sequence of coordinate changes that would facilitate our computations of F_T .

Transformation # 1. Let (r, θ) be the polar coordinates for (x, y) such that

$$x = r \cos \theta, \quad y = r \sin \theta.$$

We write Eq. (36) in (r, θ) as

$$\begin{aligned}\dot{r} &= (\mu - Er^2)r + \mathcal{O}(r^5) + \varepsilon \Phi_r P_{T,p}(t) \\ \dot{\theta} &= \omega + Fr^2 + \mathcal{O}(r^4) + \varepsilon \frac{1}{r} \Phi_\theta P_{T,p}(t)\end{aligned}\tag{37}$$

where

$$\Phi_r = \cos \theta \Phi_x + \sin \theta \Phi_y, \quad \hat{\Phi}_\theta = \cos \theta \Phi_y - \sin \theta \Phi_x.$$

Transformation # 2. Without the forcing terms, Eq. (37) has a periodic solution $r \approx \sqrt{\frac{\mu}{E}}$. To make the distance from this solution to the center

roughly one we let

$$\xi = \sqrt{\frac{E}{\mu}} r$$

and write Eq. (37) in (ξ, θ) as

$$\begin{aligned}\dot{\xi} &= \mu(1 - \xi^2)\xi + \left(\frac{\mu}{E}\right)^2 \xi^5 \mathcal{O}(1) + \varepsilon \sqrt{\frac{E}{\mu}} \Phi_r P_{T,p}(t) \\ \dot{\theta} &= \omega + \mu \frac{F}{E} \xi^2 + \left(\frac{\mu}{E}\right)^2 \xi^4 \mathcal{O}(1) + \varepsilon \frac{1}{\xi} \sqrt{\frac{E}{\mu}} \Phi_\theta P_{T,p}(t).\end{aligned}\tag{38}$$

Transformation # 3. The stable periodic solution bifurcating from the center is now close to $\xi = 1$, which we now write as $\xi = 1 + \psi(\theta)$. It is well-known that $\psi(\theta) = \mathcal{O}(\mu)$. Let us further introduce a new variable $\hat{\xi} = \xi - 1 - \psi(\theta)$ so as to move the Hopf limit cycle to $\hat{\xi} = 0$. We derive the equation for the new variable $\hat{\xi}$ and re-write $\hat{\xi}$ as ξ . Then Eq. (38) becomes

$$\begin{aligned}\dot{\xi} &= -\mu(2 + 3\xi + \xi^2 + \mathcal{O}(\mu))\xi + \varepsilon \sqrt{\frac{E}{\mu}} (\Phi_r + \mathcal{O}(\mu^2)) P_{T,p}(t) \\ \dot{\theta} &= \omega + \mu^2 g(\theta) + \mu \frac{F}{E} (2 + \xi + \mathcal{O}(\mu))\xi + \varepsilon \sqrt{\frac{E}{\mu}} \left(\frac{1}{\xi + 1} + \mathcal{O}(\mu) \right) \Phi_\theta P_{T,p}(t)\end{aligned}\tag{39}$$

where $g(\theta)$ is a function of θ of magnitude $\mathcal{O}(1)$. Note that the derivation of Eq. (37) from Eq. (36), and that of Eq. (38) from Eq. (37) are rather simple. On the other hand, the derivation of Eq. (39) from Eq. (38) is much less straight forward. We suggest that the reader work this derivation himself/herself (not a trivial one though).

Transformation # 4. Next we adjust the angular variable to remove the term $\mu^2 g(\theta)$ from the second item of Eq. (39). Let

$$s = \int_0^\theta \frac{1}{1 + \omega^{-1} \mu^2 g(\tau)} d\tau.$$

We can re-write Eq. (39) in (ξ, s) as

$$\begin{aligned}\dot{\xi} &= -\mu(2 + 3\xi + \xi^2 + \mathcal{O}(\mu))\xi + \varepsilon \sqrt{\frac{E}{\mu}} (\Phi_r + \mathcal{O}(\mu^2)) P_{T,p}(t) \\ \dot{s} &= \omega + \mu \frac{F}{E} (2 + \xi + \mathcal{O}(\mu))\xi + \varepsilon \sqrt{\frac{E}{\mu}} \left(\frac{1}{\xi + 1} + \mathcal{O}(\mu) \right) (\Phi_\theta + \mathcal{O}(\mu^2)) P_{T,p}(t).\end{aligned}\tag{40}$$

Note that $s \in S^1 = [0, L_0)$ where

$$L_0 = \int_0^{2\pi} \frac{1}{1 + \omega^{-1} \mu^2 g(\tau)} d\tau.$$

Equation (40) is the equation we use to compute F_T .

(III) Time-T map and the 1D limit. We again call $[kT, kT + p)$ a *forcing period* and $[kT + p, (k+1)T)$ a *relaxation period*. With the forcing in action for $t \in [kT, kT + p)$, Eq. (40) becomes

$$\begin{aligned} \dot{\xi} &= -\mu(2 + 3\xi + \xi^2 + \mathcal{O}(\mu))\xi + \frac{1}{p}\varepsilon \sqrt{\frac{E}{\mu}} (\Phi_r + \mathcal{O}(\mu^2)) \\ \dot{s} &= \omega + \mu \frac{F}{E} (2 + \xi + \mathcal{O}(\mu))\xi + \frac{1}{p}\varepsilon \sqrt{\frac{E}{\mu}} \left(\frac{1}{\xi + 1} + \mathcal{O}(\mu) \right) (\Phi_\theta + \mathcal{O}(\mu^2)) \end{aligned} \quad (41)$$

and with the forcing de-activated for $t \in [kT + p, (k+1)T)$, Eq. (40) becomes

$$\begin{aligned} \dot{\xi} &= -\mu(2 + 3\xi + \xi^2 + \mathcal{O}(\mu))\xi \\ \dot{s} &= \omega + \mu \frac{F}{E} (2 + \xi + \mathcal{O}(\mu))\xi. \end{aligned} \quad (42)$$

Denote $\mathbf{u}_0 = (\xi_0, s_0)$, $\mathbf{u}_p = (\xi_p, s_p)$. Let $\hat{\mathbf{u}}(\mathbf{u}_0, t)$ be the solution of Eq. (41) satisfying $\hat{\mathbf{u}}(\mathbf{u}_0, 0) = \mathbf{u}_0$, and $\mathbf{u}(\mathbf{u}_p, t)$ be the solution of Eq. (42) satisfying $\mathbf{u}(\mathbf{u}_p, 0) = \mathbf{u}_p$. Then we can write the time- T map as $F_T = G \circ \kappa$ where

$$\mathbf{u}_p := \kappa(\mathbf{u}_0) = \hat{\mathbf{u}}(\mathbf{u}_0, p), \quad G := G_{T-p}(\mathbf{u}_p) = \mathbf{u}(\mathbf{u}_p, T - p). \quad (43)$$

(A) *Solutions of Eq. (41).* Denote $U = \{(\xi, s) : |\xi| < \varepsilon\}$. For $\mathbf{u}_0 = (\xi_0, s_0) \in U$, let

$$\kappa(\mathbf{u}_0) = \mathbf{u}_p = (\xi_p, s_p).$$

We have from Eq. (41) that

$$\xi_p = \xi_0 + \varepsilon(\phi(s_0) + \mathcal{O}(\varepsilon)), \quad s_p = s_0 + \mathcal{O}(\varepsilon) \quad (44)$$

where

$$\phi(s_0) = \Psi_x(\cos s_0, \sin s_0) \cos s_0 + \Psi_y(\cos s_0, \sin s_0) \sin s_0. \quad (45)$$

Recall that $(\Psi_x, \Psi_y) := \frac{1}{r}(\Phi_x(x, y), \Phi_y(x, y))$ where $r = \sqrt{x^2 + y^2}$.

(B) *Solutions of Eq. (42).* Let $(\xi_t, s_t) = \mathbf{u}(t - p, \mathbf{u}_p)$. We have from Eq. (42)

$$\begin{aligned} |\xi_t| &< 2e^{-\frac{3}{2}\mu(t-p)} \\ s_t &= s_p + \omega(t - p) + \mu \frac{F}{E} \int_0^{t-p} (2 + \xi) \xi dt + \int_0^{t-p} \mathcal{O}(\mu^2) \xi^2 dt. \end{aligned} \quad (46)$$

Since $s \in S^1$ is represented by the interval $[0, L_0)$, s_t above is $\text{mod}(L_0)$. We have from Eq. (46)

$$|\xi_T| < 2e^{-\frac{3}{2}\mu(T-p)}|\xi_p|$$

$$s_T = s_p + \omega(T-p) + \mu \frac{F}{E} \int_0^{T-p} (2+\xi)\xi dt + \int_0^{T-p} \mathcal{O}(\mu^2)\xi^2 dt. \quad (47)$$

(C) *Parameters a, b and the 1D limit.* Let n be the largest integer such that $T-p-\omega^{-1}nL_0 > 0$. As was done in Sec. 4.1(D), we let

$$a = \omega(T-p) - nL_0; \quad b = e^{-\mu\omega^{-1}nL_0}$$

and write $F_T : (\xi_0, s_0) \rightarrow (\xi_T, s_T)$ as

$$\xi_T = bv, \quad s_T = g_a(\xi_0, s_0) + bu$$

where $g_a(\xi_0, s_0)$ is defined by replacing the integral bound $T-p$ to $+\infty$ in the equation for s_T in Eq. (47). This is to say that

$$g_a(\xi_0, s_0) = s_p + a + \mu \frac{F}{E} \int_0^\infty (2+\xi)\xi dt + \int_0^\infty \mathcal{O}(\mu^2)\xi^2 dt.$$

We have

Proposition 4.1 *Assume that $T \gg \mu^{-1}$. Then*

- (i) *for $T \gg \mu^{-1}$, we have $|u|, |v| < 1$; and*
- (ii) *for the 1D limit we have*

$$g_a(0, s_0) = a + s_0 + \varepsilon \frac{F(0)}{E(0)}(\phi(s_0) + \mathcal{O}(\varepsilon)) + \mathcal{O}(\varepsilon)$$

Proof: That $|u| < 1$ is straight forward from the first item of Eq. (47). $|v| < 1$ is from

$$|s_T - g_a| = \mu \frac{F}{E} \int_{T-p}^\infty (2+\xi)\xi dt + \int_{T-p}^\infty \mathcal{O}(\mu^2)\xi^2 dt < Ke^{-\frac{3}{2}\mu(T-p)}.$$

For (ii), we have from Eq. (42)

$$\frac{d\xi}{\xi+1} = -\mu(\xi+2)\xi dt + \mathcal{O}(\mu^2)\xi dt$$

from which it follows that

$$\int_0^\infty \mu(\xi+2)\xi dt = \ln(\xi_p+1) + \mathcal{O}(\varepsilon).$$

We then have

$$g_a = s_p + a + \frac{F}{E} \ln(\xi_p+1) + \mathcal{O}(\varepsilon). \quad (48)$$

(ii) is now obtained by combining Eqs. (44) and (48). \square

(D) *Proof of Theorem 4.* To prove Theorem 4, we need to further check (C1)-(C4) in Sec. 3.1 for F_T , among which (C2) now follows from a slightly generalized version of Claim 2.2 in Sec. 3.1 provided that $L = \varepsilon \frac{F(0)}{E(0)}$ is sufficiently large. Note that, even at this point, it is by no means easy to check other conditions. For instance, to verify (C1), being able to control the magnitude of u and v as we did above is far from being adequate. Detailed estimates on the C^4 -norms of u and v are needed in order to verify (C1). On the other hand, though mathematically important, these estimates fall in general into the category of conceptually less important details, for which we would refer the reader to [Wang & Young, 2002a] or [Lu *et al.*, 2007].

(IV) Geometric mechanism and examples. Let us now illustrate on an intuitive level how the rank one chaos is created by the external force. In Fig. 18(a), the dotted circle represents the limit cycle coming out of the center. When the external force is applied, this circle is deformed to become the solid curve in Fig. 18(a). At this point, two competing factors are in action. The first is the effect of *shearing*, meaning points at different distances from the center of the circle rotate at different speeds. Shearing acts to exaggerate the initial deformation brought in by the external forcing. The strength of shearing is measured by the ratio of the imaginary and the real parts of the constant k_1 in Eq. (32), i.e. $|F(0)/E(0)|$, which we will call from this point on as the *twist constant* for Eq. (32). The second factor is the magnitude of the forcing, which is represented by ε . If twist constant is not large enough in comparison with ε^{-1} , then the initial deformation of size ε is suppressed by the contracting force of the original limit cycle, and the attractor for the time-T map is a simple closed curve. This is a case where (C2) fails to hold. On the other hand, if the twist constant is large, then the initial deformation brought in by the kicking force is exaggerated. The attracting set starts to disintegrate into a finite collection of periodic saddles and sinks. As the twist constant gets larger, the initial deformation introduced by the kicking force is exaggerated further, getting us into a situation in which Scenarios (a) and (b) of Sec. 2.2 co-exist. In this case, the time-T maps are an admissible family of rank one maps of Sec. 3, to which the theory of Sec. 3 applies (see Fig. 18(b)).

Examples

Example 1: Let r, s be the polar coordinates for $\mathbf{x} \in \mathbb{R}^m$ and assume that

$$\Phi(\mathbf{x}) = r\psi(r, \mathbf{s})\mathbf{s}$$

where $\psi : \mathbb{R}^+ \times S^{m-1} \rightarrow \mathbb{R}$ is C^4 . Let L_μ be the linear coordinate change that transforms Eq. (33) to Eq. (34), and $\hat{r}, \hat{\mathbf{s}}$ be the polar coordinates for (x, y, \mathbf{w}) . We have

$$(\Psi_x, \Psi_y, \Psi_{\mathbf{w}}) = \psi \left(\hat{r} |L_\mu^{-1} \hat{\mathbf{s}}|, \frac{L_\mu^{-1} \hat{\mathbf{s}}}{|L_\mu^{-1} \hat{\mathbf{s}}|} \right) L_\mu^{-1} \hat{\mathbf{s}}.$$

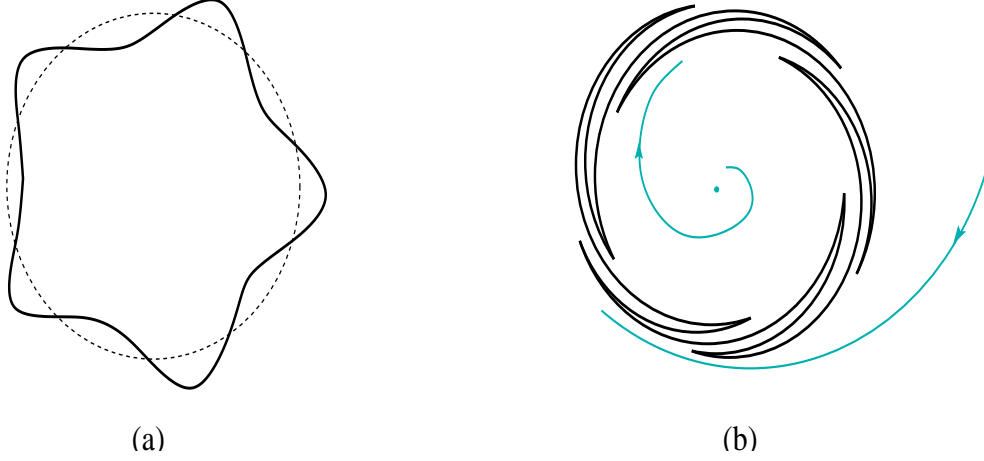


Figure 18: A Hopf attractor.

Let $L_\mu^{-1} = (\mathbf{v}_1, \dots, \mathbf{v}_m)$ where $\mathbf{v}_i = (v_{1i}, \dots, v_{mi})^T$ are vectors in \mathbb{R}^m . Then we have from Eq. (35) that

$$\phi(\theta) = \psi \left(0, \frac{\mathbf{v}_1 \cos \theta + \mathbf{v}_2 \sin \theta}{|\mathbf{v}_1 \cos \theta + \mathbf{v}_2 \sin \theta|} \right) (v_{11} \cos^2 \theta + (v_{12} + v_{21}) \sin \theta \cos \theta + v_{22} \sin^2 \theta). \quad (49)$$

Theorem 4 applies provided that $\phi(\theta)$ in Eq. (49) is a Morse function in θ .

If L_μ is the identity matrix, then $\phi(\theta) = \psi(0, (\cos \theta, \sin \theta, \mathbf{0}))$.

Example 2: We assume that, in Eq. (33), $\Phi(\mathbf{x})$ is real-analytic around $\mathbf{x} = \mathbf{0}$ and $\Phi(\mathbf{0}) = \mathbf{0}$. Then

$$\Phi(\mathbf{x}) = \mathbf{A}\mathbf{x} + h.o.t.$$

where \mathbf{A} is an m by m constant matrix, and

$$(\Psi_x, \Psi_y, \Psi_{\mathbf{w}}) = L_\mu \mathbf{A} L_\mu^{-1} \hat{\mathbf{s}} + h.o.t.$$

where $h.o.t. = \mathbf{0}$ at $\hat{r} = 0$. Let $\mathbf{B} = (b_{ij}) := L_\mu \mathbf{A} L_\mu^{-1}$. From Eq. (35) we have

$$\phi(\theta) = b_{11} \cos^2 \theta + b_{22} \sin^2 \theta + (b_{12} + b_{21}) \cos \theta \sin \theta.$$

It is straight forward to check that if

$$(b_{11} - b_{22})^2 + (b_{12} + b_{21})^2 \neq 0, \quad (50)$$

then $\phi(\theta)$ is a Morse function.

5 Application to Circuits and Systems

In this section, we give several practical examples to demonstrate the applicability of the various aspects of the theory presented in Secs. 3 and 4. The examples we use are mainly from the field of Electrical Engineering.

The study of electrical circuits has provided a major inspiration for the development of the modern theory of dynamical systems. The mathematical analysis and numerical and experimental simulations of electrical systems, such as van der Pol's equation and Duffing's equation, have helped shape the modern theories of chaos and bifurcations [Cartwright & Littlewood, 1945; Guckenheimer & Holmes, 1997; Levinson, 1949]. On the other hand, profound mathematical theories often come back to provide powerful insights, and guide the design of circuits and systems of theoretical and practical importance.

For applications presented in this section, we specifically choose the well-known Chua's [Chua, 1994; Madan, 1993] and MLC (Murali-Lakshmanan-Chua) circuits [Murali *et al.*, 1994a,b; Thamilmaran *et al.*, 2000] with a smooth nonlinearity to demonstrate the applicability of the theory to the case of periodically kicked Hopf limit cycles. We will also kick the non-Hopf limit cycles from the original piecewise linear Chua's circuit to show that the theory is applicable to arbitrary limit cycles, too. Here we mainly follow the work in [Oksasoglu *et al.*, 2006; Wang & Oksasoglu, 2005, 2007].

A generic scheme: Let us start with the following autonomous system

$$\frac{d\mathbf{u}}{dt} = f(\mathbf{u}) \quad (51)$$

where $\mathbf{u} \in \mathbb{R}^m, m \geq 2$. Assume that Eq. (51) is capable of generating a supercritical Hopf bifurcation. To obtain rank one chaos in such a system, we add to it a forcing term as shown below:

$$\frac{d\mathbf{u}}{dt} = f(\mathbf{u}) + \varepsilon \Phi(\mathbf{u}) P_{T,p}(t) \quad (52)$$

where $P_{T,p}(t)$ is a periodic pulsetrain of period T , and of pulsewidth p . If $\Phi(\mathbf{u})$ in Eq. (52) contains only first-order terms, then the forcing term in Eq. (52) can be realized by modulating the system's state variables by a periodic pulsetrain. If we deal with electrical circuits, and assume that the system state variables consist of capacitor voltages and inductor currents, we can use externally controlled switches to achieve the desired modulation scheme. Such a scheme is depicted in Fig. 19.

In Fig. 19, each switch is controlled by a periodic pulsetrain $P_{T,p}(t)$, and the governing equations for the capacitor voltage and the inductor current are given by

$$\begin{aligned} C \frac{dv_c}{dt} &= i_s(t) - v_c G_1 P_{T,p}(t) \\ L \frac{di_L}{dt} &= v_s(t) - i_L R_2 P_{T,p}(t) \end{aligned} \quad (53)$$

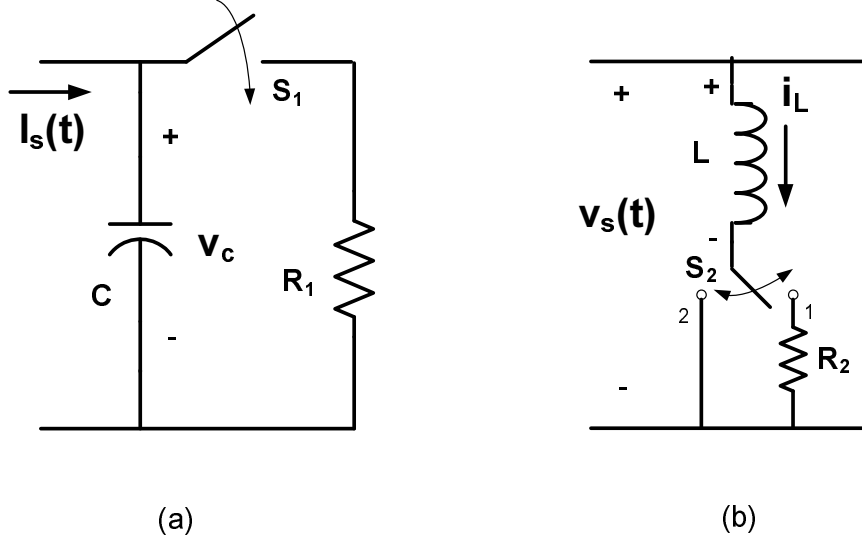


Figure 19: A switch-controlled state variable modulation scheme.

Note from Eq. (53) that the magnitude of forcing, ε , can be adjusted by the resistors R_1 , R_2 of Fig. 19 which can be done without affecting other system parameters. With the above scheme applied to a given autonomous circuit, we, then, follow a step by step procedure to prove the existence of rank one chaos in the resulting nonautonomous circuit using Theorem 4 of Sec. 4. The steps are as follows:

- (a) First, in the autonomous system, find a fixed point that is the center of a generic Hopf bifurcation with a weakly stable periodic solution coming out of the center.
- (b) Then, compute $k_1 = -E + iF$ in a normal form of the central flow. $\tau = \left| \frac{F}{E} \right|$ ought to be large for Theorem 4 of Sec. 4 to apply.
- (c) Also compute $\phi(\theta)$ following the well-defined process of Sec. 4.2 and check that $\phi(\theta)$ is a Morse function, i.e., a function of non-degenerate critical points.
- (d) Then, Theorem 4 of Sec. 4 guarantees the existence of rank one attractors on a positive measure set(s) of T and/or ε .

Once the system parameters are chosen following the steps above, we can vary T and/or ε of Eq. (52) to observe rank one chaos in simulations and experiments.

This step by step procedure is applied to the well-known Chua's circuit with smooth nonlinearity in Sec. 5.1 and the results of the numerical simulations are discussed. In Sec. 5.2 we discuss various extensions of the switch-controlled circuit design using the MLC circuit as an example. Finally in Sec. 5.3 we go back to the general setting of Sec. 4.1 to present numerical evidence of rank one attractors in periodically kicked piecewise linear Chua's circuit.

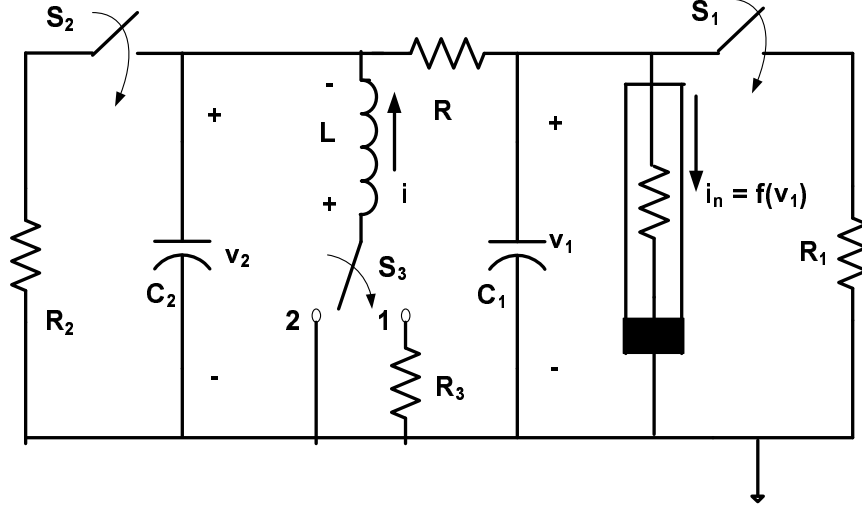


Figure 20: Switched-controlled Chua's circuit.

5.1 Rank one chaos in a switch-controlled smooth Chua's circuit

In this subsection we apply the scheme of Fig. 19 to Chua's circuit as shown in Fig. 20. The switches S_i are controlled by a periodic pulsetrain with p_0 and T_0 being the pulsewidth and the period, respectively. Let $p_0 \ll 1 \ll T_0$.

5.1.1 Derivation of equations

The governing equations for this circuit are given by

$$\begin{aligned} C_1 \frac{dv_1}{dt} &= G(v_2 - v_1) - f(v_1) - G_1 v_1 \\ C_2 \frac{dv_2}{dt} &= i + G(v_1 - v_2) - G_2 v_2 \\ L \frac{di}{dt} &= -v_2 - R_3 i \end{aligned} \quad (54)$$

for $nT_0 \leq t < nT_0 + p_0$, and by

$$\begin{aligned} C_1 \frac{dv_1}{dt} &= G(v_2 - v_1) - f(v_1) \\ C_2 \frac{dv_2}{dt} &= i + G(v_1 - v_2) \\ L \frac{di}{dt} &= -v_2 \end{aligned} \quad (55)$$

for $nT_0 + p_0 \leq t < (n+1)T_0$. Here, $f(\cdot)$ represents the $v - i$ characteristics of the nonlinear resistor in Fig. 20, and is given by

$$f(v_1) = a_1 v_1 + a_3 v_1^3 \quad (56)$$

Putting Eqs. (54) and (55) together, we obtain

$$\begin{aligned}
C_1 \frac{dv_1}{dt} &= G(v_2 - v_1) - f(v_1) - G_1 v_1 \sum_{n=0}^{\infty} F_{n,p_0,T_0}(t) \\
C_2 \frac{dv_2}{dt} &= i + G(v_1 - v_2) - G_2 v_2 \sum_{n=0}^{\infty} F_{n,p_0,T_0}(t) \\
L \frac{di}{dt} &= -v_2 - R_3 i \sum_{n=0}^{\infty} F_{n,p_0,T_0}(t)
\end{aligned} \tag{57}$$

where

$$F_{n,T_0,p_0}(t) = \begin{cases} 1 & nT_0 \leq t < nT_0 + p_0 \\ 0 & \text{elsewhere.} \end{cases} \tag{58}$$

By setting

$$x = \frac{v_1}{V_0}, \quad y = \frac{v_2}{V_0}, \quad z = \frac{i}{I_0}, \quad t \rightarrow \frac{t}{\omega_n},$$

we obtain the following dimensionless set of equations

$$\begin{aligned}
\frac{dx}{dt} &= \alpha[y - h(x)] - \varepsilon_1 x P_{p,T}(t) \\
\frac{dy}{dt} &= \gamma[x - y + \rho z] - \varepsilon_2 y P_{p,T}(t) \\
\frac{dz}{dt} &= -\beta y - \varepsilon_3 z P_{p,T}(t)
\end{aligned} \tag{59}$$

where

$$\begin{aligned}
P_{p,T} &= \frac{1}{p} \sum_{n=-\infty}^{\infty} F_{n,T,p}, \quad h(x) = b_1 x + b_3 x^3; \\
b_1 &= 1 + \frac{a_1}{G}, \quad b_3 = \frac{a_3 V_0^2}{G}; \\
p &= p_0 \omega_n, \quad T = T_0 \omega_n; \\
\alpha &= \frac{G}{C_1 \omega_n}, \quad \gamma = \frac{G}{C_2 \omega_n} = 1.0; \\
\rho &= \frac{R}{R_n}, \quad R_n = \frac{V_0}{I_0}, \quad \beta = \frac{R_n}{L \omega_n}; \\
\varepsilon_1 &= \frac{\alpha R p}{R_1}, \quad \varepsilon_2 = \frac{R p}{R_2}, \quad \varepsilon_3 = \frac{\beta R_3 p}{R_n}.
\end{aligned} \tag{60}$$

Various single- or multi-switch control schemes are easily formulated by making respective ε_i zero/non-zero. For the computations to follow in this subsection, we set $\varepsilon_2 = \varepsilon_3 = 0$, $\varepsilon_1 = \varepsilon$, i.e., we only consider the single-switch case. Other switch-control schemes, such as, multi-switch, multi-pulse, and asynchronous control, will be considered within the context of a different example in Sec. 5.2.

5.1.2 Location of supercritical Hopf bifurcation

Let us rewrite Eq. (59) as

$$\frac{d}{dt} \begin{pmatrix} x \\ y \\ z \end{pmatrix} = \begin{pmatrix} -\alpha b_1 & \alpha & 0 \\ 1 & -1 & \rho \\ 0 & -\beta & 0 \end{pmatrix} \begin{pmatrix} x \\ y \\ z \end{pmatrix} + \begin{pmatrix} -b_3 \alpha x^3 \\ 0 \\ 0 \end{pmatrix} + \begin{pmatrix} -\varepsilon x \\ 0 \\ 0 \end{pmatrix} P_{p,T}(t). \quad (61)$$

For the moment let us fix the values of α, b_1, β and regard ρ as the parameter of bifurcation. Considering the autonomous part of Eq. (61), it follows from a straight-forward computation that, at

$$\rho_0 = -\frac{\alpha(b_1 - 1)(\alpha b_1 + 1)}{\beta} > 0, \quad (62)$$

the eigenvalues of the linear part of Eq. (61) are $\pm i\omega$ and $-(\alpha b_1 + 1)$ where

$$\omega^2 = -\alpha^2 b_1 (b_1 - 1) > 0. \quad (63)$$

Consequently, for a Hopf bifurcation to occur,

$$b_1 \in (0, 1). \quad (64)$$

Assuming Eq. (64) holds true, a generic Hopf bifurcation occur at $(x, y, z) = (0, 0, 0)$ for the autonomous system obtained by setting $\varepsilon = 0$ in Eq. (61) for $\rho = \rho_0$. As ρ changes passing ρ_0 , the origin becomes unstable, but a weakly stable periodic solution comes out of it. From this point on, all computations are performed at $\rho = \rho_0$.

To convert the linear part of Eq. (61) into the standard Jordan form we let

$$\begin{pmatrix} x \\ y \\ z \end{pmatrix} = \mathbf{P} \begin{pmatrix} \xi \\ \eta \\ \zeta \end{pmatrix} = \begin{pmatrix} 1 & \frac{\omega}{\alpha b_1} & -\alpha \\ 1 & 0 & 1 \\ 0 & -\frac{\beta}{\omega} & \frac{\beta}{\alpha b_1 + 1} \end{pmatrix} \begin{pmatrix} \xi \\ \eta \\ \zeta \end{pmatrix}. \quad (65)$$

In terms of the new variables ξ, η and ζ , Eq. (61) becomes

$$\begin{aligned} \frac{d\xi}{dt} &= \omega\eta - c_0 \left(\xi + \frac{\omega}{\alpha b_1} \eta - \alpha\zeta \right)^3 + \varepsilon \Phi_\xi P_{p,T}(t) \\ \frac{d\eta}{dt} &= -\omega\xi + c_0 \frac{\omega}{1 + \alpha b_1} \left(\xi + \frac{\omega}{\alpha b_1} \eta - \alpha\zeta \right)^3 + \varepsilon \Phi_\eta P_{p,T}(t) \\ \frac{d\zeta}{dt} &= -(\alpha b_1 + 1)\zeta + c_0 \left(\xi + \frac{\omega}{\alpha b_1} \eta - \alpha\zeta \right)^3 + \varepsilon \Phi_\zeta P_{p,T}(t) \end{aligned} \quad (66)$$

where

$$c_0 = \frac{\alpha b_3 (\alpha b_1 + 1)}{\alpha^2 b_1 + 2\alpha b_1 + 1} \quad (67)$$

and

$$\begin{aligned} \Phi_\xi &= -\frac{\alpha b_1 + 1}{\alpha^2 b_1 + 2\alpha b_1 + 1} \left\{ \xi + \frac{\omega}{\alpha b_1} \eta - \alpha\zeta \right\} \\ \Phi_\eta &= \frac{\omega}{\alpha^2 b_1 + 2\alpha b_1 + 1} \left\{ \xi + \frac{\omega}{\alpha b_1} \eta - \alpha\zeta \right\} \\ \Phi_\zeta &= -\frac{(\alpha b_1 + 1)}{\alpha^2 b_1 + 2\alpha b_1 + 1} \left\{ \xi + \frac{\omega}{\alpha b_1} \eta - \alpha\zeta \right\}. \end{aligned} \quad (68)$$

5.1.3 Normal form and the twist constant

We now compute the central manifold and the normal form. Let

$$\zeta = h_2(\xi, \eta) + h_3(\xi, \eta) + \dots \quad (69)$$

be the central manifold at $\xi = \eta = \zeta = 0$ where h_i are the terms of degree i . Because the starting nonlinear term in Eq. (66) is of degree three, we have

$$h_2(\xi, \eta) = 0. \quad (70)$$

So in computing the normal form we can practically regard the central manifold as $\zeta = 0$. If we define $z = \xi + i\eta$, then

$$\xi = \frac{1}{2}(z + \bar{z}), \quad \eta = \frac{1}{2i}(z - \bar{z}). \quad (71)$$

We set $\zeta = 0$ in Eq. (66), to obtain

$$\frac{dz}{dt} = -\omega iz + \frac{1}{8}c_0(-1 + i\frac{\omega}{1 + \alpha b_1})(z + \bar{z} - \frac{\omega}{\alpha b_1}(z - \bar{z})i)^3. \quad (72)$$

Note that k_1 is the coefficient in front of $z^2\bar{z}$. Thus we have

$$k_1 = c_1[1 + 2\alpha b_1 - \alpha - \frac{\omega}{\alpha b_1}(1 + 2\alpha b_1)i] \quad (73)$$

where

$$c_1 = \frac{-3c_0}{8b_1(1 + \alpha b_1)}. \quad (74)$$

Hence the twist constant

$$\tau := \left| \frac{Im(k_1)}{Re(k_1)} \right| = \left| \frac{\omega(1 + 2\alpha b_1)}{\alpha b_1(1 + 2\alpha b_1 - \alpha)} \right|. \quad (75)$$

For the stability of the limit cycle, we must have $Re(k_1) < 0$ yielding

$$\frac{-3\alpha b_3}{8b_1(\alpha^2 b_1 + 2\alpha b_1 + 1)}[1 + 2\alpha b_1 - \alpha] < 0. \quad (76)$$

Then, for a supercritical Hopf limit cycle to occur, we must have

$$\begin{aligned} b_1 &> \frac{\alpha - 1}{2\alpha}, \quad \text{if } b_3 > 0 \\ b_1 &< \frac{\alpha - 1}{2\alpha}, \quad \text{if } b_3 < 0. \end{aligned} \quad (77)$$

Note that b_1 must also satisfy $b_1 \in (0, 1)$ for Eq. (63) to hold.

5.1.4 The function $\phi(\theta)$ and the existence of rank one chaos

The function $\phi(\theta)$ is computed by first setting $\zeta = 0$ in Φ_ξ and Φ_η to obtain

$$\begin{aligned}\Phi_\xi &= -\frac{\alpha b_1 + 1}{\alpha^2 b_1 + 2\alpha b_1 + 1} \left\{ \xi + \frac{\omega}{\alpha b_1} \eta \right\} \\ \Phi_\eta &= \frac{\omega}{\alpha^2 b_1 + 2\alpha b_1 + 1} \left\{ \xi - \frac{\omega}{\alpha b_1} \eta \right\}.\end{aligned}\tag{78}$$

We then set $\xi = \cos \theta, \eta = \sin \theta$ and

$$\begin{aligned}\phi(\theta) &= \cos \theta \Phi_\xi + \sin \theta \Phi_\eta \\ &= c_2 \left\{ \cos^2 \theta + \frac{\omega}{\alpha b_1 (\alpha b_1 + 1)} \cos \theta \sin \theta + \frac{\alpha(b_1 - 1)}{\alpha b_1 + 1} \sin^2 \theta \right\}\end{aligned}\tag{79}$$

where

$$c_2 = -\frac{\alpha b_1 + 1}{\alpha^2 b_1 + 2\alpha b_1 + 1}.$$

It is easy to verify from Eq. (79) that $\phi(\theta)$ is a Morse function.

To apply Theorem 4 of Sec. 4, we first identify the values of parameters around which we have a generic supercritical Hopf bifurcation with a large twist constant. Let $\alpha, \beta, \gamma, \rho, b_1, b_3$ be the parameters of the autonomous part of Eq. (61), and p, ε, T be the parameters of the periodic forcing in Eq. (61). We fix the values of all parameters except T as follows:

- (i) *Parameter values for Hopf bifurcation:* $b_3 \neq 0$, $\beta > 0$, $\alpha > 1$ are arbitrarily fixed, and ρ is around $\rho_0 = -\frac{\alpha(b_1-1)(\alpha b_1+1)}{\beta}$.
- (ii) *Strong shearing:* choose $b_1 \in (0, 1)$ sufficiently close to $b_1 = \frac{\alpha-1}{2\alpha}$ either from above or below depending on the sign of b_3 (see Eq. (77) for stability criterion).
- (iii) *Parameters of forcing:* p, ε and T are such that $p \ll \varepsilon \ll 1$, $T \gg |\rho - \rho_0|^{-1}$.

Then we have

Proposition 5.1 *Let the values of parameters $(\alpha, \beta, \rho, b_1, b_3)$ and p, ε be fixed as in the above, and F_T be the time- T map for Eq. (61). Then there exists a positive measure set Δ for T such that $F_T, T \in \Delta$ has an attractor Λ satisfying (i) There exists an open neighborhood U of Λ , such that F_T admits no periodic sinks in U ; (ii) Λ admits an ergodic SRB measure, with respect to which Lebesgue almost every point in U is generic.*

This proposition is a direct corollary of Theorem 4 of Sec. 4. It establishes rank one chaos as an observable phenomenon in both the parameter and the phase spaces.

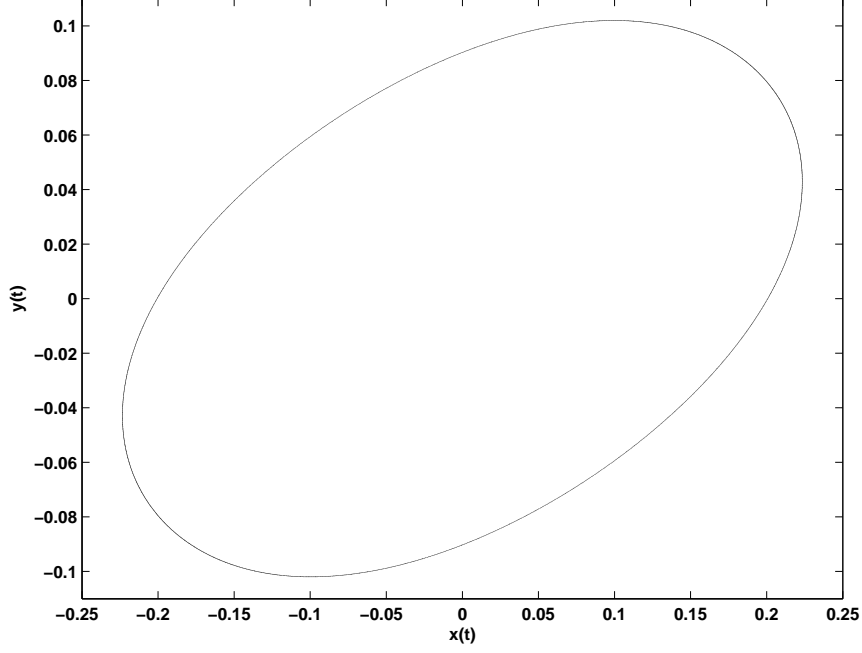


Figure 21: A Hopf limit cycle from smooth Chua's circuit ($\varepsilon = 0$).

5.1.5 Numerical simulations

In this subsection we present results of numerical simulations for the switch-controlled smooth Chua's circuit of Sec. 5.1. Proposition 5.1 serves not only as a theoretical assurance, but also as a practical guidance in searching for rank one chaos in numerical simulations. Simulation results presented in this subsection are in perfect match with the theories of Secs. 3 and 4. Our simulations are performed using the fourth-order Runge-Kutta routine starting at $t_0 = 0^+$.

In what follows, one orbit that is close to the attracting set of the time- T map for Eq. (61) is plotted in each picture. For all pictures presented, we keep $\alpha = 2$, $\beta = 2$, $b_3 = -1$, $|\rho - \rho_0| = 0.005$ and experiment with ε , b_1 , and T . With the choices of these parameter values we are close to a Hopf bifurcation. The magnitude of the twist constant is adjusted through b_1 . Since the values of α and β are already fixed, b_1 also determines the value of ρ_0 .

For Fig. 21, we set $\varepsilon = 0$ and $b_1 = 0.242$ for which $\rho_0 = 1.119872$. The value of T is irrelevant. What is depicted in Fig. 21 is the limit cycle emerging from the center of a Hopf bifurcation for the autonomous part of Eq. (61).

A. Case of small L . We now set $\varepsilon > 0$ and consider the case of small L . Recall that $L = \varepsilon \left| \frac{Im(k_1)}{Re(k_1)} \right|$ and, for the values chosen above, i.e., $\alpha = 2$, $\beta = 2$, $b_1 = 0.242$, we have

$$\left| \frac{Im(k_1)}{Re(k_1)} \right| = 108.84 \quad (80)$$

The graph of $\left| \frac{Im(k_1)}{Re(k_1)} \right|$ as a function of b_1 is depicted in Fig. 22.

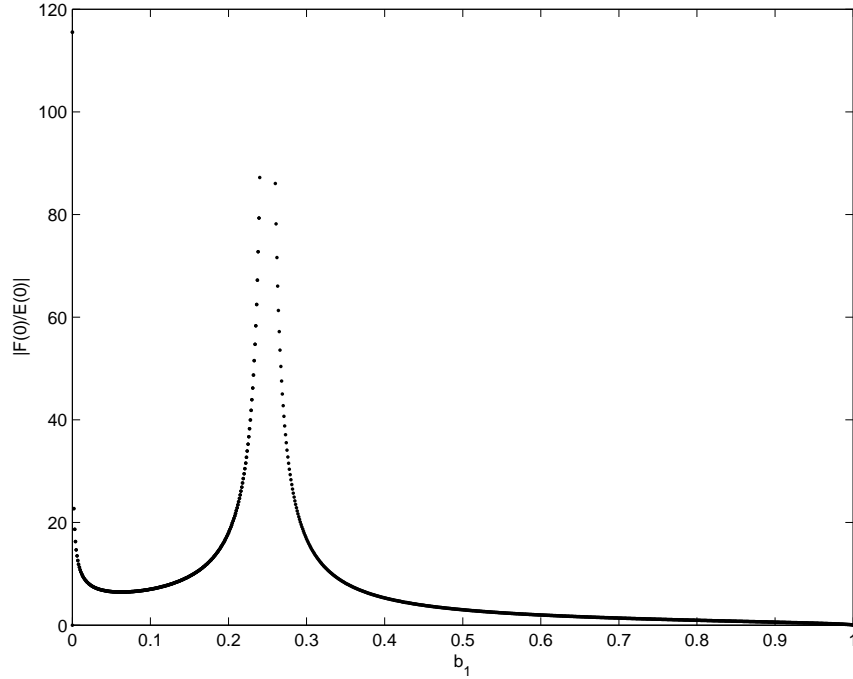


Figure 22: Twist constant as a function of b_1 (Eq. (75)).

Figure 23 is for the case where L is small. It is obtained by letting $\varepsilon = 0.03$, $T = 107$ with α, b_3, ρ, b_1 being the same as those chosen for Fig. 21. In this case $L \approx 3.26$ is not strong enough to create expansion against the strength of attraction so there is no rank one chaos. In Figs. 23-27, part (a) (top) is the plot of an orbit of the time- T map on the $x - y$ plane; part (b) (bottom left) is the plot of the x -coordinate of this orbit versus discrete time k ; and part (c) (bottom right) the frequency spectrum of the x -coordinate for the orbit plotted.

B. Case of larger L . We now move to the parameter values for which strange attractors are observable. For this we surely want ε larger. On the other hand, to make the orbit of interest stay in a reasonably small neighborhood of the center of the associated Hopf bifurcation, ε should be kept appropriately small. To balance these considerations, we set $\varepsilon = 0.2$, which serves our purpose well. For Fig. 24, we set $\varepsilon = 0.2$, $T = 107$, and adjust $|L|$ by varying b_1 . The size of $|L|$ is determined now by the distance of b_1 from 0.25 (refer again to Fig. 22). For $b_1 = 0.246$, Fig. 24 shows an observable strange attractor. In this case $L \approx 43.4$

For the remaining figures of this subsection (Figs. 25-27) we follow a different venue by keeping $\alpha = 2$, $\beta = 2$, $b_3 = -1$, $b_1 = 0.246$ ($\rho_0 = 1.119968$) and varying T to show the existences of periodic sinks and strange attractors with regards to T as the parameter of the system. Fig. 25 is obtained for $T = 106.5$ where the visible part of the attractor is a periodic sink. Another strange attractor is obtained for $T = 106.8$ as depicted in Fig. 26. Figure 27 is another

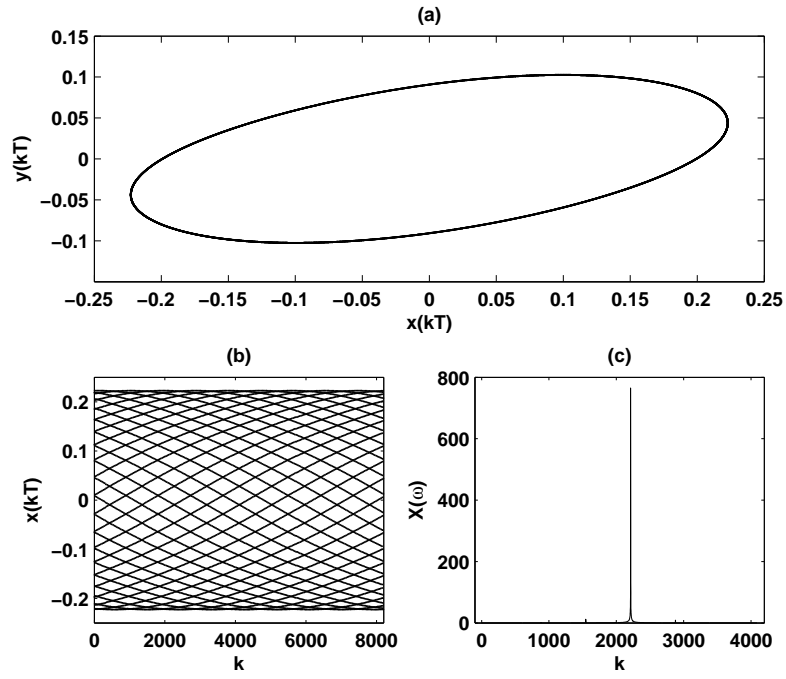


Figure 23: Limit cycle not broken for $(T = 107, \varepsilon = 0.03)$.

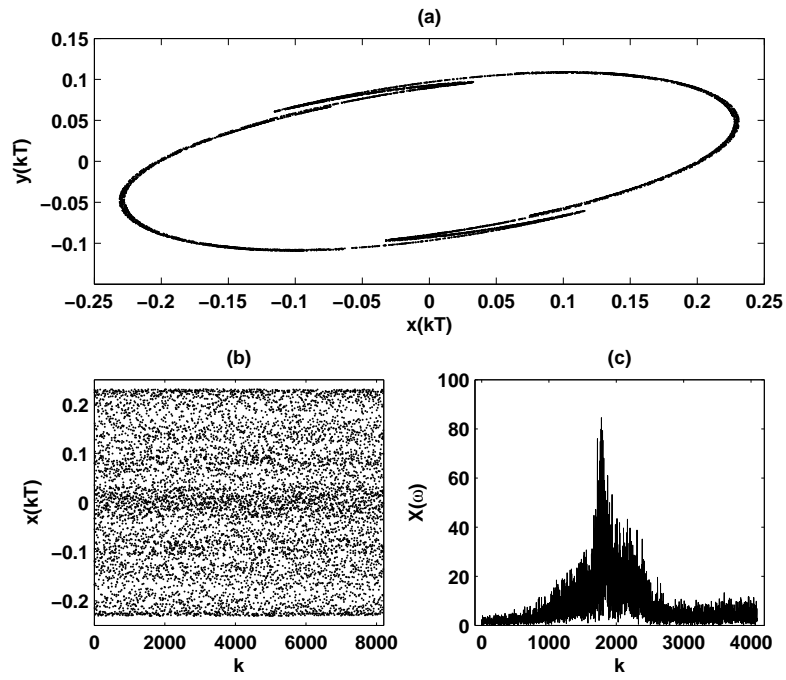


Figure 24: A strange attractor from smooth Chua's circuit for $T = 107, \varepsilon = 0.2$.

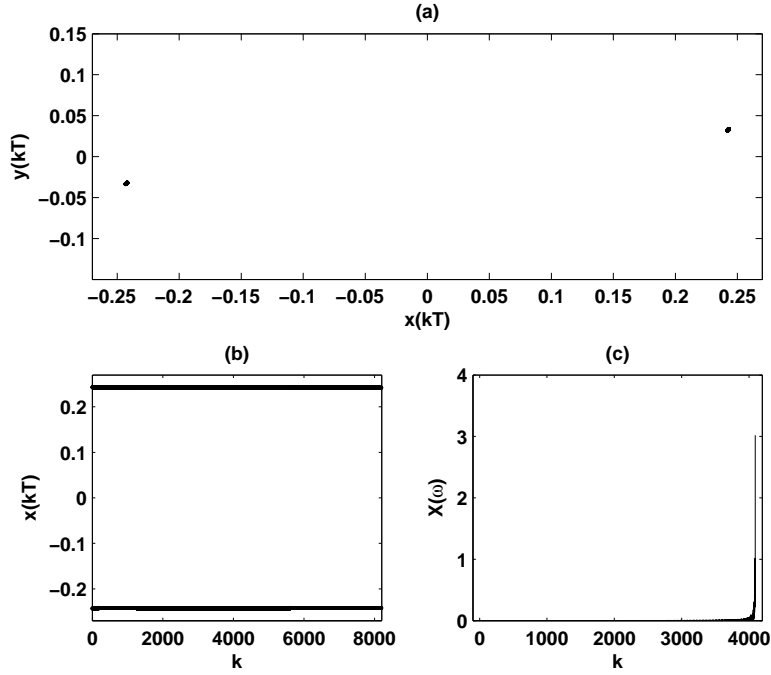


Figure 25: A periodic sink from smooth Chua's circuit for $T = 106.5$, $\varepsilon = 0.2$.

example of a periodic sink for $T = 107.5$. Note that, in the plot of $x(kT)$ versus k in Figs. 25 and 27, the number of horizontal lines represents the period of the periodic sink plotted. Chaotic attractors occur more frequently as b_1 approaches to 0.25. This is consistent with the predictions of the theory. Figures 25-27 also confirm our earlier claim that periodic sinks and chaotic attractors are the two main dynamical scenarios competing in the space of parameters.

In summary, when the smooth Chua's system undergoing a generic Hopf bifurcation is subjected to periodic kicks, rank one chaos occurs if the value of twist constant is sufficiently large. The results of our numerical simulations are in perfect agreement with the theoretical predictions of Secs. 3 and 4. Periodic sinks and rank one chaos are the two main competing dynamical scenarios, and the dynamical behavior of the time-T maps are similar to that of $T_{a,b,L}$ numerically studied in Sec. 2.2.

5.2 Multiple switches and asynchronous kicks

In this subsection we extend the scheme of Fig. 19 to those of multi-pulse and asynchronous switch control. The multi-pulse scheme refers to controlling the switches by a periodic signal of multiple pulses. Asynchronous control refers to the application of the control pulses to the switches at different times. This approach is depicted in Fig. 28.

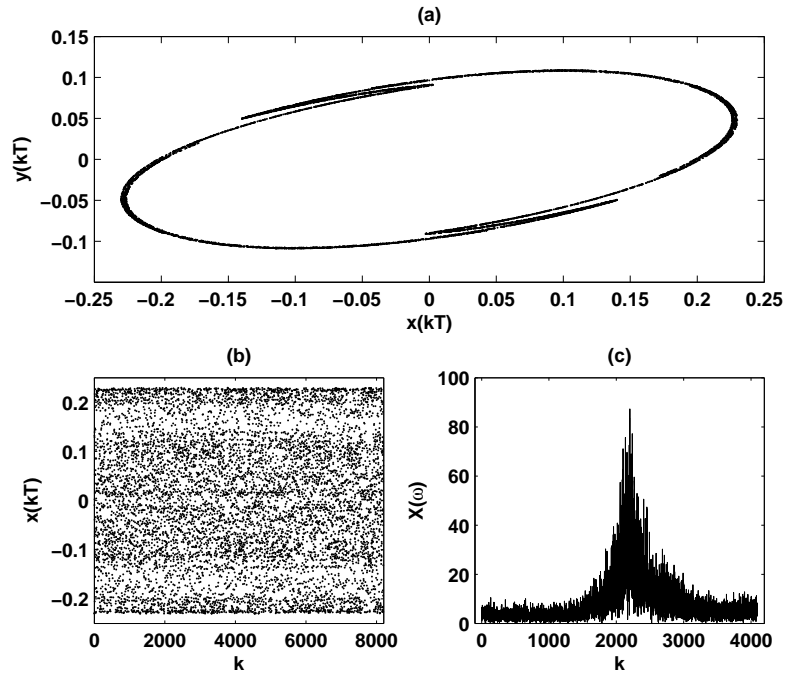


Figure 26: A strange attractor from smooth Chua's circuit for $T = 106.8$, $\varepsilon = 0.2$.

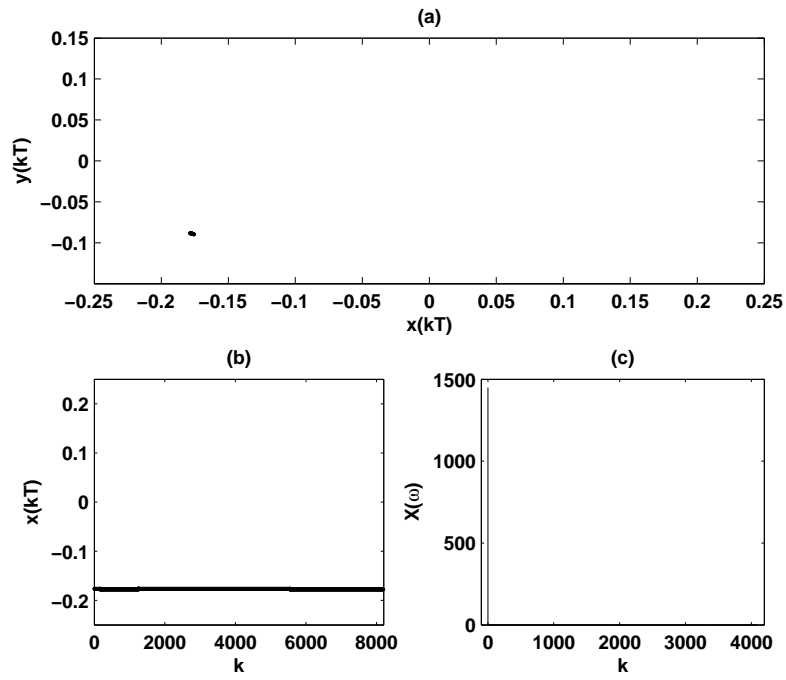


Figure 27: A periodic sink from smooth Chua's circuit for $T = 107.5$, $\varepsilon = 0.2$.

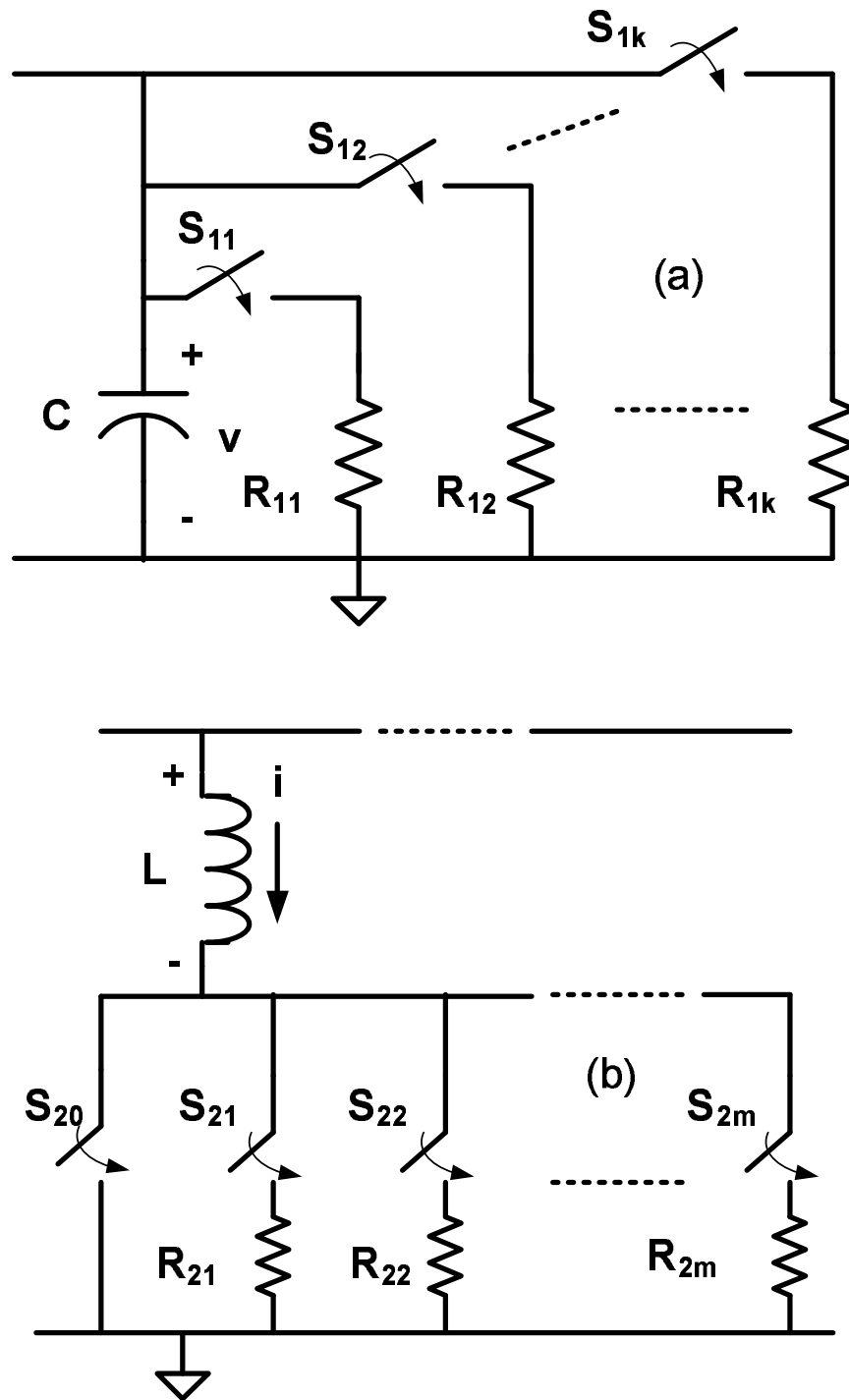


Figure 28: A switch control scheme for employing multiple kicks of different magnitude.

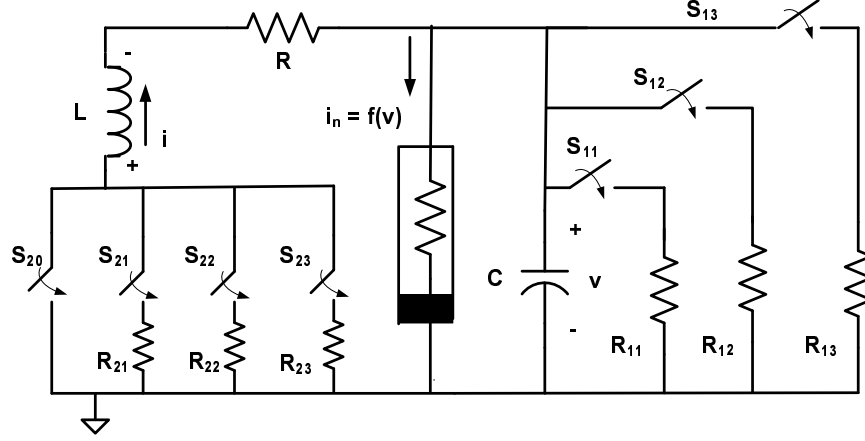


Figure 29: Switch-controlled MLC circuit based on different magnitude, multi-pulse control scheme.

The system we study in this subsection is the switch-controlled MLC (Murali-Lakshmanan-Chua) circuit [Murali *et al.*, 1994b] as shown in Fig. 29. Note that Fig. 29 employs a three-pulse switch control scheme. By choosing different values for the resistors R_{jk} , each resulting pulse can have a different magnitude. We denote the switches of Fig. 29 as S_{1k} , S_{20} and S_{2k} , $k = 1, 2, 3$. Let s_{1k} , s_{2k} , $k = 1, 2, 3$ be the times at which S_{1k} and S_{2k} are to be turned on, respectively. Note that S_{20} is closed whenever all S_{2k} , $k \neq 0$ are open. We assume that each periodic pulsetrain has the same period T_0 , and the pulsewidth p_0 . For $k = 1, 2, 3$, S_{1k} is closed for $s_{1k} + nT_0 \leq t < s_{1k} + nT_0 + p_0$ (ON time), and is open elsewhere (OFF time) within a single period. Similarly, S_{2k} is closed for $s_{2k} + nT_0 \leq t < s_{2k} + nT_0 + p_0$ (ON time), and is open elsewhere (OFF time). We also assume that at any given time there is at most one switch (discounting the default switch S_{20} , of course) that is turned on.

5.2.1 Derivation of equations

From Fig. 29, we have for $k = 1, 2, 3$,

$$\begin{aligned} C \frac{dv}{dt} &= i - f(v) - G_{1k}v \\ L \frac{di}{dt} &= -v - Ri \end{aligned} \quad (81)$$

if S_{1k} is turned on, and

$$\begin{aligned} C \frac{dv}{dt} &= i - f(v) \\ L \frac{di}{dt} &= -v - Ri - R_{2k}i \end{aligned} \quad (82)$$

if S_{2k} is turned on. If all switches (except S_{20}) are turned off, then

$$\begin{aligned} C \frac{dv}{dt} &= i - f(v) \\ L \frac{di}{dt} &= -v - Ri. \end{aligned} \quad (83)$$

Putting these equations together and assuming a three-pulse control signal, we obtain

$$\begin{aligned} C \frac{dv}{dt} &= i - f(v) - v \sum_{k=1}^3 \sum_{n=0}^{\infty} G_{1k} F_{n,T_0,p_0,s_{1k}}(t) \\ L \frac{di}{dt} &= -v - Ri - i \sum_{k=1}^3 \sum_{n=0}^{\infty} R_{2k} F_{n,T_0,p_0,s_{2k}}(t) \end{aligned} \quad (84)$$

where

$$F_{n,T_0,p_0,s_{jk}}(t) = \begin{cases} 1 & s_{jk} + nT_0 \leq t < s_{jk} + nT_0 + p_0 \\ 0 & \text{elsewhere.} \end{cases} \quad (85)$$

By setting

$$x = \frac{v}{V_0}, \quad y = \frac{i}{I_0}, \quad t \rightarrow \frac{t}{\omega_n},$$

we obtain the following dimensionless set of equations

$$\begin{aligned} \frac{dx}{dt} &= \alpha[y - h(x)] - x \sum_{k=1}^3 \varepsilon_{1k} P_{T,p,d_{1k}}^{(1)} \\ \frac{dy}{dt} &= -\beta[x + \gamma y] - y \sum_{k=1}^3 \varepsilon_{2k} P_{T,p,d_{2k}}^{(2)} \end{aligned} \quad (86)$$

where

$$\begin{aligned} P_{T,p,d_{jk}}^{(j)} &= \frac{1}{p} \sum_{n=0}^{\infty} F_{n,T,p,d_{jk}}; \\ d_{1k} &= s_{1k}\omega_n, \quad d_{2k} = s_{2k}\omega_n; \\ p &= p_0\omega_n, \quad T = T_0\omega_n, \quad R_n = \frac{V_0}{I_0}; \\ h(x) &= b_1x + b_2x^2 + b_3x^3, \quad b_m = a_m R_n V_0^{m-1}; \\ \alpha &= \frac{1}{R_n C \omega_n}, \quad \beta = \frac{R_n}{L \omega_n}, \quad \gamma = \frac{R}{R_n}; \\ \varepsilon_{1k} &= \frac{\alpha R_n p}{R_{1k}}, \quad \varepsilon_{2k} = \frac{\beta R_{2k} p}{R_n} \end{aligned} \quad (87)$$

for $j = 1, 2, k, m = 1, 2, 3$. The general form of the resulting periodic pulsetrain in Eq. (86) for one period is depicted in Fig. 30.

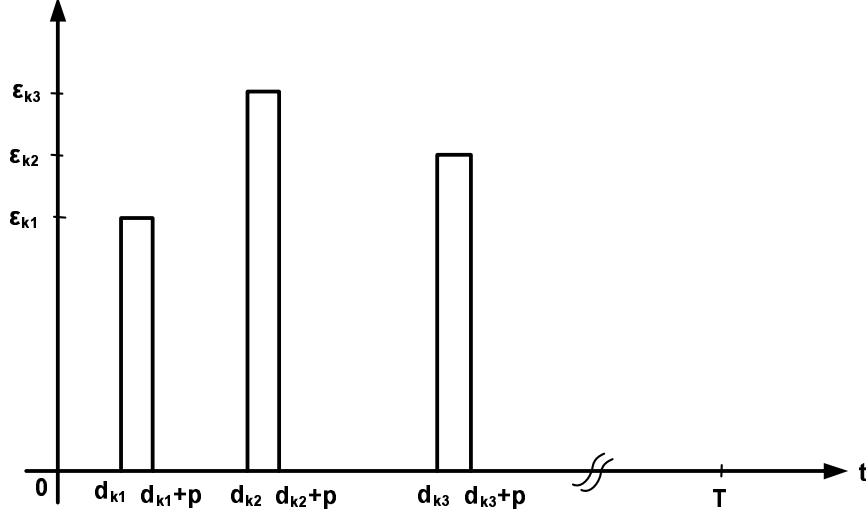


Figure 30: Periodic pulsetrain with multiple kicks of different magnitude.

5.2.2 Hopf bifurcations and normal form

Let us observe that the theory of Sec. 4.2 is established only for synchronized forcing of a single kick in one period. So by directly quoting Theorem 4, the existence of rank one chaos could only be rigorously established in the restricted context of the scheme of a synchronized single kick. In principle, however, the method of Sec. 4.2 should also apply to systems employing synchronized multiple kicks.

To apply Theorem 4 to the synchronized single kick setting we set in Eq. (86)

$$\begin{aligned} d_{1k} &= d_{2k} = 0, \quad k = 1, 2, 3 \\ \varepsilon_{1k} &= \varepsilon_{2k} = 0, \quad k = 2, 3. \end{aligned} \quad (88)$$

Equation (86) is now written as

$$\frac{d}{dt} \begin{bmatrix} x \\ y \end{bmatrix} = \begin{bmatrix} -\alpha b_1 & \alpha \\ -\beta & -\beta\gamma \end{bmatrix} \begin{bmatrix} x \\ y \end{bmatrix} + \begin{bmatrix} -b_2\alpha x^2 - b_3\alpha x^3 \\ 0 \end{bmatrix} + \varepsilon_{11} \begin{bmatrix} -x \\ -\frac{\varepsilon_{21}}{\varepsilon_{11}}y \end{bmatrix} P_{T,p,0}(t). \quad (89)$$

We fix the values of α, b_1, β and regard γ as a parameter of bifurcation. It follows from a straight forward computation that, at

$$\gamma_0 = -\frac{\alpha b_1}{\beta} > 0, \quad (90)$$

the eigenvalues of the linear part of Eq. (89) are purely imaginary, and a supercritical Hopf bifurcation occurs at $(x, y) = (0, 0)$ for the autonomous system. The eigenvalues of the linear part of Eq. (89) are $\sigma \pm i\omega$ with

$$\sigma = -\frac{1}{2}(\alpha b_1 + \beta\gamma), \quad \omega^2 = \alpha\beta - \frac{1}{4}(\alpha b_1 - \beta\gamma)^2. \quad (91)$$

From Eq. (91), we have at $\gamma = \gamma_0$,

$$\sigma = 0, \quad \omega^2 = \alpha(\beta - \alpha b_1^2) > 0 \quad (92)$$

which implies that

$$b_1 \in (-\sqrt{\frac{\beta}{\alpha}}, 0). \quad (93)$$

To convert the linear part of Eq. (89) into the standard Jordan form we let

$$\begin{bmatrix} x \\ y \end{bmatrix} = \begin{bmatrix} 1 & 0 \\ b_1 + \frac{\sigma}{\alpha} & -\omega/\alpha \end{bmatrix} \begin{bmatrix} \xi \\ \eta \end{bmatrix}. \quad (94)$$

In terms of the new variables ξ and η , Eq. (89) becomes

$$\begin{aligned} \frac{d\xi}{dt} &= \sigma\xi - \omega\eta - \alpha(b_2\xi^2 + b_3\xi^3) - \varepsilon_{11}\xi P_{T,p,0}(t) \\ \frac{d\eta}{dt} &= \omega\xi + \sigma\eta - \frac{\alpha(\sigma + \alpha b_1)}{\omega}(b_2\xi^2 + b_3\xi^3) + \varepsilon_{11}\left[\frac{\sigma + b_1\alpha}{\omega}\left(\frac{\varepsilon_{21}}{\varepsilon_{11}} - 1\right)\xi - \frac{\varepsilon_{21}}{\varepsilon_{11}}\eta\right]P_{T,p,0}(t). \end{aligned} \quad (95)$$

Next, we rewrite Eq. (95) in a complex variable $z = \xi + i\eta$ and derive a normal form for the autonomous part in z . From $z = \xi + i\eta$, $\bar{z} = \xi - i\eta$, we have

$$\xi = \frac{1}{2}(z + \bar{z}), \quad \eta = \frac{1}{2i}(z - \bar{z}). \quad (96)$$

We obtain from Eq. (95) that

$$\frac{dz}{dt} = (\sigma + i\omega)z - \frac{\alpha}{8}\left[1 + i\frac{\sigma + b_1\alpha}{\omega}\right][2b_2(z + \bar{z})^2 + b_3(z + \bar{z})^3]. \quad (97)$$

According to the standard normal form theory, there exists a change of variables near identity, which we write as

$$z = Z + c_2 Z^2 + c_3 Z^3 + \dots, \quad (98)$$

that transfers Eq. (97) to

$$\frac{dZ}{dt} = (\sigma + i\omega)Z + k_1 Z^2 \bar{Z} + \mathcal{O}(|Z|^5) \quad (99)$$

where the term $\mathcal{O}(|Z|^n)$ represents the terms of magnitude $< K|Z|^n$ in a sufficiently small neighborhood of $Z = 0$ for some constant K . Using the formula given in [Guckenheimer & Holmes, 1997, p. 155], we have

$$k_1 = \frac{i}{2\omega}(h_{zz}h_{z\bar{z}} - 2|h_{z\bar{z}}|^2 - \frac{1}{3}|h_{\bar{z}\bar{z}}|^2) + \frac{1}{2}h_{zz\bar{z}} \quad (100)$$

where, in our case,

$$\begin{aligned}
h_{zz} &= -\frac{\alpha b_2}{2} \left[1 + i \frac{\sigma + b_1 \alpha}{\omega} \right] \\
h_{z\bar{z}} &= -\frac{\alpha b_2}{2} \left[1 + i \frac{\sigma + b_1 \alpha}{\omega} \right] \\
h_{\bar{z}z} &= -\frac{\alpha b_2}{2} \left[1 + i \frac{\sigma + b_1 \alpha}{\omega} \right] \\
h_{zz\bar{z}} &= -\frac{3\alpha b_3}{4} \left[1 + i \frac{\sigma + b_1 \alpha}{\omega} \right]
\end{aligned} \tag{101}$$

are the normalized coefficients of the terms z^2 , $z\bar{z}$, $\bar{z}z$ and $zz\bar{z}$ on the right hand side of Eq. (97), respectively. By a straight forward computation, we obtain

$$\begin{aligned}
Re(k_1) &= -\frac{\alpha}{8\omega^2} [2\alpha^2 b_2^2 (b_1 + \sigma/\alpha) + 3b_3 \omega^2] \\
Im(k_1) &= -\frac{\alpha^2}{24\omega^3} [(b_1 + \sigma/\alpha)(9b_3 \omega^2 + 10\alpha^2 b_2^2 (b_1 + \sigma/\alpha)) + 4b_2^2 \omega^2].
\end{aligned} \tag{102}$$

5.2.3 Twist constant and rank one chaos

A periodic solution emerges from $Z = 0$ when the value of γ passes γ_0 in Eq. (89) provided that $Re(k_1) \neq 0$. This periodic solution is asymptotically stable if $Re(k_1) < 0$. Thus, from Eq. (102), we need

$$2\alpha^2 b_2^2 (b_1 + \sigma/\alpha) + 3b_3 \omega^2 > 0. \tag{103}$$

Note that we have, at $\gamma = \gamma_0$,

$$\begin{aligned}
Re(k_1) &= \frac{-\alpha}{8(\beta - \alpha b_1^2)} [2\alpha b_2^2 b_1 + 3b_3(\beta - \alpha b_1^2)] \\
Im(k_1) &= -\frac{\alpha^2}{24\omega(\beta - \alpha b_1^2)} [10\alpha^2 b_2^2 b_1^2 + (\beta - \alpha b_1^2)(4b_2^2 + 9b_1 b_3)],
\end{aligned} \tag{104}$$

and the stability condition of Eq. (103) becomes

$$2\alpha^2 b_2^2 b_1 + 3b_3 \alpha (\beta - \alpha b_1^2) > 0. \tag{105}$$

Let us also note that, at $\gamma = \gamma_0$ we have

$$\left| \frac{Im(k_1)}{Re(k_1)} \right| = \frac{\alpha}{3\omega} \left| \frac{[10\alpha^2 b_2^2 b_1^2 + (\beta - \alpha b_1^2)(4b_2^2 + 9b_1 b_3)]}{2\alpha b_2^2 b_1 + 3b_3(\beta - \alpha b_1^2)} \right|. \tag{106}$$

This ratio is the twist constant, the magnitude of which needs to be large for chaotic attractors to exist.

To apply Theorem 4 we also need to compute $\phi(\theta)$. Following the definition of Sec. 4.2 we have in this case

$$\begin{aligned}
\Phi_\xi &= -\xi \\
\Phi_\eta &= \frac{\sigma + b_1 \alpha}{\omega} \left(\frac{\varepsilon_{21}}{\varepsilon_{11}} - 1 \right) \xi - \frac{\varepsilon_{21}}{\varepsilon_{11}} \eta.
\end{aligned} \tag{107}$$

Let

$$\xi = \cos \theta, \quad \eta = \sin \theta. \quad (108)$$

We have

$$\begin{aligned} \phi(\theta) &= \cos \theta \Phi_\xi + \sin \theta \Phi_\eta \\ &= -\cos^2 \theta + \left(\frac{\sigma + \alpha b_1}{\omega} \right) \left(\frac{\varepsilon_{21}}{\varepsilon_{11}} - 1 \right) \cos \theta \sin \theta - \frac{\varepsilon_{21}}{\varepsilon_{11}} \sin^2 \theta. \end{aligned} \quad (109)$$

$\phi(\theta)$ is indeed a Morse function. We can now formulate a statement parallel to Proposition 5.1, the details of which we leave to the reader.

5.2.4 Numerical simulations

We now present a few new pictures of rank one chaos in the multi-switch-controlled MLC circuit. Again, our simulations are performed using the fourth-order Runge-Kutta routine starting at $t = 0$. For each picture presented, one discrete orbit starting near the attractor of the time-T map is plotted.

A. Initial Choice of Parameter Values. Computations performed earlier on the parameters of Hopf bifurcation and on the twist constant are instrumental for our choice of the parameter values below. Our main considerations are to be reasonably close to a point of supercritical Hopf bifurcation, and to have a relatively large twist constant.

- (1) The parameters $\alpha = 10, \beta = 1, \gamma = 0.99, b_1 = -0.1, b_2 = 1.165, b_3 = 1$ ($|\gamma - \gamma_0| = 0.01$) are fixed throughout. With these parameter values we are close to a Hopf bifurcation (appears at $\gamma_0 = 1$) with a relatively large twist constant (≈ 2850). There is nothing more that is intentional in our specification of these parameter values.
- (2) In all cases, we let p , the length of time the switches are on, be fixed at $p = 0.5$.
- (3) With the parameter values specified as above, the things left for us to vary at the moment are (i) the forcing period T , (ii) the magnitude of the kicks in one period (ε_{ik}), and (iii) the times at which the kicks are initiated (d_{ik}).
- (4) To further remove (3)(iii) from this list of uncertainties we set $d_{11} = 0, d_{12} = 50, d_{13} = 85, d_{21} = 25, d_{22} = 110, d_{23} = 130$ throughout. These specific choices for d_{ik} are rather arbitrary but the unevenness in the spacing of consecutive pulses is intentional.

The weakly stable limit cycle, obtained by setting all $\varepsilon_{ik} = 0$, is depicted in Fig. 31. This limit cycle is then kicked periodically to create various pictures of chaos. For the figures of this subsection, the following convention is adopted: For Figs. 32-40, part (a) (top) is the plot of an orbit of the time-T map on the $x - y$ plane; part (b) (middle left) is the plot of the x -coordinate of this orbit versus discrete time k ; part (c) (middle right) is the frequency spectrum

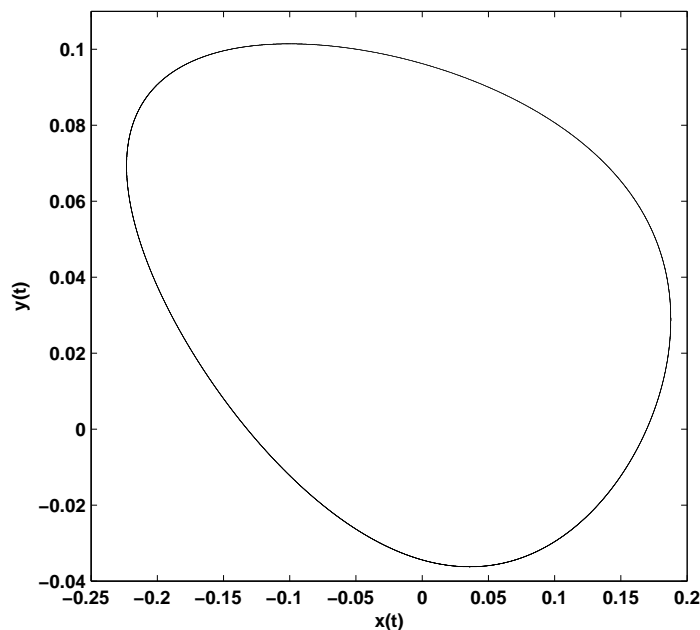


Figure 31: A Hopf limit cycle from MLC circuit.

of the x -coordinate for the orbit plotted; and part (d) (bottom) is the two-dimensional density function $z(x, y)$, which represents the SRB measure of the corresponding attractor. For Fig. 41, part (a) (top left) is the plot of an orbit of the time- T map on the $x - y$ plane; part (b) (top right) shows the locally magnified version of the indicated area in part (a); part (c) (middle left) is the plot of the x -coordinate of this orbit versus discrete time k ; part (d) (middle right) is the frequency spectrum of the x -coordinate for the orbit plotted; and part (e) (bottom) is the two-dimensional density function $z(x, y)$, which represents the SRB measure of the corresponding attractor.

B. Observable Chaos: Multiple Kicks of the Same Magnitude. For the simulations we now present, ε_{ik} is either 0.33 or 0. In this case the circuit is controlled by the simpler scheme of Fig. 19. We are free to take away any one of the six potential kicks by setting its corresponding magnitude to 0. Figures 32-37 are a set of pictures of chaotic attractors obtained by numerical simulations. These pictures are presented in the ascending order in the number of kicks involved (from one to six).

The geometric complexity of the chaotic attractors appears to increase as more kicks are employed within one period. Also, observe that, for the simulations presented above, the length of the last relaxation interval, i.e., the time from the last kick in one forcing period to the end of the same forcing period, is not very long. Consequently, the rank one character present in these pictures is not yet dominating.

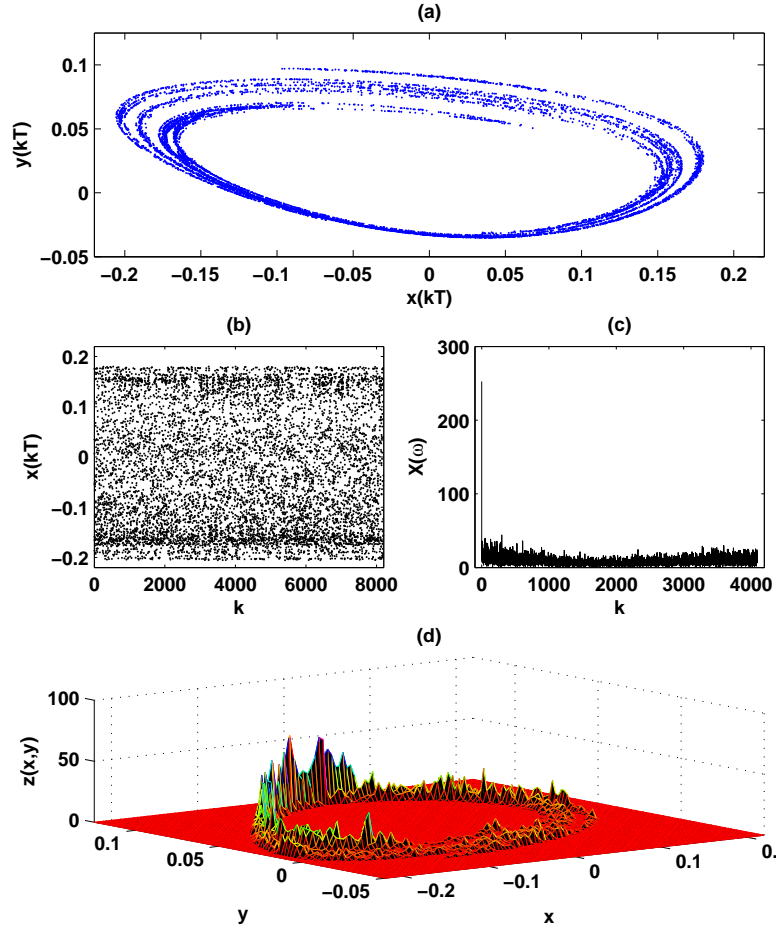


Figure 32: A strange attractor from MLC circuit for $T = 60$, and a single kick $\varepsilon_{11} = 0.33$.

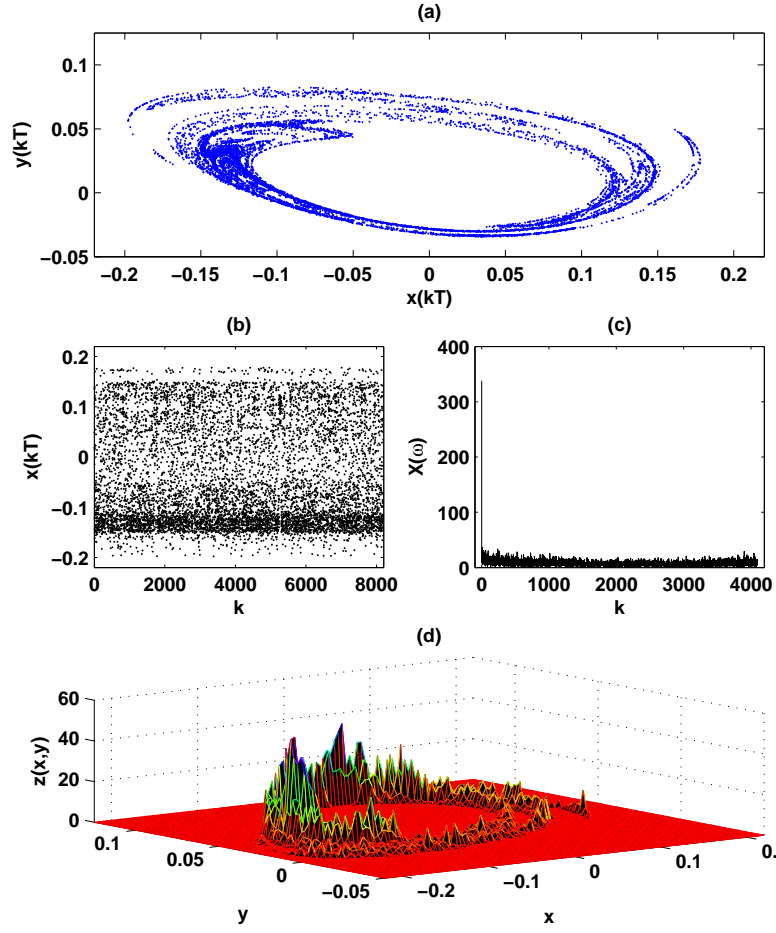


Figure 33: A strange attractor from MLC circuit for $T = 85$, and two kicks $\varepsilon_{11} = \varepsilon_{12} = 0.33$.

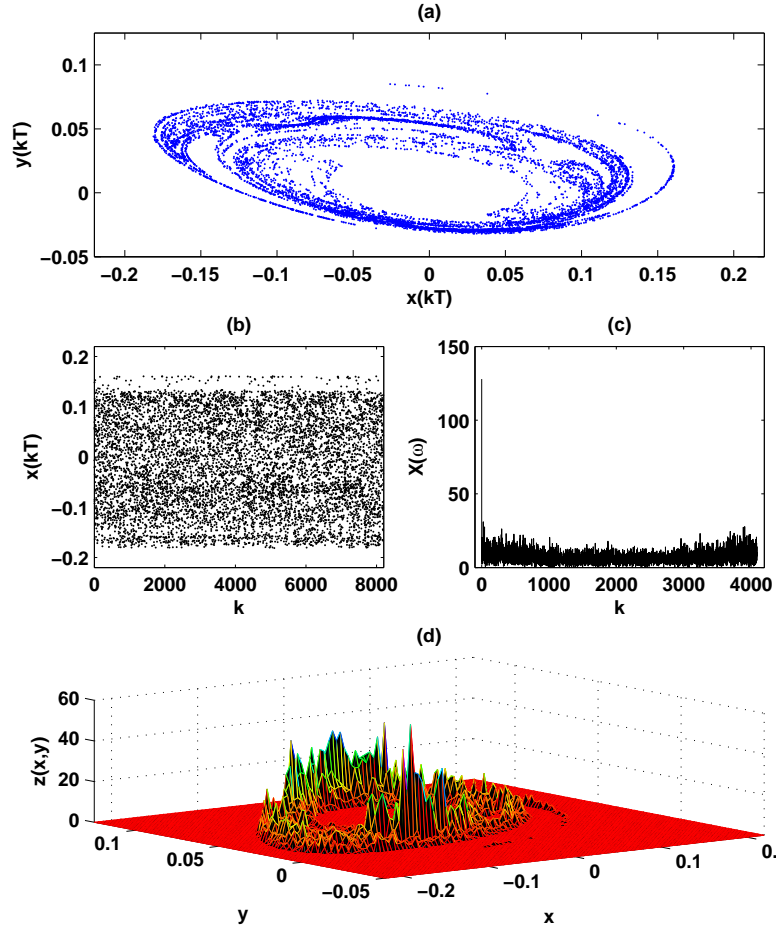


Figure 34: A strange attractor from MLC circuit for $T = 116$, and three kicks $\varepsilon_{11} = \varepsilon_{12} = \varepsilon_{13} = 0.33$.

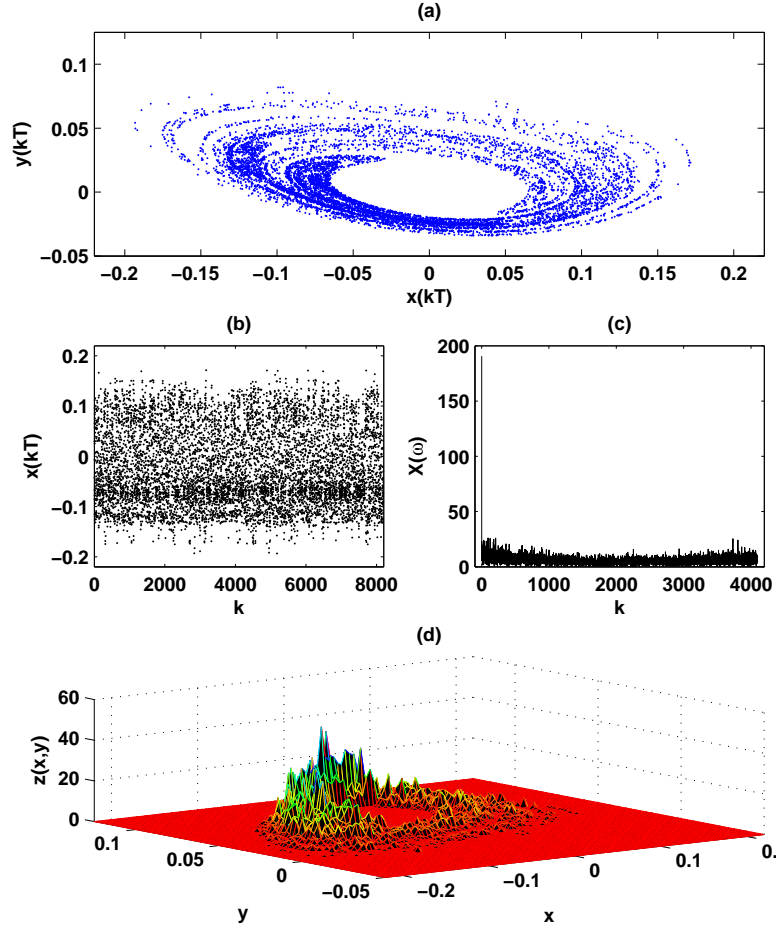


Figure 35: A strange attractor from MLC circuit for $T = 146.5$, and four kicks $\varepsilon_{11} = \varepsilon_{12} = \varepsilon_{13} = 0.33$, $\varepsilon_{21} = 0.33$.

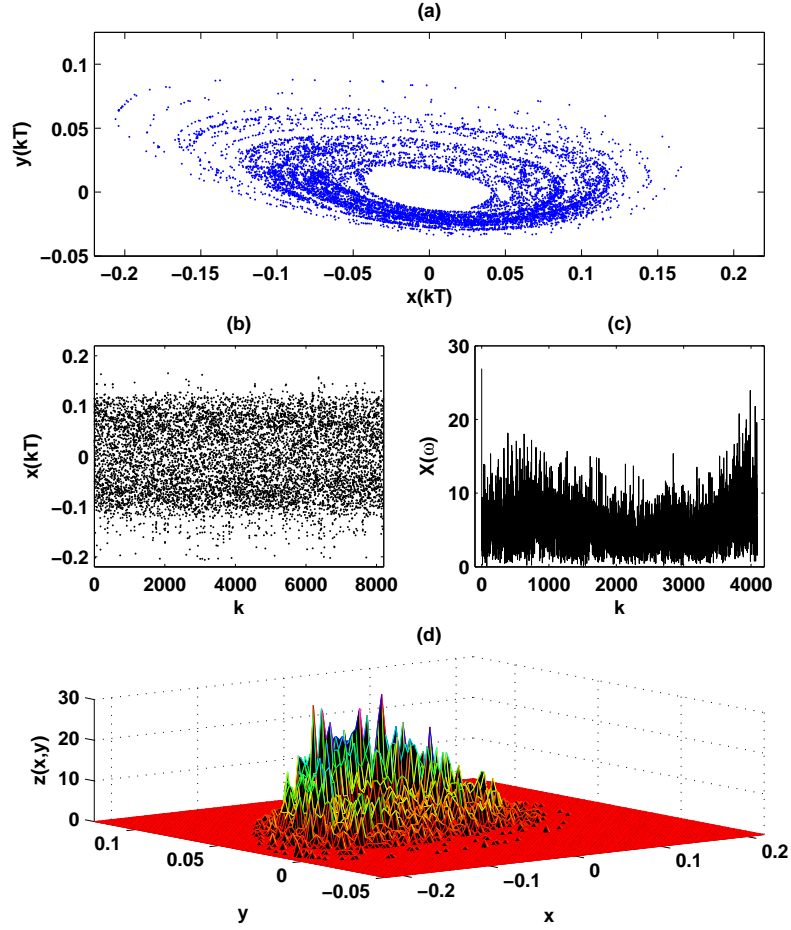


Figure 36: A strange attractor from MLC circuit for $T = 169.5$, and five kicks $\varepsilon_{11} = \varepsilon_{12} = \varepsilon_{13} = 0.33$, $\varepsilon_{21} = \varepsilon_{22} = 0.33$.

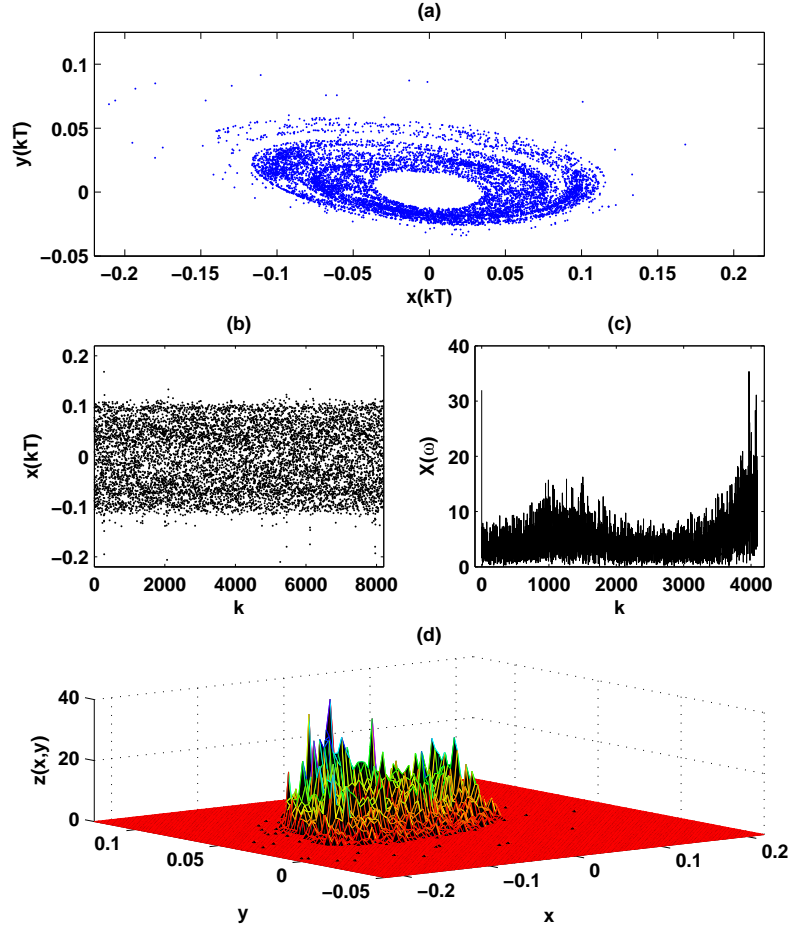


Figure 37: A strange attractor from MLC circuit for $T = 199$, and six kicks $\varepsilon_{ij} = 0.33$, $i = 1, 2$, $j = 1, 2, 3$.

C. Observable Chaos: Multiple Kicks of Varying Magnitudes. We now present pictures of chaotic attractors allowing multiple kicks of different magnitude. All parameters except ε_{ik} and T are the same as before. We set $\varepsilon_{1k} = 0.22$, $\varepsilon_{2k} = 0.12$, $k = 1, 2, 3$ and $T = 160$ for Fig. 38. Here the circuit is controlled by two switches according to the scheme of Fig. 28, each admitting three pulses in one forcing period. To adjust ε_{1k} and ε_{2k} we adjust the values of R_1 and R_2 in Fig. 28 as given by Eq. (87). For Fig. 39, we use $\varepsilon_{11} = \varepsilon_{13} = 0.12$, $\varepsilon_{12} = 0.52$, $\varepsilon_{2k} = 0.22$, $k = 1, 2, 3$ and $T = 169$. And for Fig. 40, we use $\varepsilon_{11} = 0.32$, $\varepsilon_{12} = 0.52$, $\varepsilon_{13} = 0.12$, $\varepsilon_{21} = 0.22$, $\varepsilon_{22} = 0.32$, $\varepsilon_{23} = 0.42$ and $T = 218$. The differences in these two pictures are caused by varying magnitudes of the control pulses. These pictures do indicate that utilizing kicks of varying magnitudes does contribute to the generation of chaotic attractors of interesting geometric structure.

Note that in favor of getting chaotic pictures of complicated structure, so far the forcing periods are intentionally set short to minimize the compressing effect in the radial direction. By making T larger, rank one character for these chaotic attractors can be made more dominating. Figure 41 is an example of a truly rank one strange attractor. This is obtained by setting $\varepsilon_{ij} = 0.32$, $i = 1, 2$ $j = 1, 2, 3$ and $T = 468$. With a very long relaxation period ($T = 468$) the attractor of Fig. 41(a) is pressed down in the radial direction, getting the look of a simple curve. However, this is a picture of a chaotic attractor, the complexity of which is illustrated through Fig. 41(b),(c), (d) and (e).

It is important to note that the two-dimensional density function $z(x, y)$ in each of Figs. 32-41 reflects the SRB measure for its respective attractor shown in part (a) of each figure.

5.3 Non-Hopf periodic solutions

Around supercritical Hopf bifurcations, the combined effect of forcing, shearing and attraction is represented by $L = \varepsilon \left| \frac{Im(k_1)}{Re(k_1)} \right|$, a number that can be analytically computed. For the more general setting of Sec. 4.1, analytic computation of similar quantities does not appear feasible. However, to be restricted to the setting of a Hopf bifurcation is to impose serious restrictions in practical implementations. In order to have a generic supercritical Hopf bifurcation, local nonlinearity is a necessity. For instance, in Sec. 5.1, a cubic nonlinearity for the nonlinear resistor characteristics is used in the Chua's circuit, replacing the original piecewise linear design that is much easier to implement in practice. Moreover, being restricted to a small neighborhood of some tiny Hopf limit cycle might very well be a serious drawback in terms of practical implementations and detections of rank one attractors.

In this subsection we explore the possibility of using the original *piecewise linear* Chua's circuit of Fig. 20 to generate rank one attractors by following mainly the work in [Wang & Oksasoglu, 2007]. For simplicity, we only use one switch. By the piecewise linear character, generic Hopf bifurcations do not exist.

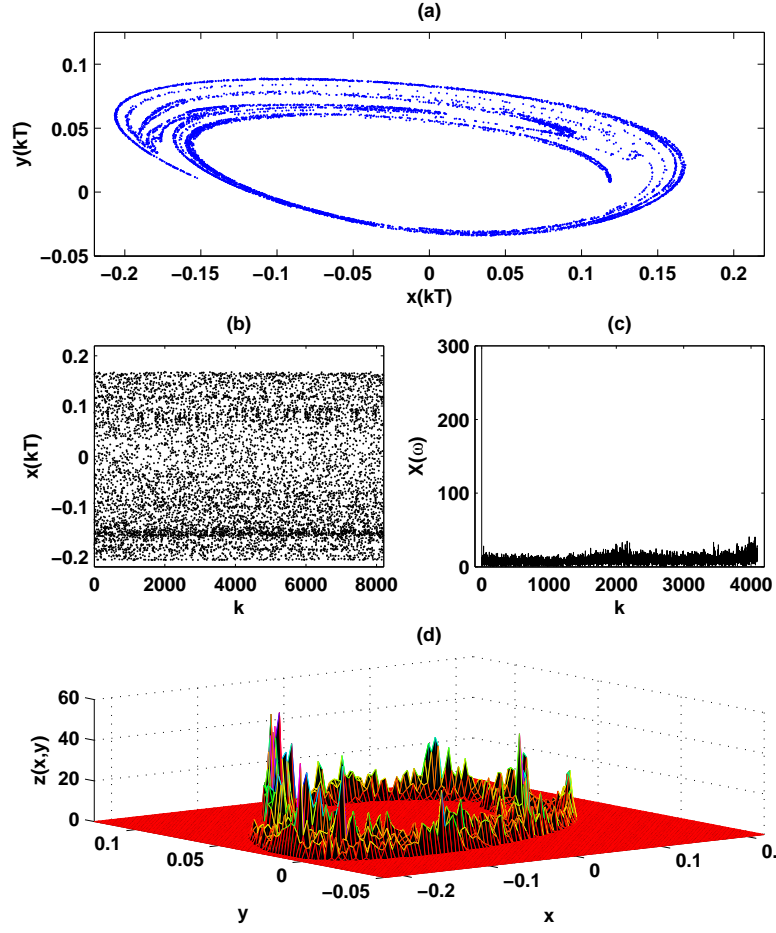


Figure 38: A strange attractor from MLC circuit for $T = 160$, $\varepsilon_{1j} = 0.22$, $\varepsilon_{2j} = 0.12$, $j = 1, 2, 3$.

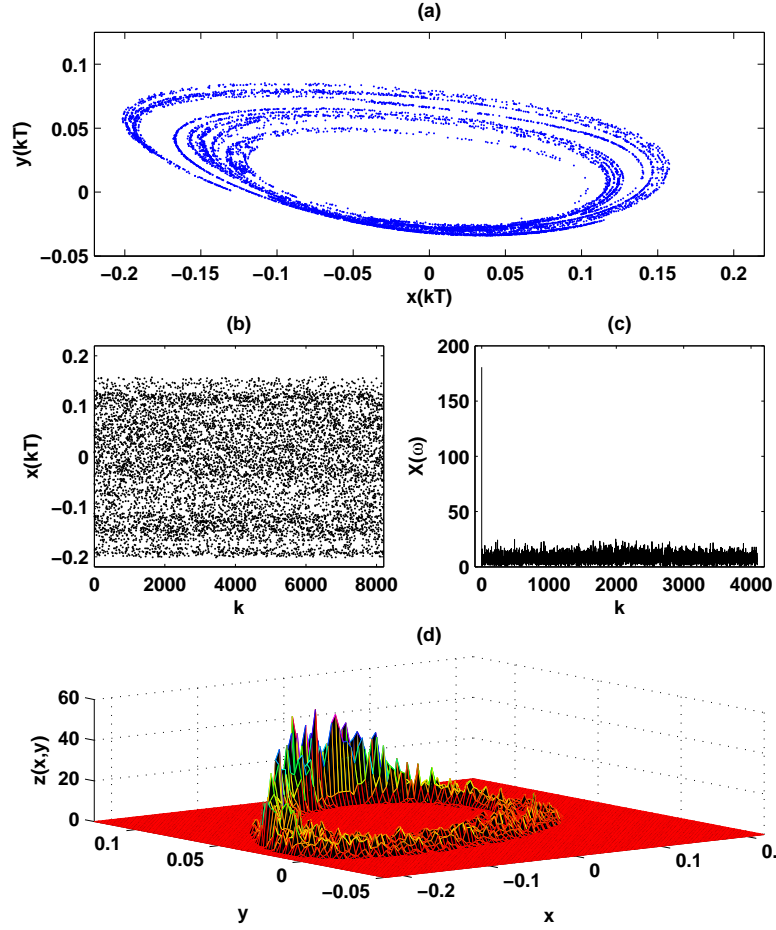


Figure 39: Strange attractor for $T = 169$, $\varepsilon_{11} = \varepsilon_{13} = 0.12$, $\varepsilon_{12} = 0.52$, $\varepsilon_{2j} = 0.22$, $j = 1, 2, 3$.

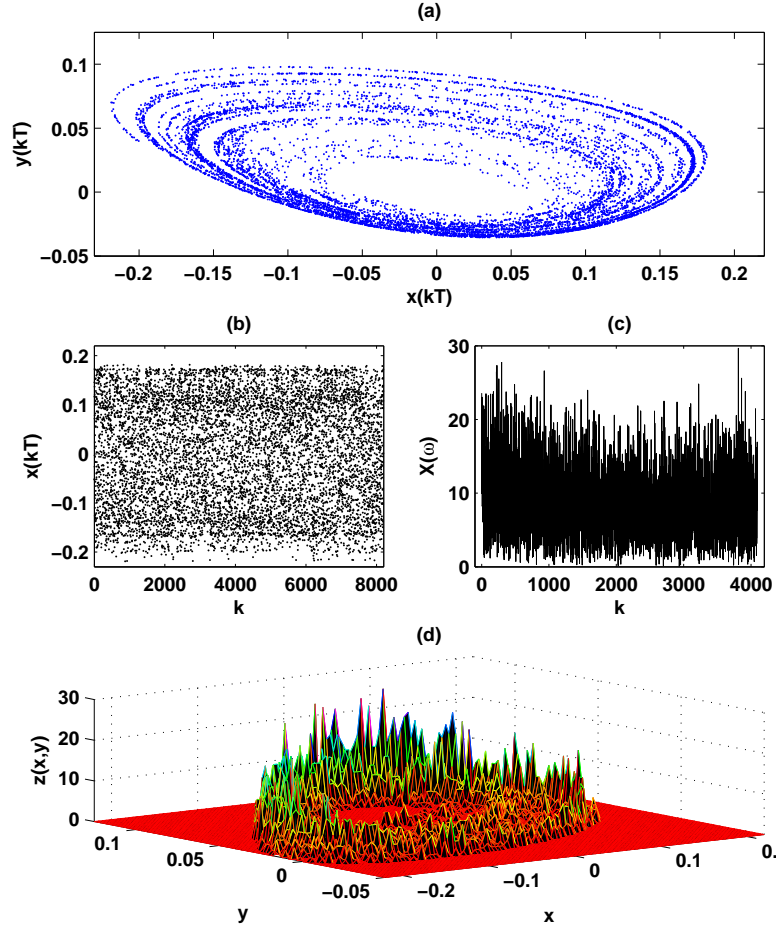


Figure 40: A strange attractor from MLC circuit for $T = 218$, $\varepsilon_{11} = 0.32$, $\varepsilon_{12} = 0.52$, $\varepsilon_{13} = 0.12$, $\varepsilon_{21} = 0.22$, $\varepsilon_{22} = 0.32$, $\varepsilon_{23} = 0.42$.

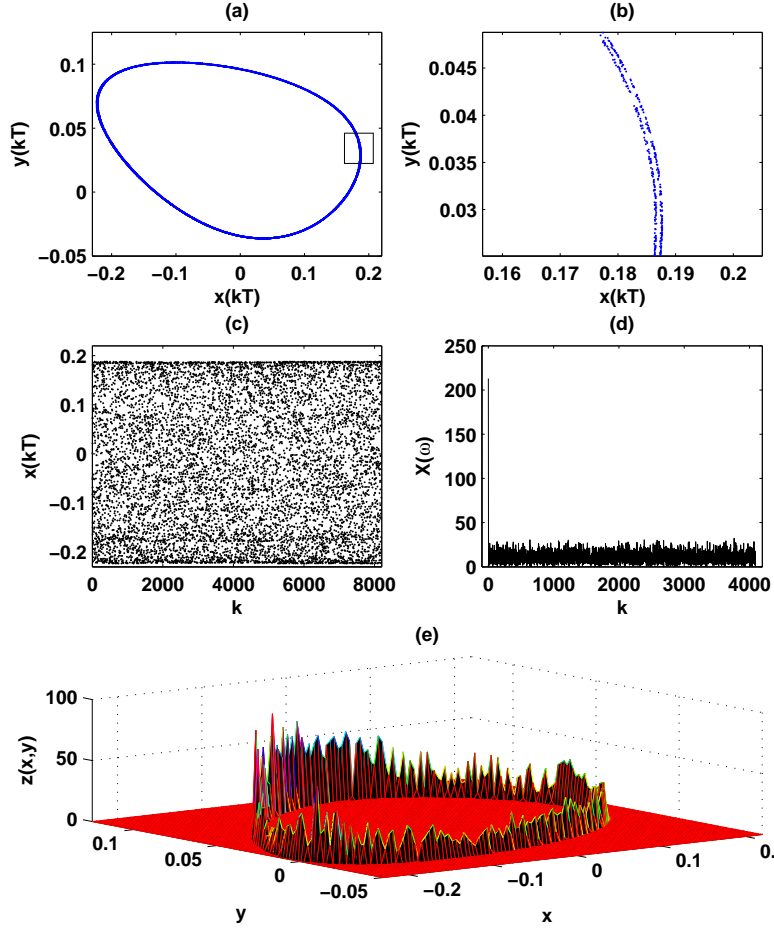


Figure 41: A rank one attractor from MLC circuit for $T = 468$, $\varepsilon_{ij} = 0.32$, $i = 1, 2$, $j = 1, 2, 3$.

5.3.1 Derivation of equations

The set of nondimensional equations for the original Chua's system is given by

$$\begin{aligned}\frac{dx}{dt} &= \alpha[y - h(x)] \\ \frac{dy}{dt} &= \gamma[x - y + \eta z] \\ \frac{dz}{dt} &= -\beta y\end{aligned}\tag{110}$$

where $h(x) = m_1x + 0.5(m_0 - m_1)(|x + B| - |x - B|)$. Equation (110) is obtained from the original piecewise linear Chua's circuit (Fig. 20 when all the switches are off) with $f(v_1) = G_bv_1 + 0.5(G_a - G_b)(|v_1 + V_b| - |v_1 - V_b|)$, through the following change of variables:

$$x = v_1/V_0 \quad y = v_2/V_0 \quad z = i/I_0 \quad t \rightarrow t/\omega_n \tag{111}$$

where V_0 , I_0 , and ω_n are the arbitrary voltage, current, and frequency scaling constants, respectively. In this case, in terms of the physical system parameters, the nondimensional system parameters in Eq. (110) are given by

$$\begin{aligned}\alpha &= \frac{G}{C_1\omega_n}, \quad \gamma = \frac{G}{C_2\omega_n}, \quad \eta = \frac{RI_0}{V_0}, \quad \beta = \frac{V_0}{L\omega_n I_0} \\ m_0 &= \frac{G_a}{G}, \quad m_1 = 1 + \frac{G_b}{G}, \quad B = \frac{V_b}{V_0}.\end{aligned}\tag{112}$$

Again, each switch in Fig. 20 is controlled by an external periodic pulsetrain with a pulsewidth of p_0 and a period of T_0 . When all the switches in Fig. 20 are kept open or at their default positions, we have the original Chua's circuit. The nondimensional set of equations for the circuit of Fig. 20 can be given by

$$\begin{aligned}\frac{dx}{dt} &= \alpha[y - h(x)] - \varepsilon x P_{T,p}(t) \\ \frac{dy}{dt} &= \gamma[x - y + \eta z] \\ \frac{dz}{dt} &= -\beta y.\end{aligned}\tag{113}$$

The relationship between the new parameters of the nondimensional system of Eq. (113) and those of the physical circuit of Fig. 20 can be given by

$$\begin{aligned}p &= p_0\omega_n, \quad T = T_0\omega_n \\ P_{T,p} &= \frac{1}{p} \sum_{n=0}^{\infty} [u(t - nT) - u(t - nT - p)] \\ \varepsilon &= \frac{\alpha R p}{R_1}\end{aligned}\tag{114}$$

where $P_{T,p}(t)$ is a periodic pulsetrain with a pulsewidth of p and a period of T , and ε represent the magnitude of the periodic pulses.

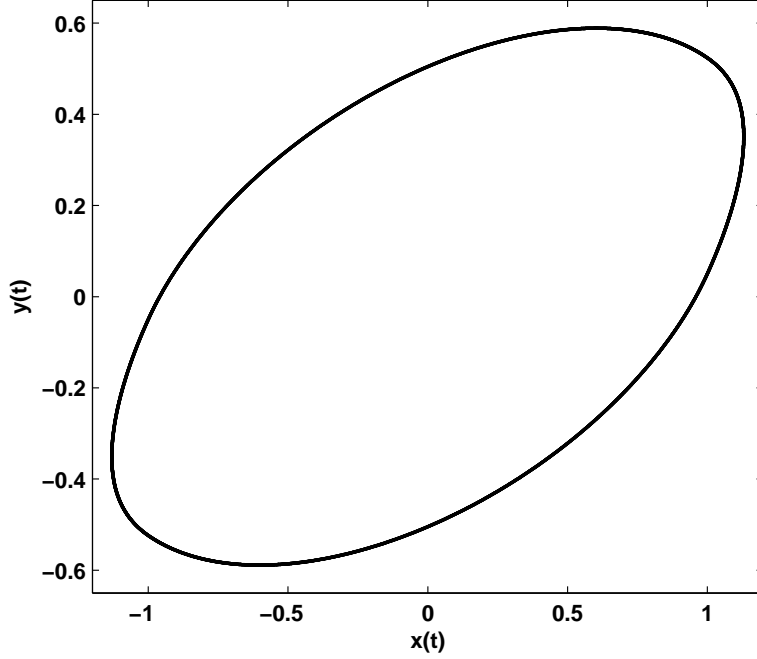


Figure 42: A non-Hopf limit cycle from PWL Chua's circuit ($\varepsilon = 0$).

5.3.2 Numerical simulations

We now present some results from our numerical simulations. The autonomous part of Eq. (113), obtained by setting $\varepsilon = 0$, has a limit cycle, as shown in Fig. 42, for

$$(\alpha, \gamma, \beta, \eta, m_0, m_1, B) = (2.0, 1.0, 2.0, 1.12, -0.75, -0.225, 1.0). \quad (115)$$

This limit cycle is the one that is going to be forced to obtain rank one chaos. We let

$$\alpha = 2, \quad \gamma = 1, \quad \eta = 1.12, \quad m_0 = -0.75, \quad m_1 = 0.225, \quad B = 1, \quad p = 0.5 \quad (116)$$

be fixed throughout and only allow T and ε to vary. Figures 43-45 are examples of rank one chaos obtained for $T = 247.5$, $\varepsilon = 0.5$; $T = 75$, $\varepsilon = 0.5$ and $T = 39$, $\varepsilon = 0.96$, respectively. In terms of what each of the plots of Figs. 43-45 represents, the same convention as that of Sec. 5.1 is employed. Once again, due to the large period of forcing ($T = 247.5$) the attractor in Fig. 43(a) appears to be a simple closed curve, but it is, in fact, a chaotic attractor of a very complicated geometric and dynamical structure, see Fig. 43(b) and (c). To reveal more of the structure in the radial direction, we reduce T to $T = 75$ and $T = 39$ for Figs. 44 and 45, respectively.

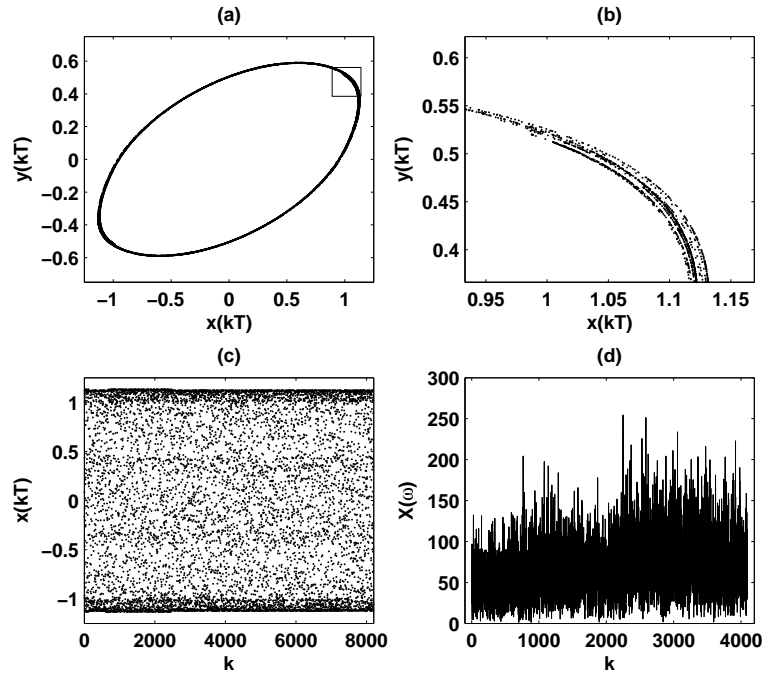


Figure 43: A strange attractor from PWL Chua's circuit for $T = 247.5, \varepsilon = 0.5$.

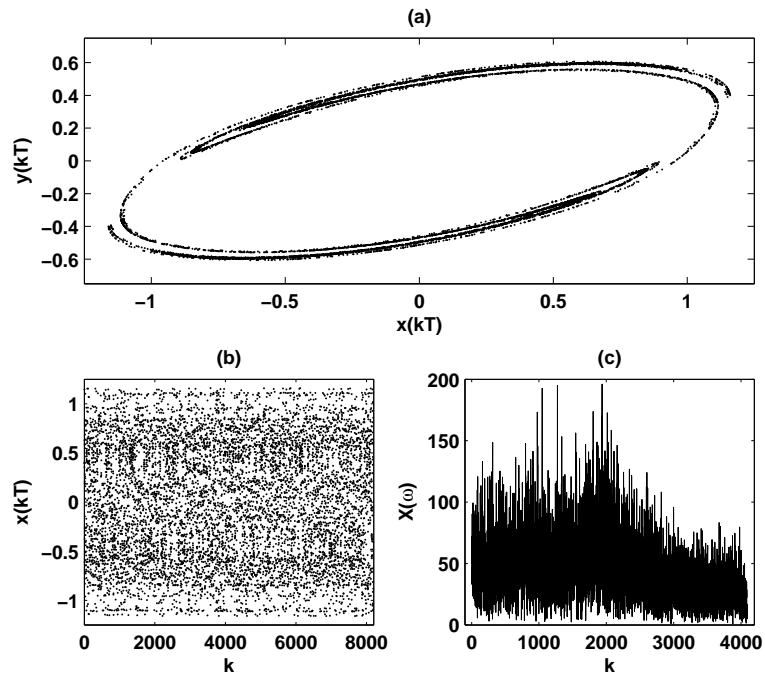


Figure 44: A strange attractor from PWL Chua's circuit for $T = 75, \varepsilon = 0.5$.

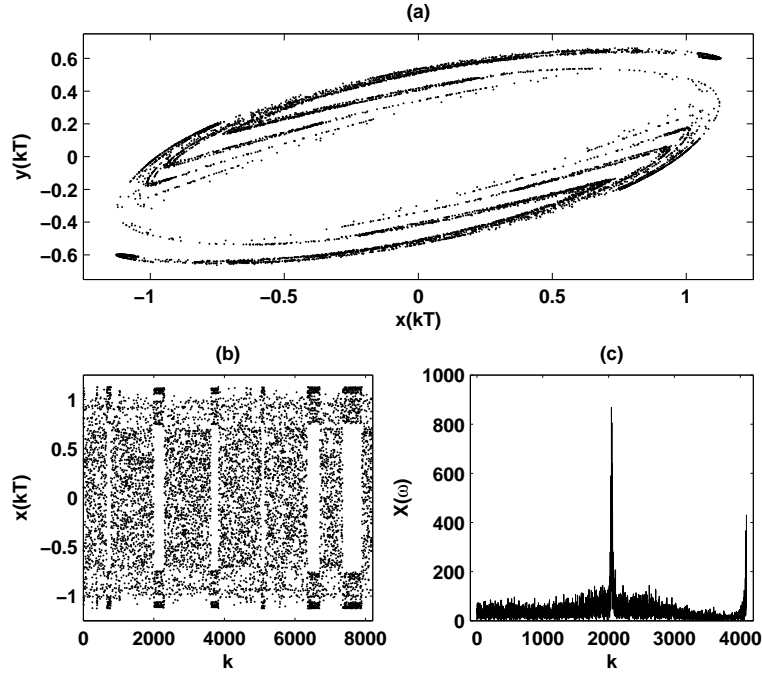


Figure 45: A strange attractor from PWL Chua's circuit for $T = 39, \varepsilon = 0.96$.

Remarks: (1) For this specific example, there is no theoretical assurance that rank one chaos would occur. However, we know that they are more likely to occur if the periodic solution is weakly stable, and the shearing (see Sec. 4) around this solution is relatively strong. In the case of a supercritical Hopf bifurcation, the stability of the Hopf limit cycle can be controlled as desired and the strength of shearing can be analytically computed. For a stable periodic solution arbitrarily picked, however, finding weakly stable limit cycles with strong shearing through analytical computations is usually not a realistic option. We would have to rely more on trial and error in simulations.

(2) The phase space is divided into three regions (for each segment of the piecewise linear characteristic) where the original circuit is defined by three different linear equations. When restricted completely to one of the linear regions, shearing is obviously non-existent so the ultimate reason for the creation of rank one chaos is the jumps of a solution from one region of linearity to another. The lack of smoothness seen in Fig. 45 is a reflection of these sudden jumps.

(3) Nevertheless, the chaos seen in our simulations is the type of chaos the theory predicts. Once again, the fact that these chaotic attractors are observable is due to the existence of homoclinic tangles admitting *no* periodic sinks.

6 Concluding Remarks

In this tutorial we systematically presented, at an introductory level, a new chaos theory for non-uniformly hyperbolic systems developed by the pure mathematics side of the dynamical systems community in the recent years. This new dynamics theory, namely, the theory of rank one chaos, establishes a comprehensive understanding of the complicated geometric and dynamical structures for a class of non-uniformly hyperbolic tangles. Inside of these homoclinic tangles, periodic sinks representing stable equilibrium, and SRB measures representing certain statistical law for chaos are the two main dynamical phenomena that are observable in both physical and parameter spaces.

This tutorial also addresses the applications of this new chaos theory. For certain systems of differential equations, the existence of the indicated class of homoclinic tangles can be verified through a well-defined computational process. In particular, switched-controlled Chua's circuit [Chua, 1994; Madan, 1993] and MLC circuit [Murali *et al.*, 1994a,b; Thamilmaran *et al.*, 2000] were used as examples to demonstrate how to apply the theory to concrete systems. Numerical simulations were used throughout to motivate, and to confirm the predications of the theory.

We started in Sec. 2 with a brief discussion of the well-known theories of homoclinic tangles and Smale's horseshoes. We then used a three-parameter family of 2D maps as an example to demonstrate the existing gap between the theories discussed and the results of simple numerical simulations. The conclusions from the theory of Newhouse sinks [Newhouse, 1974; Palis & Takens, 1993] and the theory of rank one chaos were then introduced to explain the simulation results. We concluded at the end of this section that, for the three-parameter family of 2D maps studied, periodic sinks and SRB measures are the two primary observable phenomena competing in the parameter space.

Section 3 includes a systematic introduction of theory of rank one maps [Wang & Young, 2001, 2006a,b]. We started with the rigorous definition of admissible 1D maps, and gradually moved to the definitions of admissible families of rank one maps in higher dimensions. Then the conclusions of the new chaos theory on rank one maps were stated in precise mathematical terms, and the significance and implications of these conclusions were discussed in some detail.

With the mathematical setting of Sec. 3 in mind, we moved in Sec. 4 to introduce a general frame work for applications. In Sec. 4.1, we showed, through detailed computations, that periodically kicked systems around weakly stable limit cycles induce time-T maps that fit naturally into the settings of Sec. 3. In Sec. 4.2, we presented the results from the studies of Wang & Young [2002a,b] on rank one chaos in periodically kicked systems of Hopf bifurcations.

In Sec. 5 we presented in some detail the studies of Wang and Oksasoglu on rank one attractors in switch-controlled circuits and systems [Oksasoglu & Wang, 2006; Oksasoglu *et al.*, 2006; Wang & Oksasoglu, 2005, 2007]. Based on the theory of Sec. 4.2, a step by step algorithm was introduced to verify the existence of rank one attractors in switch-controlled circuits. Switch-controlled

Chua's and MLC circuits were studied carefully following the algorithm outlined, and many of the results of numerical simulations were presented to confirm the theoretical findings, and to show the usefulness of the theory.

Overall, we have tried to introduce a long and complicated new chaos theory by using a balanced combination of examples, numerical simulations and theoretical discussions. We hoped to introduce, with this tutorial, the theory of rank one maps to the circuit and systems community. Although the applications presented in Sec. 5 are from the field of Electrical Engineering, the theory is also potentially applicable to other systems whose behavior can be characterized by Eq. (51). We also aimed at creating a standard reference for the theory that is hopefully accessible to a more application-oriented audience.

References

- Anosov, D. [1967] “Geodesic flows on compact Riemannian manifolds of negative curvature,” *Proc. Steklov Inst. Math.* **90**, 1–209.
- Benedicks, M. & Carleson, L. [1985] “On iterations of $1 - ax^2$ on $(-1, 1)$,” *Ann. Math.* **122**, 1–25.
- Benedicks, M. & Carleson, L. [1991] “The dynamics of the Hénon map,” *Ann. Math.* **133**, 73–169.
- Benedicks, M. & Young, L.-S. [1993] “Sinai-Bowen-Ruelle measure for certain Hénon maps,” *Invent. Math.* **112**, 541–576.
- Bowen, R. [1975] *Equilibrium States and the Ergodic Theory of Anosov Diffeomorphisms* volume 470 of *Lecture Notes in Math.* Springer-Verlag Berlin, Germany.
- Cartwright, M. L. & Littlewood, J. E. [1945] “On nonlinear differential equations of the second order,” *J. London Math. Soc.* **20**, 180–189.
- Chua, L. O. [1994] “Chua’s circuit. An overview ten years later,” *J. Circuits Syst. Comput.* **4**, 117–159.
- Collet, P. & Eckmann, L. P. [1983] “Positive Liapunov exponents and absolute continuity for maps of the interval,” *Ergodic Theory and Dynamical Systems* **3**, 13–46.
- Guckenheimer, J. & Holmes, P. [1997] *Nonlinear Oscillations, Dynamical Systems and Bifurcations of Vector Fields* page 155 Applied Mathematical Sciences. Springer-Verlag New York fifth edition.
- Guckenheimer, J., Wechselberger, M., & Young, L.-S. [2006] “Chaotic attractors of relaxation oscillators,” *Nonlinearity* **19**(3), 701–720.
- Hénon, M. [1976] “A two-dimensional mapping with a strange attractor,” *Comm. Math. Phys.* **50**, 69–77.
- Hopf, E. [1947] “Abzweigung einer periodischen lösung von einer stationären lösung eines differential systems,” *Ber. Verh. Sächs. Acad. Wiss. Leipzig Math. Phys.* **95**, 3–22.
- Jakobson, M. [1981] “Absolutely continuous invariant measures for one-parameter families of one-dimensional maps,” *Comm. Math. Phys.* **81**, 39–88.
- Katok, A. & Hasselblatt, B. [1995] *Introduction to the Modern Dynamical Systems* Cambridge University Press Cambridge.
- Ledrappier, F. & Young, L.-S. [1985] “The metric entropy of diffeomorphisms,” *Ann. Math.* **122**, 509–574.

- Levinson, N. [1949] “A second order differential equation with singular solutions,” *Ann. Math.* **50**(1), 127–153.
- Lin, K. [2006] “Entrainment and chaos in a pulse-driven Hodgkin-Huxley oscillator,” *SIAM J. Appl. Dyn. Syst.* **5**(2), 179–204.
- Lu, K., Wang, Q., & Young, L.-S. [2007] “Strange attractors for periodically forced parabolic equations,” *In preparation*.
- Madan, R. N. [1993] *Chua’s Circuit: A Paradigm for Chaos* World Scientific Singapore.
- Marsden, J. & McCracken, M. [1976] *The Hopf Bifurcation and its Applications* volume 19 of *Applied Mathematical Sciences* Springer-Verlag Berlin, Germany.
- Misiurewicz, M. [1981] “Absolutely continuous invariant measures for certain maps of an interval,” *Publ. Math. IHES.* **53**, 17–51.
- Mora, L. & Viana, M. [1993] “Abundance of strange attractors,” *Acta. Math.* **171**, 1–71.
- Murali, K., Lakshmanan, M., & Chua, L. O. [1994a] “Bifurcation and chaos in the simplest dissipative nonautonomous circuit,” *Int. J. Bifurc. Chaos* **4**(6), 1511–1524.
- Murali, K., Lakshmanan, M., & Chua, L. O. [1994b] “The simplest dissipative nonautonomous chaotic circuit,” *IEEE Trans. Circuits Syst. I* **41**(6), 462–463.
- Newhouse, S. E. [1974] “Diffeomorphisms with infinitely many sinks,” *Topology* **13**, 9–18.
- Oksasoglu, A. & Wang, Q. [2006] “A new class of chaotic attractors in Murali-Lakshmanan-Chua circuit,” *Int. J. Bifurcation & Chaos* **16**(9), 2659–2670.
- Oksasoglu, A., Ma, D., & Wang, Q. [2006] “Rank one chaos in switch-controlled Murali-Lakshmanan-Chua circuit,” *Int. J. Bifurcation & Chaos* **16**(11), 3207–3234.
- Oseledec, V. I. [1968] “A multiplicative ergodic theorem: Liapunov characteristic numbers for dynamical systems,” *Trans. Moscow Math. Soc.* **19**, 197–231.
- Palis, J. & Takens, F. [1993] *Hyperbolicity & sensitive chaotic dynamics at homoclinic bifurcations* volume 35 of *Cambridge Studies in Advanced Mathematics* Cambridge University Press Cambridge.

- Pesin, J. B. [1977] “Characteristic Lyapunov exponents and smooth ergodic theory,” *Russ. Math. Surv.* **32**(4), 55–114.
- Poincaré, H. [1890] *Les méthodes Nouvelles de la Mécanique Céleste, 3 Vols.* Gauthier-Villa Paris.
- Ruelle, D. [1976] “A measure associated with Axiom A attractors,” *Amer. J. Math.* **98**, 619–654.
- Rychlik, M. [1988] “Another proof of Jakobson’s theorem and related results,” *Ergodic Theory and Dynamical Systems* **8**, 83–109.
- Sinai, Y. G. [1970] “Dynamical systems with elastic reflections: Ergodic properties of dispersing billiards,” *Russ. Math. Surv.* **25**, 137–189.
- Sinai, Y. G. [1972] “Gibbs measure in ergodic theory,” *Russ. Math. Surv.* **27**, 21–69.
- Smale, S. [1967] “Differentiable dynamical systems,” *Bull. Amer. Math. Soc.* **73**, 747–817.
- Thamilmaran, K., Lakshmanan, M., & Murali, K. [2000] “Rich variety of bifurcations and chaos in a variant of Murali-Lakshmanan-Chua circuit,” *Int. J. Bifurc. Chaos* **10**(7), 1781–1785.
- Thieullen, P., Tresser, C., & Young, L.-S. [1994] “Positive exponent for generic 1-parameter families of unimodal maps,” *J’Analyse* **64**, 121–127.
- Viana, M. [1993] “Strange attractors in higher dimensions,” *Bull. Braz. Math. Soc.* **24**, 13–62.
- Wang, Q. & Oksasoglu, A. [2005] “Strange attractors in periodically kicked Chua’s circuit,” *Int. J. Bifurcation & Chaos* **15**(1), 83–98.
- Wang, Q. & Oksasoglu, A. [2007] “Rank one chaos in switch-controlled piecewise linear Chua’s circuit,” *Accepted for publication in J. Cir. Sys. & Comp.*
- Wang, Q. & Young, L.-S. [2001] “Strange attractors with one direction of instability,” *Commun. Math. Phys.* **218**, 1–97.
- Wang, Q. & Young, L.-S. [2002a] “From invariant curves to strange attractors,” *Commun. Math. Phys.* **225**, 275–304.
- Wang, Q. & Young, L.-S. [2002b] “Strange attractors in periodically-kicked limit cycles and Hopf bifurcations,” *Commun. Math. Phys.* **240**, 509–529.
- Wang, Q. & Young, L.-S. [2006a] “Non-uniformly expanding 1D maps,” *To appear, Commun. Math. Phys.*

- Wang, Q. & Young, L.-S. [2006b] “Toward a theory of rank-one attractors,”
To appear, Annal. Math.
- Wojtkowski, M. [1983] “Invariant family of cones and Lyapunov exponents,”
Ergodic Theory and Dynamical Systems **5**, 145–161.
- Young, L.-S. [1995] *Ergodic Theory of Differentiable Dynamical Systems* pages
 293–336 Real and Complex Dynamical Systems. Kluwer Acad. Press Netherlands.
- Young, L.-S. [2002] “What are SRB measures, and which dynamical systems
 have them?,” *J. Stat. Phys.* **108**, 733–754.